

ISSN number 0971 - 9709



The Journal of Indian Geophysical Union

AN OPEN ACCESS BIMONTHLY JOURNAL OF IGU

Volume 20, Issue 6 | November 2016



Journal of Indian Geophysical Union Editorial Board	Indian Geophysical Union Executive Council
Chief Editor P.R. Reddy (Geosciences), Hyderabad	President Prof. Shailesh Nayak, Distinguished Scientist, MoES, New Delhi
Associate Editors B.V.S. Murthy (Exploration Geophysics), Hyderabad D. Srinagesh (Seismology), Hyderabad Nandini Nagarajan (Geomagnetism & MT), Hyderabad M.R.K. Prabhakara Rao (Ground Water Geophysics), Hyderabad	Vice-Presidents Dr. Satheesh C. Shenoi, Director, INCOIS, Hyderabad Prof. Talat Ahmad, VC, JMI, New Delhi Dr. V.M. Tiwari, Director, CSIR-NGRI, Hyderabad Director, CSIR-NIO, Goa
Editorial Team Solid Earth Geosciences: Vineet Gahlaut (Seismology), New Delhi B. Venkateswara Rao (Water resources Management), Hyderabad N.V. Chalapathi Rao (Geology, Geochemistry & Geochronology), Varanasi V.V. Sessa Sai (Geology & Geochemistry), Hyderabad Marine Geosciences: K.S.R. Murthy (Marine Geophysics), Visakhapatnam M.V. Ramana (Marine Geophysics), Goa Rajiv Nigam (Marine Geology), Goa Atmospheric and Space Sciences: Ajit Tyagi (Atmospheric Technology), New Delhi Umesh Kulshrestha (Atmospheric Sciences), New Delhi P. Sanjeeva Rao (Agrometeorology & Climatoplogy), New Delhi U.S. De (Meteorology), Pune Archana Bhattacharya (Space Sciences), Mumbai Editorial Advisory Committee: Walter D Mooney (Seismology & Natural Hazards), USA Manik Talwani (Marine Geosciences), USA T.M. Mahadevan (Deep Continental Studies & Mineral Exploration), Ernakulum D.N. Avasthi (Petroleum Geophysics), New Delhi Larry D Brown (Atmospheric Sciences & Seismology), USA Alfred Kroener (Geochronology & Geology), Germany Irina Artemieva (Lithospheric Structure), Denmark R.N. Singh (Theoretical & Environmental Geophysics), Ahmedabad Rufus D Catchings (Near Surface Geophysics), USA Surjalal Sharma (Atmospheric Sciences), USA H.J. Kumpel (Geosciences, App. Geophysics, Theory of Poroelasticity), Germany Saulwood Lin (Oceanography), Taiwan Jong-Hwa Chun (Petroleum Geosciences), South Korea Xiujuan Wang (Marine Geology & Environment), China Jiro Nagao (Marine Energy and Environment), Japan Information & Communication: B.M. Khanna (Library Sciences), Hyderabad	Hon. Secretary Dr. Kalachand Sain, CSIR-NGRI, Hyderabad Joint Secretary Dr. O.P. Mishra, MoES, New Delhi Org. Secretary Dr. ASSRS Prasad, CSIR-NGRI, Hyderabad Treasurer Mr. Rafique Attar, CSIR-NGRI, Hyderabad Members Prof. Rima Chatterjee, ISM, Dhanbad Prof. P. Rama Rao, Andhra Univ., Visakhapatnam Prof. S.S. Teotia, Kurukshetra Univ., Kurukshetra Mr. V. Rama Murty, GSI, Hyderabad Prof. B. Madhusudan Rao, Osmania Univ., Hyderabad Prof. R.K. Mall, BHU, Varanasi Dr. A.K. Chaturvedi, AMD, Hyderabad Mr. Sanjay Jha, Omni Info, NOIDA Mr. P.H. Mane, ONGC, Mumbai Dr. Rahul Dasgupta, OIL, NOIDA Dr. M. Ravi Kumar, ISR, Gujarat Prof. Surjalal Sharma, Univ. of Maryland, USA Dr. P. Sanjeeva Rao, Advisor, SERB, DST, New Delhi Dr. N. Satyavani, CSIR-NGRI, Hyderabad Prof. Devesh Walia, North Eastern Hills Univ., Shillong
EDITORIAL OFFICE Indian Geophysical Union, NGRI Campus, Uppal Road, Hyderabad- 500 007 Telephone: +91 -40-27012799; 23434631; Telefax: +91-04-27171564 E. mail: jigu1963@gmail.com, website: www.j-igu.in	
The Open Access Journal with six issues in a year publishes articles covering Solid Earth Geosciences; Marine Geosciences; and Atmospheric, Space and Planetary Sciences.	
Annual Subscription Individual Rs. 1000 per issue and Institutional Rs. 3500 for four issues (from 2017 onwards, six issues Rs.5000/-) Payments should be sent by DD drawn in favour of "The Treasurer, Indian Geophysical Union", payable at Hyderabad, Money Transfer/NEFT/RTGS (Inter-Bank Transfer), Treasurer, Indian Geophysical Union, State Bank of Hyderabad, Habsiguda Branch, Habsiguda, Uppal Road, Hyderabad- 500 007 A/C: 52191021424, IFSC Code: SBHY0020087, MICR Code: 500004020, SWIFT Code: SBHYINBB028. For correspondence, please contact, Hon. Secretary, Indian Geophysical Union, NGRI Campus, Uppal Road, Hyderabad - 500 007, India; Email: igu123@gmail.com; Ph: 040 27012799	

CONTENTS

Editorial

S.No.	Title	Authors	Pg.No.
1	The Stress State of The Region around İnönü-Eskişehir active fault system (Turkey); kinematic analysis accompanied with GPS Data	A.Sağlam Selçuk, Y.E.Gökten and B. Aktuğ	527
2	Imaging of seismic discontinuities of the upper mantle in the western Himalaya through Receiver Function analysis	Nagaraju Kanna, K.S. Prakasam, Sandeep Gupta, K. Sivaram, Sudesh Kumar, Somasish Bose and B.N.V. Prasad	536
3	Microscopic Evidences for the Impact Origin of Ramgarh Structure, Rajasthan, India	Satyanarayan Rana and Vinod Agrawal	544
4	Petrology and geochemistry of the troctolite and ultramafic from the Paleoproterozoic Kandra Ophiolite Complex, Eastern Dharwar Craton, SE India	V.V. Sesha Sai	551
5	The effect of 10.7 cm solar flux on the monsoon rainfall over India	S. K. Midya, S. Goswami and K. Sengupta	558
6	Chaotic analysis of daily and weekly rainfall time series over Chennai	S. Tamil Selvi and R. Samuel Selvaraj	566
7	Characteristics of pre-monsoon convective activity over two contrasting environments from microwave radiometer data – A case study	P.P. Leena, S. Sakharam, V. Anilkumar, S.K. Das and G. Pandithurai	575
8	Long range forecast of rainfall during southwest monsoon in the states of Maharashtra and Goa	Onkari Prasad, O.P. Singh and K. Prasad	586
9	Cloud Aerosol Interactions and its influence on Cloud Microphysical parameters during Dry and Wet spells of Indian Summer Monsoon using CAIPEEX data	G.R. Chinthalu, T. Dharmaraj, M.N. Patil, A.R. Dhakate and Devendraa Siingh	596
	News at a Glance		606
10	In the absence of a robust controlling mechanism Sand mining will be more disastrous compared to Global warming	P.R. Reddy	609
	20 th Convention of the Indian Geological Congress (IGC)	Announcement	614

Editorial

I have returned from the KIMS hospital on 8th September, after undergoing treatment for STROKE for 6 days starting from 2nd September. Fortunately, due to God's grace, prayers of my family, friends and well wishers I could regain my voice, and minor setbacks.

I have learnt from this setback----- No matter how intelligent and rich you are, you cannot transport yourself to the future or the past. You have to be present, awake and happy now. If you believe that time has passed you by, your best days are behind you, or that somehow you've failed too many times to have another chance, nothing could be further from the truth. Indecision often blurs your vision making you to fail to focus. As many learned have propagated one should not leave a decision for tomorrow that needs to be made today. You can do everything you ought to do once you make a decision. I have decided to serve JIGU, until my physical and mental faculties permit and the readers want me to contribute. I will not continue once any of the first two fail and the third find me unsuitable.

An interesting topic is covered below, as part of the editorial.

The Anthropocene:

The Anthropocene concept is "stratigraphically real" and "potentially a valid chronostratigraphic unit," according to working group members. AWG secretary Colin Waters presented the assessment during a session at the International Geological Congress (IGC) in Cape Town, South Africa.

In his presentation, Waters noted that as a preliminary step, 30 out of 35 AWG members favored formalizing the Anthropocene in a recent nonbinding vote. A majority voted in favor of designating the Anthropocene as an "**epoch/series**," according to the working group, which would mean that the current Holocene epoch, which began about 11,700 years ago, has terminated. Anthropocene Working Group members recently voted to pin the start of the Anthropocene in the 1950s, when atmospheric nuclear bomb blasts deposited radioactive plutonium in sediment layers. (Source: Showstack, R. (2016), Scientific study group favors recognizing human-influenced epoch, *Eos*, 97, doi: 10.1029/2016EO058567).

This is a major scientific decision, as present day Man's contribution is significantly evident in obliterating number of species with his overambitious self destructing "developmental programs". While this decision been taken, some new findings have come up with specific findings.

Two recent papers in *Earth's Future* examine the meaning and formalization of an Anthropocene Epoch, a geological era in which humans have a major impact on surface processes and the environment. *Steffen et al.* [2016] take an Earth systems approach while *Williams et al.* [2016] focus on biospheric signals. Both papers are informative and data-based and should become required reading for anyone interested in the proposed change to Earth's geologic timescale and, especially, modern global change. The field of stratigraphy is explicitly recognized in each analysis, as it provides the foundation of the Geologic Timescale.

A quick primer on stratigraphy: for the past 2.5 million years, we have lived in the Cenozoic Era's Quaternary Period, which started with the Pleistocene Epoch and, currently, the Holocene Epoch. The addition of an Anthropocene Epoch into the geological time scale is a key motivation behind these papers, which will be decided by the International Commission on Stratigraphy, supported by an Anthropocene Working Group that includes the leads and several authors of these two papers.

Steffen and colleagues use Earth systems science to describe our planet's evolution from an evolving Precambrian environment into a life-dominated Phanerozoic one (since ~540Ma). They conclude that today's Earth system has undergone a substantial transition away from the Holocene (interglacial) state, toward a world with much less polar ice, changed atmospheric composition, and accelerated plant and animal species extinction. Williams and colleagues' biotic approach emphasizes that modern humans are changing our relationship with the planet through human consumption of Earth's resources, with major consequences for the ecosphere and a change in evolutionary state. Using different perspectives, both papers reach the same conclusion of an Anthropocene state that is unlike the Holocene, supporting the need for a new epoch. Both also favor a chemical tracer from mid-20thC nuclear activity as

its lower timescale boundary, though that seems less compelling from their descriptions.

The stratigraphic foundation of the Phanerozoic Eon's geologic timescale is the preservation of hard-bodied life. Extinctions, a relatively sudden, large decline of species, punctuate the record with five major events (excluding today) and multiple smaller events, providing global markers for stratigraphic boundaries in the geologic record. Some extinctions were relatively fast (thousands of years), while others reflect longer times (millions of years). The species extinction of modern time, which started with the rise of humans as the planet's dominant consumer of resources can likewise become the base of the Anthropocene. This latest (6th) major extinction is already underway, and continuing for decades to centuries, perhaps even culminating in human extinction. Life, notably the radiation of species, offers another global stratigraphic marker in the tradition of the geologic timescale. Humans exploring and conquering the world transported other life, including plants and seeds, small animals (like insects and rodents), and even large animals (like horses) that since became entrained as fossils in modern depositional strata. This biomarker would place the start of the Anthropocene well before the 20th century, as far back as 15th century, following Medieval times. Arguably, the current 6th extinction also started around that time. Unlike the Holocene, which started ~12,000 years ago as a garden-variety interglacial, the Anthropocene involves vast and fast changes on a global scale, involving life, atmosphere, land, and oceans. This pattern is not a mere extension or acceleration of the Holocene interglacial. The Anthropocene signature is unlike that of our planet's icehouse-greenhouse system, leading to my earlier suggestion in *van der Pluijm* [2014] to adopt a Pleistocene-Anthropocene boundary that reflects this fundamental change in Earth system from an externally-driven Milankovitch state to a human-driven state. As we move toward a decision, these authors contribute to the compelling

case for an Anthropocene Epoch, while reminding us of the environmental state change that is underway.

(**Source:** Ben van der Pluijm, Editor-in-Chief, *Earth's Future*; email: efbvdp@gmail.com).

Even though the impact of 1950s series of nuclear explosions on the earth's environment was significant, to categorically state that the suggested Anthropocene supports the theory that 11,700 year back started Holocene epoch got terminated is rather difficult to digest. Even though an Epoch is defined as "a division of time that is a subdivision of a period and is itself subdivided into ages, corresponding to a series in chronostratigraphy" to pin point the onset of Anthropocene epoch was started in 1950s is difficult. It is true that Man has devastated our environment and the devastation started with large scale introduction of chemicals in every walk of our life and over exploitation of our non renewable natural resources. In spite of this one cannot categorically state that the man made destruction is comparable to series of naturally induced evolutionary processes. Before coining this biomarker at par with significant evolutionary changes let the learned debate it in a detailed way and introduce a more viable alternative. Otherwise we will be only opening a new scientific issue for scientific debates and nothing else. I do agree with Ben Van der Pluijm's suggestion "to adopt a Pleistocene-Anthropocene boundary that reflects this fundamental change in Earth system from an externally-driven Milankovitch state to a human-driven state".

In this issue:

This issue contains 9 research articles, News at a glance, one research note cum opinion and a scientific convention circular.

I thank all those who have extended support to JIGU. I do wish from 2017 a new era begins with due recognition from Thomson Reuters

P.R.Reddy

The Stress State of The Region around İnönü-Eskişehir active fault system (Turkey); kinematic analysis accompanied with GPS Data

A.Sağlam Selçuk*¹, Y.E.Gökten² and B.Aktuğ³

¹ Van Yüzüncü Yıl University, Department of Geology, Van, Turkey

² Ankara University, Department of Geology, Ankara, Turkey

³Ankara University, Department of Geophysics, Ankara, Turkey

*Corresponding Author: azadsaglam@gmail.com

ABSTRACT

The İnönü-Eskişehir Fault System (IEFS) exhibits WNW–ESE striking right-lateral strike-slip character with a normal component that extends from Uludağ (Bursa) in the west to Sivrihisar (Eskişehir) in the east and separates the west Anatolian extensional region from the central Anatolia to the northeast. This fault system consists of E–W and NW–SE trending fault sets and segments which have potential to produce destructive earthquakes. In this study, we aim to identify the stress regime of the region around İnönü-Eskişehir active fault system by correlating the fault-slip data and GPS data. The strain rates are computed using the velocity vectors from 5 Turkish National Fundamental GPS Network (TUTGA) data, acquired from the General Command of Mapping (Turkey). Fault-slip data have been analysed using the stress inversion method of Angelier. The obtained contraction rate for the studied area is about 65 ± 15 nanostrain/yr, which corresponds to a contraction rate of 0.7 ± 0.15 mm/yr over 10 km. The strain rate results of last ten years calculated from the TUTGA-99 data suggest approximately NW-SE trending compressional tectonic regime in the region. This strain rate and orientations are confirmed by the Plio-Quaternary slip surface data collected along the İnönü-Eskişehir Fault System.

Key words: İnönü-Eskişehir Fault System, contraction rate, Kinematic analysis, TUTGA data and Central Anatolia.

INTRODUCTION

The Central parts of the Anatolian block plays the role of stress transferring zone between East Anatolian contractional province and West Anatolian Extensional region in the west during its drive towards west along North and East Anatolian Fault systems. Together with this tectonic escape of the Anatolian block towards to the west, new small plate boundaries and related neotectonic elements are created with several intra-block strike slip faults (Gökten et al., 2013). The rotations of the blocks bounded by these intra-block strike slip faults (Şaribudak et al., 1990; Tatar et al., 1995; Kaymakçı 2000; Kaymakçı et al., 2003 a,b; Gökten et al., 2013) during the westward movement of the Anatolian block as a whole, caused the rising of various stress regimes which characterize and control different sub-regions of the Central Anatolia giving rise to regional seismicity in the region. Besides, the relative movements of the small blocks are characterized by different stress orientations, although most of the sub-region boundaries are controlled by the strike-slip faults. In this context, IEFS is one of the major neotectonic structures of the central Anatolia which separates the southwestern Turkey Extensional and the North Anatolian strike-slip neotectonic domains (Özsayın and Dirik, 2007) (Figure 1). Regarding active tectonic regimes and related structures in the Central Anatolian region, IEFS has a considerable role in the stress distribution in the region. The IEFS, extending

from Uludağ (Bursa) to the west and Lakesalt(Konya) to the east, is a 400-km long and 15-25-km wide right-lateral transtensional strike-slip fault belt (Koçyiğit 2003; Koçyiğit 2005) (Figure 1). In general, the fault belt is mainly composed of WNW-ESE trending right-lateral strike-slip faults and also includes NE-SW trending left-lateral strike-slip and NW-SE trending dip-slip normal faults.

During the time interval between late Pliocene and recent the central Anatolia deformed at a low velocity strain rate (>20 cm/yr) under two diverse cogenetic neotectonic regimes (Reilinger et al., 2006). Recent GPS studies indicate that there are velocity differences between eastern and western parts of central Anatolia and deformation type of the region is not uniform; while the western part of the Anatolia has been shaping under the extensional-dominated tectonic regime, the eastern part has been deformed under the contractional tectonic regime (Aktuğ et al., 2013). Deformation rate on the IEFS is estimated as 0.15 mm/yr using GPS data (Aktuğ et al., 2013). The rate in the western sector is $0.1 \mu\text{strain/yr}$ which sharply falls to $0.02 \mu\text{strain/yr}$ to the east (Kahle et al., 1998). Based on geologic observations, Koçyiğit et al., (2000) suggest a deformation rate of $0.07 - 0.13$ mm/yr for this region. However, some recent works on dating of terrace deposits (Ocakoglu, 2007; Ocakoglu and Açikalın 2009) yield a strain rate of 1 mm/yr. The IEFS has undertaken different roles at different periods in the tectonic evolution of Central Anatolia. The segmentation of this fault system around Kaymaz was

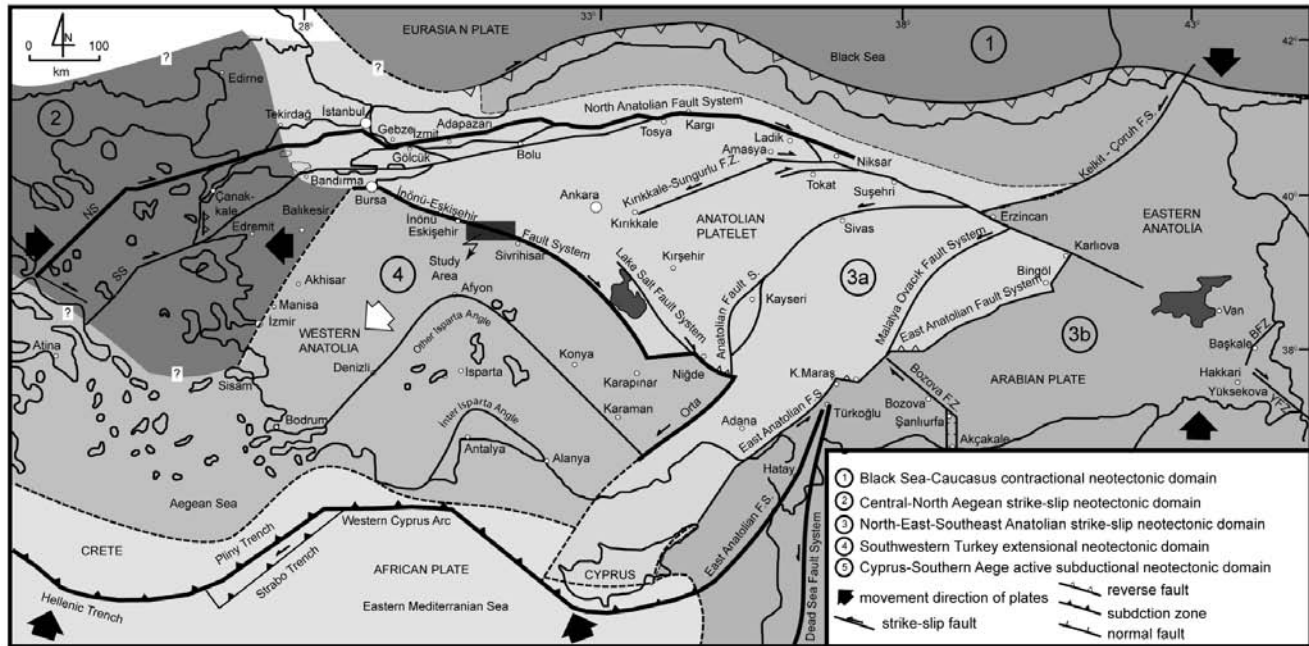


Figure 1. Simplified tectonic map of Turkey and surrounding areas showing major tectonic structures and neotectonic provinces (Koçyiğit and Özacar, 2003).

developed in three different zones which are Alpu fault zone, Eskişehir fault zone and Orhaniye fault zone from north to the south (Figure 2) (Sağlam Selçuk and Gökten, 2012). Tectonic analyses of the faults are made with the help of slip vectors measured on the fault planes. These analyses are based on stress-shearing relation developed by Wallace (1951) and Bott (1959). If the slip vector on each fault plane is in the same direction of effective resolved shear stress (Bott, 1959), then the most suitable stress tensor can be computed from the inversion of the fault slip vectors measured from fault (Carey and Brunier, 1974; Angelier 1984). Angelier’s direct inversion method, one of the mostly used methods in the inversion solutions, is based on functions established by mathematical approaches. This technique using the fault properties enables the calculation of principle stress vectors and their ratio. These properties include character, strike and dip of the fault and the fault striae with rake angles. In this study, we aim to identify the stress regime of the region around İnönü-Eskişehir active fault system by correlating the fault-slip data and GPS data by using the stress inversion method of Angelier and TUTGA network data.

Eskişehir Fault Zone

Eskişehir fault zone which has been active possibly since Pliocene (Sağlam Selçuk and Gökten, 2012) generated moderate size earthquakes during the instrumental

period. The most recent destructive earthquakes occurred on Eskişehir fault zone in 1956, with a magnitude of $M=6.4$ (Öcal, 1956) is an important one with reference to Neotectonic and seismicity of the region (Figure 3).

This fault zone exhibits right-lateral strike-slip character with a normal component and extends between Uludağ (Bursa) to the west and Sivrihisar (Eskişehir) to the east. In the study area, this fault zone is composed of three distinct segments, namely Yörükkaracaören segment (YF) (between Yörükkaracaören and Sarıkavak), Bardakçı-Kaymaz segment (BKF) (between Sarıkavak and Kaymaz) and Paşakadın segment (PF) (between Kaymaz and Sivrihisar) (Figure 2). The basement rocks consisting of mostly Mesozoic marbles and Quaternary units comprising alluvial sediments are tectonically juxtaposed along these segments. Furthermore, morphotectonic structures such as fault terraces, hanging alluvium fans, and several kinematic data on the fault planes are also observed. While we were not able to observe slip surface data along the Yörükkaracaören segment, we observed and measured some kinematic indicators along the Bardakçı-Kaymaz and Paşakadın segments. The 28-km-long Bardakçı-Kaymaz segment is a $N25^{\circ}W$ trending right-lateral strike-slip fault with a normal component. 14 slip data were measured at three locations along the Bardakçı-Kaymaz segment. Fault-slip data have been analysed, using the stress inversion method of Angelier (1990, 1994). From the direct inversion method the orientations of the stress tensors are $\sigma_1=138^{\circ}/7^{\circ}$, $\sigma_2=20^{\circ}/76^{\circ}$ and $\sigma_3=230^{\circ}/12^{\circ}$ and

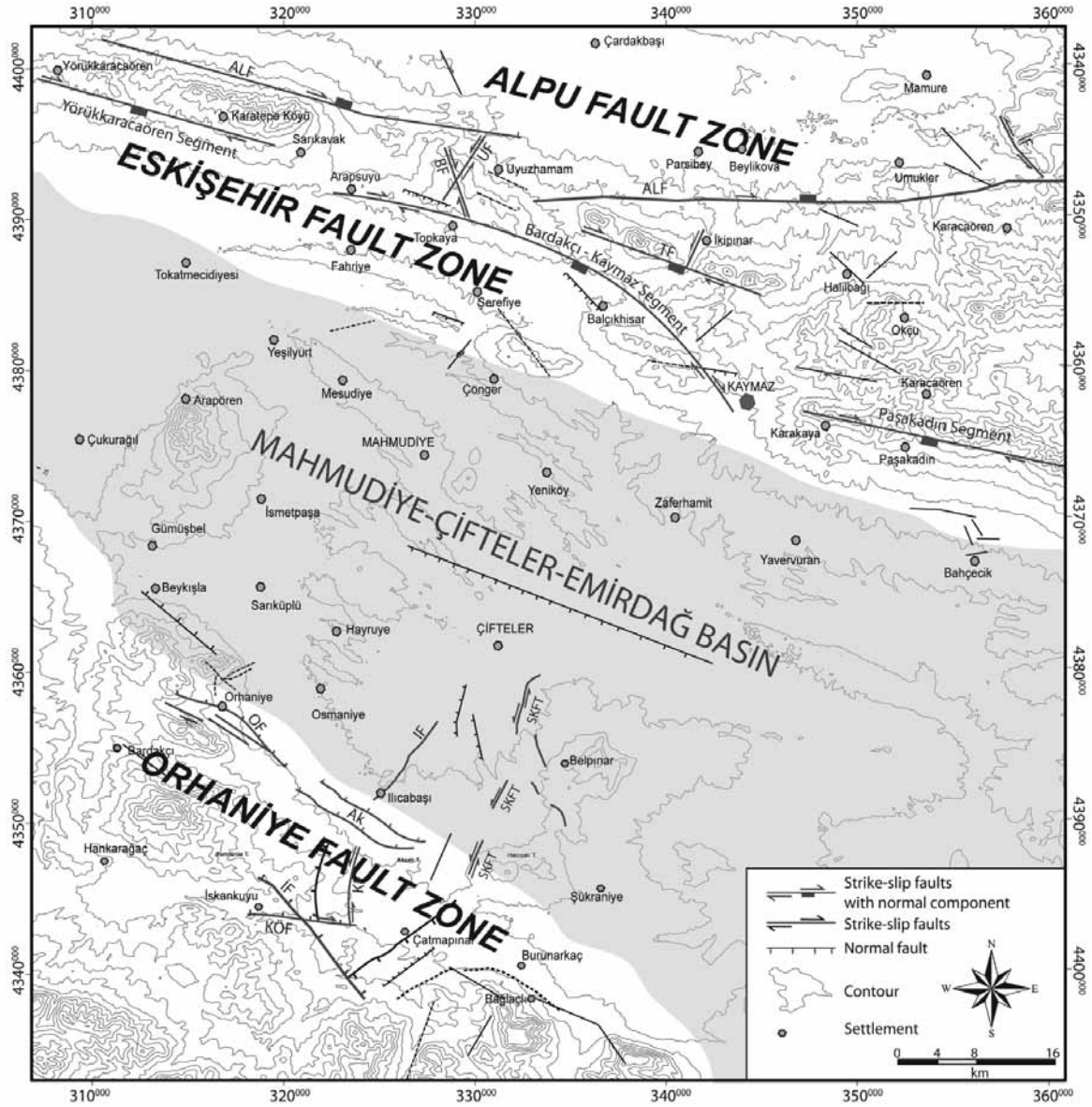


Figure 2. Simplified structural map of Mahmudiye-Çifteler-Emirdağ basin. Abbreviations: OF: Orhaniye fault, İF: İskankuyu fault, Ak: Akçalıtepe fault, SKFT: Sakaryabaşı fault, İF: İlicabaşı fault, KF: Kızıltepe fault, KÖF: Kötütepe fault, TF: Tepecik fault, BF: Bardakçı fault, UF: Uyuzhamam fault, İF: İncecik fault, ALF: Alpu fault.

Φ is 0.524 (Table 1). The computed results of the inverse analysis of fault-slip measurements are consistent with the behavior of principal stresses, as expected in strike-slip faults, while σ_2 is vertical and σ_1 and σ_3 are nearly horizontal. These results revealed a NW-SE trending compression and NE-SW trending extension on Bardakçı-Kaymaz segment (Figure 3). In the study area, the eastern segment of Eskişehir fault zone is Paşakadın fault. The N85°W trending and 65°SW dipping Paşakadın fault is a 16-km long right-lateral strike-slip fault with a dip slip component. The stress field orientations along the fault suggest an approximately NW-SE trending compression and NE-SW trending extension.

Alpu Fault Zone

Alpu fault zone is a structural contact between the Kaymaz uplift and Alpu basin while the southern side of the Kaymaz uplift is bordered by the Eskişehir fault zone (Figure 4). Tepecik, Uyuzhamam, and İncecik faults are the main segments within the Alpu fault zone. Kinematic properties of these structural elements define the characteristics of recent stress field in the region.

Data obtained along the fault surfaces of Tepecik fault indicate that IEFs has a significant right-lateral character. The N80°W trending and 45°SW dipping Tepecik fault is

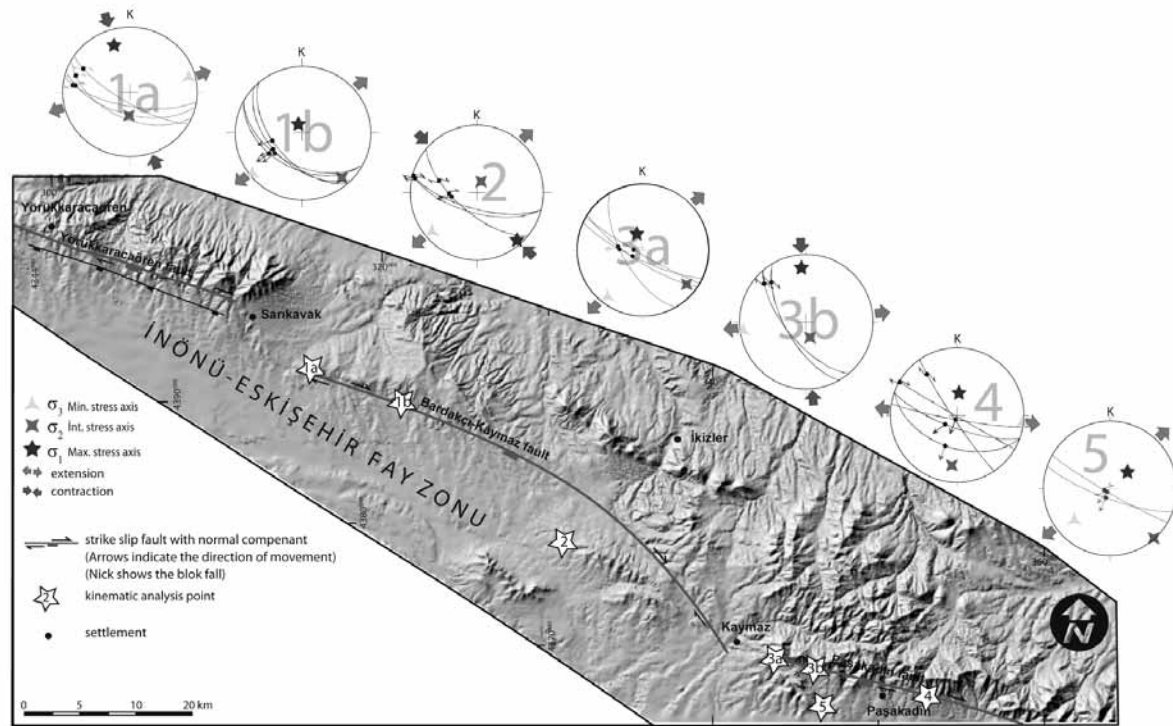


Figure 3. Digital Elevation Model (DEM) showing general outline of the Eskişehir fault zone (Sağlam Selçuk and Gökten, 2012). Numbers in stars refers to location of fault slip data (see, Table 1 for slip data).

Table 1. Results of paleostress analysis from measurement of slickensides in the Eskişehir fault zone. (see Figure 3 for locations).

Name of fault	Location no	Nature of fault	Number of slip data	σ_1	σ_2	σ_3	ϕ
Bardakçı-Kaymaz F.	1a	Oblique-slip	4	337°/23°	181°/67°	076°/02°	0.527
Bardakçı-Kaymaz F.	1b	Oblique-slip	5	339°/78	140°/11°	231°/04°	0.191
Bardakçı-Kaymaz F.	2	Oblique-slip	5	138°/07°	20°/76°	230°/12°	0.524
Paşakadın F.	3a	Oblique-slip	7	357°/67°	126°/15°	221°/17°	0.103
Paşakadın F.	3b	Oblique-slip	2	357°/07°	157°/83°	265°/09°	0.101
Paşakadın F.	4	Oblique-slip	5	005°/63°	186°/27°	096°/01°	0.346
Paşakadın F.	5	Oblique-slip	2	045°/63°	138°/02°	229°/29°	0.342

a 13-km long right-lateral strike-slip fault with a dip slip component. A total of 8 measurements were taken from fault planes as fault striae and deviation angle at two stations along Tepecik fault. From the direct inversion method, following values are estimated, $\sigma_1=8^\circ/65^\circ$, $\sigma_2=152^\circ/21^\circ$ and $\sigma_3=247^\circ/13^\circ$ and Φ is 0.282 (Table 2). Regarding the behavior of three principal stresses, σ_1 is vertical, σ_2 and σ_3 are almost horizontal indicating the dip slip normal faulting character of Tepecik fault. The stress field orientations along the Tepecik fault suggest an approximately NE–SW-directed extension (Figure 4).

The N25°E trending, 60° to 85° southward dipping Uyuzhamam fault is an 8-km long strike slip fault. The fault is located between Esenler village to the north and Uyuzhamam village to the south. The striation set has an

average rake of 18°N. Kinematic analysis indicates that the Uyuzhamam fault operates as a left-lateral strike slip fault. A total of 4 measurements were taken from fault planes at one station as fault striae and deviation angle at one station on the Uyuzhamam fault. From the direct inversion method, $\sigma_1=227^\circ/12^\circ$, $\sigma_2=346^\circ/67^\circ$ and $\sigma_3=133^\circ/20^\circ$ and Φ is 0.353 (Table 2). At station 9, where the left-lateral strike slip character of the fault is clearly seen, a deformation domain of NW-SE trending compression and NE-SW trending extension is suggested (Figure 4).

İncecik fault starts from just northeast of the Beylikova village, and changes its direction from N60°W to N30°W along its 6 km long length. A total of 4 measurements were taken from fault planes, fault striae and deviation angle at one station on the İncecik fault. From the direct inversion

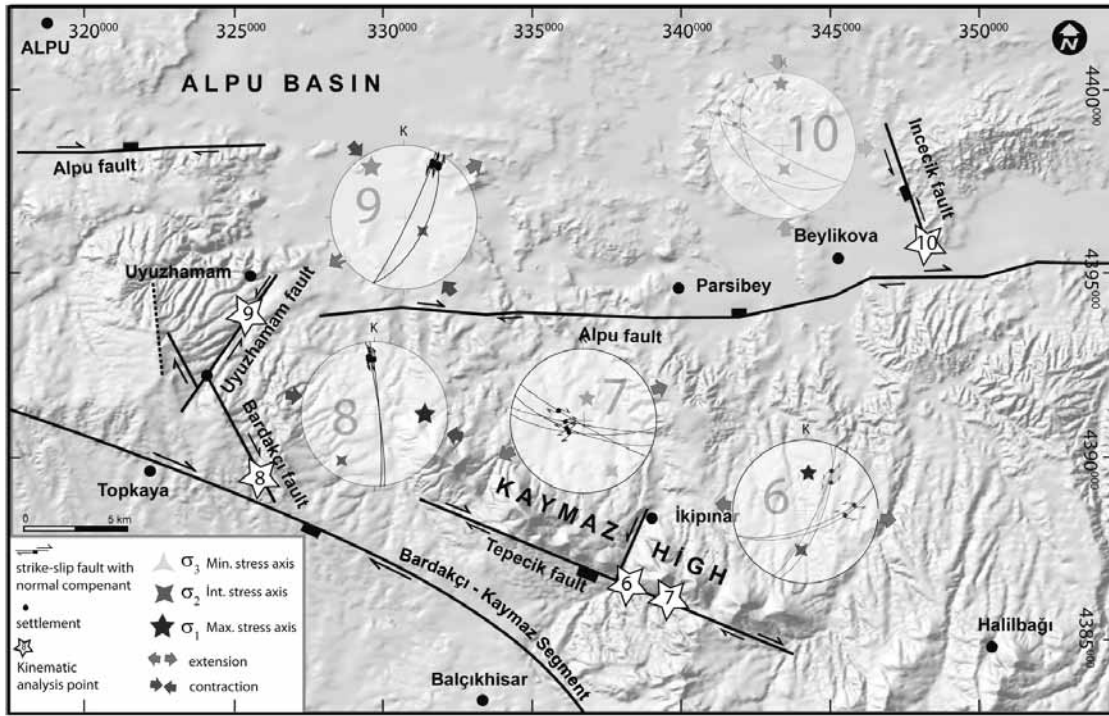


Figure 4. DEM showing general outline of the Alpu fault zone (Sağlam Selçuk and Gökten, 2012). Nick shows the block fall, arrows indicate local compression and extension directions respectively (see, Table 2 for slip data).

Table 2. Results of paleostress analysis from measurement of slickensides in the Alpu fault zone. (see Figure 4 for locations).

Name of fault	Location no	Nature of fault	Number of slip data	σ_1	σ_2	σ_3	ϕ
Tepecik F.	6	Oblique-slip	4	337°/65°	170°/21°	074°/06°	0.444
Tepecik F.	7	Oblique-slip	4	327°/71°	162°/19°	071°/05°	0.770
Uyuzhamam F.	8	Strike-slip	4	098°/28°	204°/29°	303°/38°	0.289
Alpu F.	9	Oblique-slip	4	326°/14°	138°/58°	233°/04°	0.613
İncecik F.	10	Oblique-slip	5	357°/26°	175°/64°	266°/01°	0.253

method, $\sigma_1=357°/26°$, $\sigma_2=175°/64°$ and $\sigma_3=266°/01°$ and Φ is 0.653 (Table 2). At station 10, the NE-SW trending right-lateral strike slip character of the fault is analysed. The result suggests a N-S compression associated with an E-W extension (Figure 4).

Orhaniye Fault Zone

The Orhaniye fault zone (OFZ) is composed of faults with dissimilar character extending in varying directions. They are OFZ, Sakaryabaşı fault, İskankuyu fault, Akçalıtepe fault, Ilıcabaşı fault, Kötütepe fault and Kızılkaya fault. Among them, Orhaniye fault set, Kötütepe and Kızılkaya faults are the younger ones and yield important kinematic data (Figure 5). OFZ consists dominantly of NW-SE striking fault segments with an average length of 40 km between Dede area and Sünnürüz hill (Figure 5). It is mostly composed of normal faults with a right-lateral component.

During the field studies, a total of 9 measurements were taken from the fault planes of Orhaniye fault zone, fault striae and deviation angle at one station. From the direct inversion method, $\sigma_1=326°/13°$, $\sigma_2=185°/74°$ and $\sigma_3=28°/10°$ and $\Phi =0.196$, are obtained. Regarding the behavior of three principal stresses, σ_2 is vertical and σ_1 and σ_3 are nearly horizontal. In the fault plane solution, it indicates the NNW-SSW trending compression and NNE-SSW trending extension (Figure 5).

The N70°E trending Kötütepe fault, located around the İskankuyu village, is a normal fault with an oblique slip component. During the field studies, 4 measurements were taken from fault planes, fault striae and deviation angle at one station. Based on the results from direct inversion method, $\sigma_1=204°/72°$, $\sigma_2=310°/5°$ and $\sigma_3=41°/17°$ and $\Phi =0.373$ are obtained (Table 3). Regarding the behavior of three principal stresses, σ_1 is vertical and σ_2 and σ_3 are nearly horizontal indicating dip slip normal character of

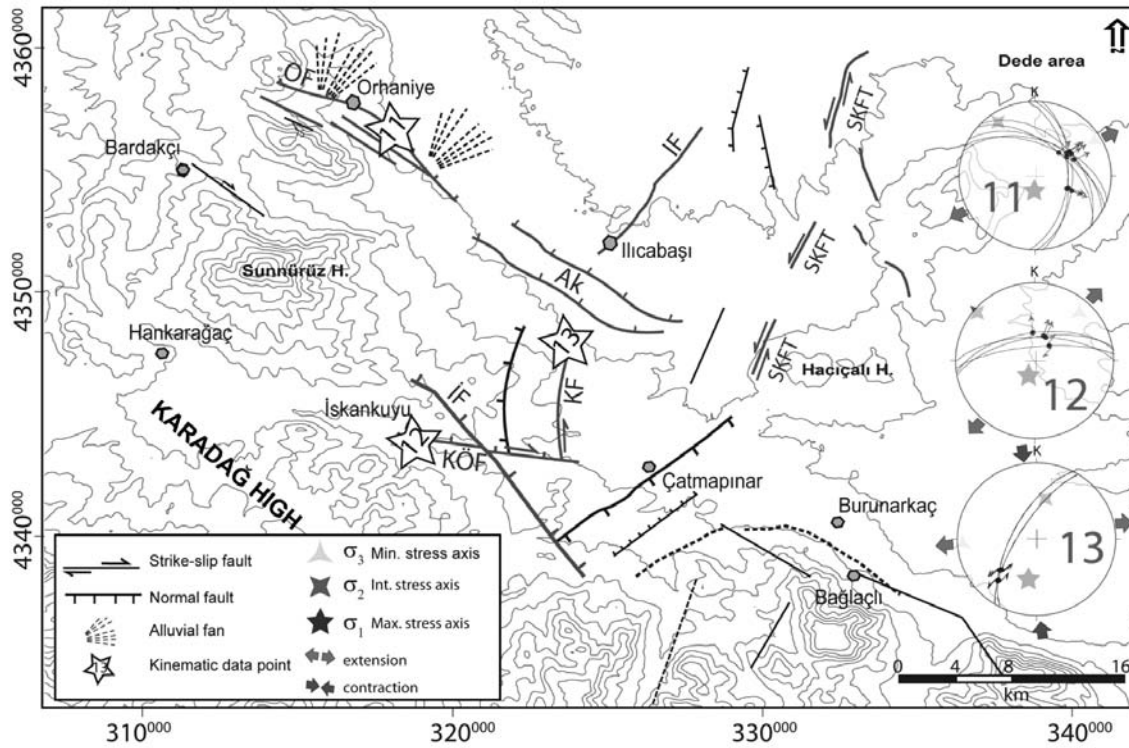


Figure 5. General outline of the Orhaniye fault zone. Numbers 11 through 13 shows the locations of the fault slip data, (see, Table 3 for slip data), OF: Orhaniye fault, KÖF: Kötütepe fault, KF: Kızıltepe fault, İF: İskankuyu fault, SKFT: Sakaryabaşı fault.

Table 3. Results of paleostress analysis from measurement of slickensides in the Orhaniye fault zone. (see Figure 5 for locations).

Name of fault	Location no	Nature of fault	Number of slip data	σ_1	σ_2	σ_3	ϕ
Orhaniye F.	11	Normal	9	185°/74°	326°/13°	048°/10°	0.196
Kötütepe F.	12	Oblique-slip	4	204°/72°	310°/05°	041°/17°	0.373
Kızıltepe F.	13	Strike-slip	2	171°/34°	001°/46°	261°/00°	0.315

Kötütepe fault. Fault plane solutions indicate the presence of a NE-SW trending extension (Figure 5). The N28E trending Kızıltepe fault is a left-lateral strike-slip. During the field studies conducted on the Kızıltepe fault, measurements were taken from fault planes, fault striae and deviation angle at only one station. Based on the results from direct inversion method, $\sigma_1=191^\circ/44^\circ$, $\sigma_2=12^\circ/46^\circ$ and $\sigma_3=281^\circ/0^\circ$ and $\Phi=0.315$ (Table 3) are obtained. Another fault approximately parallel to Kızıltepe fault was determined in this part of the field which is a NE-SW trending normal fault with a left-lateral strike slip component, and as a whole the region is characterized by a NW-SE trending compression and NE-SW trending extension (Figure 5).

Stress Analysis of the Region and Relative Velocity Vector

TUTGA network has been established between 1997 and 1999, covering the Anatolian block, and considering the

deformation due to active tectonic movements of Turkey, the GPS sites have been selected. The coordinate variations of the particular points via tectonic plate movements are caused by inter seismic, co seismic, and post seismic effects. The coordinates and the velocities of five fundamental stations (MIH, KRCT, EMRD, KYMZ, TRMN and ESKI) located in the study area were obtained from the national mapping agency of Turkey (General Command of Mapping). The interseismic velocities of the sites along with formal uncertainties are shown in Figure 6. To determine the strain rates, Delaunay Triangulation algorithm and a linear estimation methodology were employed in which the rigid body rotations and the translations were estimated simultaneously with the strain parameters (Feigl et al., 1990; Turcotte and Schubert, 1982).rain axes are shown in Figure 7.

The results obtained from the kinematic data Angelier (1990, 1994) and the analysis in the study area show NNW-SSE compression and ENE-WSW extension. Other

The Stress State of The Region around İnönü-Eskişehir active fault system (Turkey); kinematic analysis accompanied with GPS Data

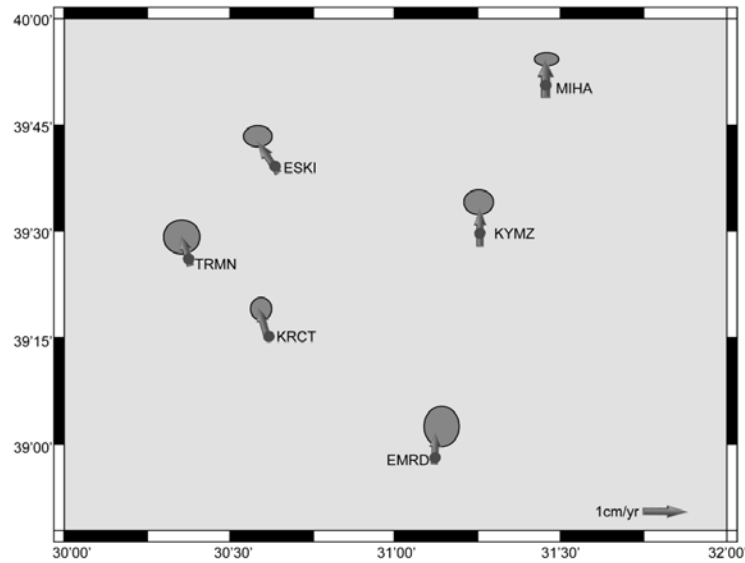


Figure 6. The study area and obtained velocity vectors in ITRF96.

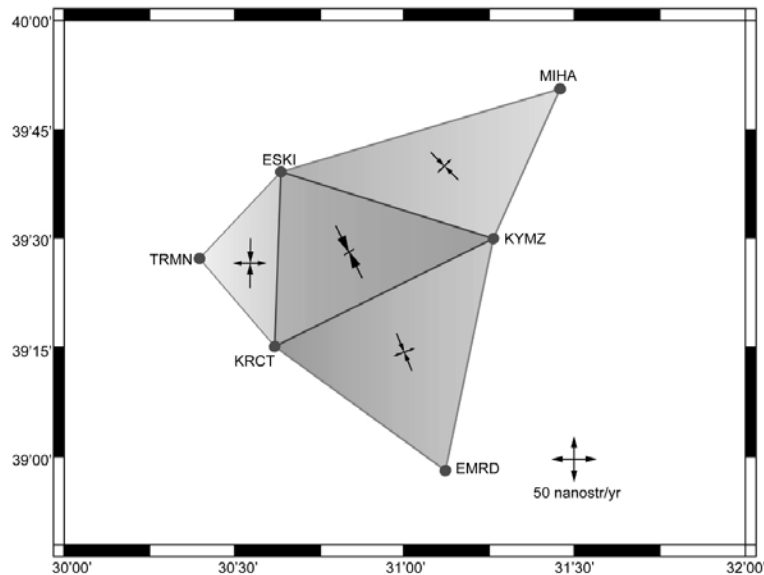


Figure 7. The elements of main warp calculated for study area.

kinematic analyses based on GPS data also support in general the same conclusion, although with a slightly more dominant regional NNW-SSE compression. On the other hand, Kaymakçı et al., (2003a) showed that this region has experienced a NNW-SSE compression from Late Paleocene to Early Miocene in their paleomagnetic studies carried out in the Çankırı basin located east of study area. This study confirms that the same stress conditions are continuing in a broad part of central Anatolia today.

GPS-derived strain rates in the ESKI-KRCT-KYMZ main warp block which lies in the southern part of the NW-SE striking Eskişehir Fault Zone exhibits some differences

in the orientation, which is possibly due to the variations in the direction of the faults located in the in this western part of the basin. On the other hand, the results of the ESKI-MIH-KYMZ and KRCT-EMRD-KYMZ blocks show that they have nearly the same compression and extension orientations. Especially, TRMN-ESKI-KRCT block, which is in the southern part of the province of Eskişehir, shows N-S compression and E-W extension. ESKI-KRCT-KYMZ block shows a contraction of about 65 ± 15 nanostr/yr which approximately corresponds to a quantity of 0.7 mm/yr over 10 km. ESKI-MIH-KYMZ and KRCT-EMRD-KYMZ blocks have strain rates of approximately 50 ± 15 nanostr

/ yr, corresponding a contraction of 0.6 mm/yr over 10 km. KRCTTRMN-ESKI block has a strain rate of 60 ± 15 nanostr / yr, which corresponds to 0.75 mm / yr over 10 km.

CONCLUSIONS

Six GPS sites of TUTGA-99 in the region of interest have been used for calculating the strain rate of the central Anatolia. These data comprise the measurements of 10 years of period starting from 1999. According to the TUTGA data from the region, the average strain rate along the 10 km length of the zone is 0.7 mm/year which corresponds to the compression in the region. The NW-SE direction of a compression is consistent with the fault plane kinematic data.

It is considered that such stress system is responsible for the westward escape of the Anatolian block in the late Pliocene time. With the advent of the Neotectonic period, several kinds of tectonic regimes have also been effective in the overall region including the study area. However, it is shown that the study area is under the influence of a compression in NNW-SSE trend in a simple-shear system, and an expansion raised in NNE-SSW trend related to this compression.

ACKNOWLEDGMENTS

This paper comprises part of the PhD Thesis of the first author which was supported by the Ankara University Research Fund (Project No: 20050745- 013HBP). The manuscript was much improved by the constructive critical reviews by anonymous reviewers. We also thank Dr.MRK Prabhakar Rao and Chief Editor for constructive suggestions and apt editing of the manuscript.

Compliance with Ethical Standards

The authors declare that they have no conflict of interest and adhere to copyright norms.

REFERENCES

Aktuğ, B., Parmaksız, E., Kurt, M., Lenk, O., Kılıçoğlu, A., Gürdal, M.A., and Özdemir, S., 2013. Deformation of Central Anatolia: GPS Implications, *Journal of Geodynamics*, pp: 67-78.

Angelier, J., 1984. Tectonic analysis of fault slip data sets. *Journal of Geophysical Research* 89/B7, pp: 5835-5848.

Angelier, J., 1990. Inversion of field data in fault tectonics to obtain the regional stress. III. A new rapid direct inversion method by analytical means. *Geophysical Journal International*, v.103, pp: 363-376.

Angelier, J., 1994. Fault slip analysis and paleostress reconstruction. In: Hancock, P.L. (ed), *Continental Deformation*. Pergamon Press, Oxford, pp: 53-100.

Bott, M.H.P., 1959. The mechanism of oblique slip faulting. *Geological Magazine*, v.96, pp: 109-117.

Carey, E., and Brunier, B., 1974. Analyse théorique et numérique d'une modèle mécanique élémentaire appliqué a l'etude d'une population des failles. *Comptes Rendus de l'Académie des Sciences*, Paris 279, pp: 891-894.

Feigl, K.L., King, R.W., and Jordan, T.H., 1990. Geodetic measurements of Tectonic Deformation in the Santa Maria Fold and Thrust Belt, California. *J. Geophys. Res.*, v.95 (B3), pp: 2679-2699.

Gökten, E., Kelling, G., and Meydan, M., 2013. The kinematic significance of rotation-related deformation features in a fault-defined wedge associated with the North Anatolian Fault, central Turkey. *Journal of Geodynamics.*, v.65, pp: 228-243.

Kahle, K.G., Straub, C., Reilinger, R., McClusky, S., King, R., Hurst, K., Veis, G., Kastens, K., and Cross, P., 1998. The strain field in the Eastern Mediterranean estimated by repeated GPS measurements. *Tectonophysics*, v.294, pp: 237-252.

Kaymakçı, N., 2000. Tectono-stratigraphical evolution of the Çankırı basin (Central Anatolia, Turkey). PhD Thesis. *Geologica Ultraieictina, Mededelingen van de Faculteit Aardwetenschappen, Universiteit Utrecht*, no.120, pp: 247.

Kaymakçı, N., White, S.H., and Van Dijk, P.M., 2003a. Kinematic and structural development of the Çankırı basin (Central Anatolia Turkey): a paleostress inversion study. *Tectonophysics*, v.364, pp: 85-113.

Kaymakçı, N., Duermeijer, C.E., Langereis, C., White, S.H., and Van Dijk, P.M., 2003b. Palaeomagnetic evolution of the Çankırı Basin (central Anatolia) Turkey: implications for oroclinal bending due to indentation. *Geological Magazine*, v.140, no.3, pp: 343-355.

Koçyiğit, A., 2003. Orta Anadolu'nun genel neotektonik özellikleri ve deprenselliği [General neotectonic characteristics and seismicity of central Anatolia] *Turkish Association of Petroleum Geologists Special Publication*, [in Turkish with English abstract], v.5, pp: 1-26.

Koçyiğit, A., 2005. Türkiye ve yakın çevresinin neotektonik bölümlenmesi: Güneybatı Türkiye'de neotektonik rejimin gelişim tarihçesi, çok yönlü genişleme ve deprem tehlikesi [The neotectonic subdivision of Turkey and its surroundings: the history of neotectonic regime in southwest Turkey, multidirectional extension and seismic hazard]. *Abstracts, Eskişehir Fault Zone and Seismicity of Its systems Workshop, Eskişehir, Osmangazi University, Eskişehir*, pp: 1-2.

Koçyiğit, A., and Özacar, A. A., 2003. Extensional Neotectonic Regime through the NE Edge of the Outer Isparta Angle, SW Turkey: New field and seismic data. *Turkish J. Earth Sci.*, v.12, pp: 67-90.

The Stress State of The Region around İnönü-Eskişehir active fault system (Turkey); kinematic analysis accompanied with GPS Data

- Koçyiğit A., Ünay, E., and Saraç, G., 2000. Episodic graben formation and extensional neotectonic regime in west central Anatolia and the Isparta Angle: a case study in the Akşehir-Afyon Graben, Turkey. In: Bozkurt, E., Winchester, J.A. & Piper, J.D.A. (eds), *Tectonics and Magmatism in Turkey and Surrounding Area*. Geological Society, London, Special Publications, v.173, pp: 405–421.
- Ocakoglu, F., 2007. A re-evaluation of the Eskişehir Fault Zone as a Recent extensional structure in NW Turkey. *Journal of Asian Earth Sciences* v.31, pp: 91–103.
- Ocakoglu, F., and Açikalin, S., 2009. Late Pleistocene fault-induced uplift and consequent fluvial response in Eskişehir Fault Zone, NW Anatolia. *Zeitschrift für Geomorphologie*, v.53, pp: 121–136.
- Öcal, N., 1956. Eskişehir Depremi Makro ve Mikrosismik Gözlemleri. Sismoloji Enstitü Yayınları, İstanbul Teknik Üniversitesi, İstanbul, 1959.
- Özsayın, E., and Dirik, K., 2007. Quaternary activity of the Cihanbeyli and Yeniceoba fault zones: İnönü Eskişehir fault system, Central Anatolia. *Turkish Journal of Earth Sciences* v.16, pp: 471-492.
- Reilinger, R., McClusky, S., Vernant, P., Lawrance, S., Ergintav, S., Çakmak, R., Özener, H., Kadirov, F., Guliev, I., Stepanyan, R., Nadariya, M., Hahubia, G., Mahmoud, S., Sakr, K., Arrajehi, A., Paradissis, D., Al-Aydrus, A., Prilepin, M., Guseva, T., Evren, E., Dmitrotsa, A., Filikov, S.V., Gomez, F., Alghazzi, R. and Karam, G., 2006. GPS constraints on continental deformation in the Africa-ArabiaEurasia continental collision zone and implications for the dynamics of plate interactions. *Journal Geophysical Research* B05411, doi:10.1029/2005JB004051.
- Sağlam Selçuk, A., and Gökten Y.E., 2012. Neotectonic Characteristics Of The İnönü-Eskişehir Fault System Around Kaymaz (Eskişehir) Region: Influence On The Development Of The Mahmudiye- Çifteler Emirdağ Basin. *Turkish Journal of Earth Sciences*, v.21, no.4, pp: 521-547.
- Sarıbudak, M., Sanver, M., Şengör, A.M.C., and Görür, N., 1990. Palaeomagnetic evidence for substantial rotation of the Almacık flake within the North Anatolian Fault Zone. *Geophysical Journal International*, v.102, no.3, pp: 563–568.
- Tatar, O., Piper, J.D.A., Park, R.G., and Gürsoy, H., 1995. Paleomagnetic study of block rotations in the Niksar overlap region of the North Anatolian Fault Zone, Central Turkey. *Tectonophysics*, v.244, pp: 251–66.
- Turcotte, D.L., and Schubert G., 1982. *Geodynamics: Applications of Continuum Physics to Geological Problems*, John Wiley & Sons, New York.
- Wallace, R.E., 1951. Geometry of shearing stress and relation to faulting. *Journal of Structural Geology*, v.13, pp: 118–130.

Imaging of seismic discontinuities of the upper mantle in the western Himalaya through Receiver Function analysis

Nagaraju Kanna^{*}, K.S. Prakasam, Sandeep Gupta, K. Sivaram, Sudesh Kumar, Somasish Bose and B.N.V. Prasad

CSIR-National Geophysical Research Institute, Uppal Road, Hyderabad-500007, India

^{*}Corresponding Author: nagarajugeo@gmail.com

ABSTRACT

We present image of seismic velocity discontinuities of the upper mantle in the depth range of 200 to 800 km beneath the western Himalaya from Gangetic Plain (27.5°N latitude) to Ladakh-Karakoram region (35°N latitude), an active collision zone of Indo-Eurasian plates. We use 2088 Receiver Functions calculated from the data obtained from 44 digital broadband seismological stations. The results show a sharp 410 km discontinuity in the range of ~393 – 406 km from Gangetic Plain till Indus Zangpo Suture (IZS), and disturbed (double peaked) further north of the IZS. The 660 km discontinuity shows flat and sharp discontinuity in the Gangetic Plain through Himalaya and elevated ~12 to 17 km beneath Tibetan Himalaya to the north of IZS. We observe a distinct northward dipping velocity interface to the north of IZS in the depth range of ~460 to 490 km which indicates down going Indian subducting slab reported in earlier studies. This velocity interface may be responsible for earlier 660 km phase beneath this region. Thickened mantle transition zone (~255-262 km) is observed beneath Gangetic Plain and NW Himalaya than Tibetan Himalaya due to presence of cold material within (~100° C less than normal).

Key words: Receiver Function, Common Depth Point Stacking, 410 and 660 global discontinuities, Mantle Transition Zone and Western Himalaya.

INTRODUCTION

Deep imaging of Indo-Eurasian Plates collision zone is essential to understand the evolution of the Himalaya-Tibetan belt. Majority of the previous studies reveal that the Himalaya-Tibetan belt is evolved mainly by underthrusting of the Indian crust with mantle lithosphere (e.g., Argand, 1924; Ni and Barazangi, 1984; Mattayer, 1986; Oreshin et al., 2008). Two different hypotheses exist about the nature of the collision zone. Argand (1924) proposed a flat underthrusting of Indian plate beneath Eurasian plate and later supported by many others (e.g., Ni and Barazangi, 1984; Zhou and Murphy, 2005). Another one suggests that the Indian plate, with its crust scraped off plunges steeply into the asthenosphere (e.g., Mattayer, 1986; Replumaz et al., 2004). Many seismic experiments have been carried out in the Himalaya-Tibetan belt to understand the nature of crust and upper mantle (e.g., Molnar, 1988; Hirn et al., 1995; Van der Voo et al., 1999; Zhao et al., 2001; Kind et al., 2002; Ritzwoller et al., 2002; Tilman et al., 2003; Replumaz et al., 2004; Wittlinger et al., 2004; Schulte-Pelkum et al., 2005; Kumar et al., 2006; Li et al., 2006; Priestley et al., 2006; Rai et al., 2006; Oreshin et al., 2008; Caldwell et al., 2009; Nábělek et al., 2009; Zhang et al., 2012; Devi et al., 2011; Caldwell et al., 2013). Most of these studies are carried out using the data from Tibetan side and revealed the nature of collision zone is not unique from east to west along the Himalaya-Tibetan belt and different in different parts of the Himalaya-Tibetan collision

zone. This non-uniqueness might arise from insufficient resolution of the data or complexity of the actual deep structure. However, the internal structure of the upper mantle of Indian plate still is not well understood due to data paucity from Indian side.

Several investigations have been carried out to understand nature of upper mantle using seismic discontinuities at 410 and 660 km which are most significant and best observed seismic reflectors in the mantle and associated with phase transformations within the olivine dominated peridotite system (Agee, 1993), leading to an increase in compressional and shear wave velocities across them. The 410 km discontinuity marks the transformation from olivine to α - spinel, and the 660 km discontinuity marks the transformation from β - spinel to perovskite + magnesiowüstite (Kind et al., 2002). Both the reactions are sensitive to the temperature and have Clapeyron slopes of opposite signs. The zone between these two discontinuities is called Mantle Transition Zone (MTZ). The thickness of the MTZ provides direct information about temperature within it and adjacent part of the mantle and thus constitutes an important constraint on geodynamic and geochemical models for mantle processes. The expected magnitude of the effect is about ~100° C per ~10 km thickness change of the transition zone (Kind et al., 2002). Thickened mantle transition zone is found in subduction and colder region and thinner mantle transition zone is found in oceanic plates, the region having mantle plumes and warmer region. The structure

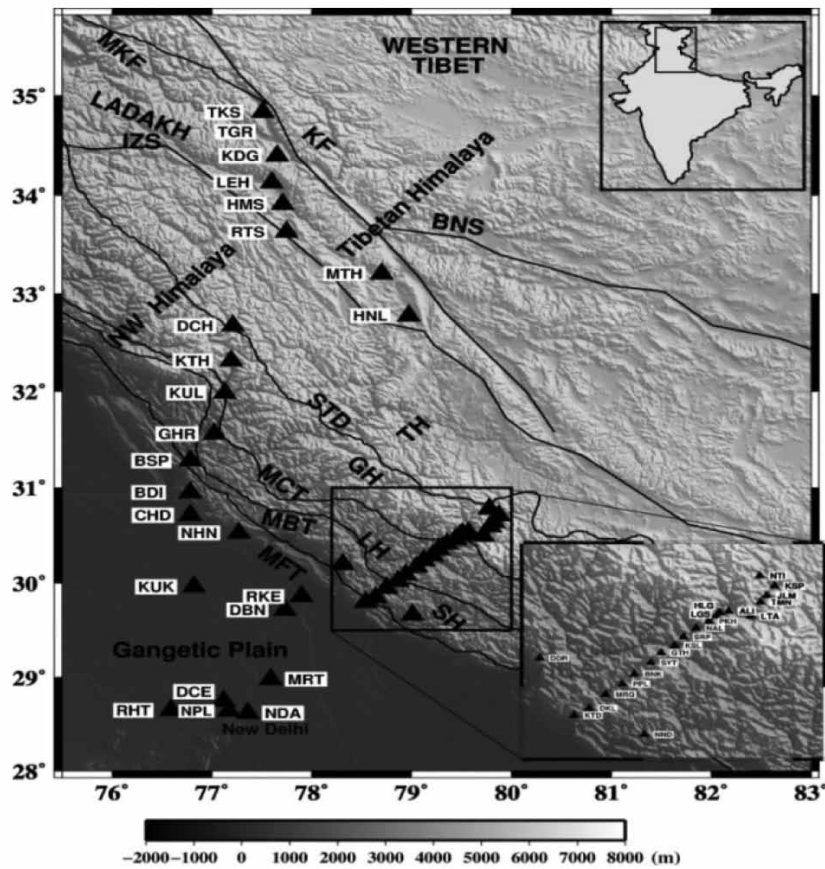


Figure 1. The tectonic map, projected over topography of the study region showing subdivisions of Gangetic Plain, NW Himalaya and Ladakh by the major thrusts with solid continuous lines from south: MFT- Main Frontal Thrust, MBT- Main Boundary Thrust, MCT- Main Central Thrust, STD- Southern Tibet Detachment, IZS- Indus Zangpo Suture, KF- Karakoram Fault, MKF- Main Karakoram Fault, BS- Bangang Nuziang Suture, SH- Sub Himalaya, LH- Lesser Himalaya, GH- Greater Himalaya, TH-Tethys Himalaya. The triangles represent the seismic stations used in this study.

of mantle transition zone provides good constraint to understand the evolution of the Himalaya-Tibetan belt.

Earlier study of mantle transition zone by Wittlinger et al., (2004) reported ~ 10 km elevated 410 km discontinuity beneath the southern part of western Tibet due to the presence of colder material ($\sim 100^\circ$ C less temperature), whereas, Kind et al., (2002) reported late arrival of 410 and 660 discontinuities beneath central Tibet due to presence of hotter material (more than $\sim 300^\circ$ C temperature).

A study of MTZ for whole of India, from southern tip of India to Karakoram, was carried out by Rai et al., (2009) using 1957 Receiver Functions of Gaussian width 0.6 from 54 broadband seismographs operated during 1999-2004 with depth interval of 5 km using the Receiver Functions and presented a ~ 10 km thickened mantle transition zone in the Gangetic Plain than India. The number of stations was limited to 16 for the Himalayan region. Singh et al., (2015) present the review of the crust and upper mantle structure from the Indian subcontinent to Himalaya. With large data available for the Western Himalaya from the

seismic stations operated during 2005-2008 and 2011-2012, we study the western Himalaya region in more detail.

Geological Settings

The long ~ 2400 km Himalaya-Tibetan belt is formed by underthrusting of the Indian plate that continues to push the Eurasian plate since ~ 50 Ma (Patriat and Achache, 1984). During this process, several fault systems have been created from south to north, as: Main Frontal Thrust (MFT), Main Boundary Thrust (MBT), Main Central Thrust (MCT), South Tibetan Detachment (STD), Indus Zangpo Suture (IZS), Main Karakoram Fault (MKF), Karakoram Fault (KF), and Bangang Nuziang Suture (BS). The present study area is the western extremity of the Himalaya-Tibet orogen and comprises of three major structural blocks, the Tibetan Himalaya and NW Himalaya separated by the Southern IZS and the Gangetic Plain to the south of MFT. The Tibetan block consists of Ladakh and Karakoram to the north of IZS. To the south of IZS

lies the Tethys Himalaya with the STD as the southern boundary. To the south of the STD lies the Himalayan sequence, consisting of the Higher (or Greater) Himalaya, Lesser (or Lower) Himalaya and Sub (or Outer) Himalaya, which are bounded between the STD - MCT, MCT - MBT and MBT - MFT thrust zones, respectively. Figure 1 shows the study region and major geological boundaries with the topography of the region. Its evolution and internal structure has been subject of numerous geological and geophysical studies (e.g., Molnar, 1988; Klemperer, 2006).

Data

In the present study, we use data of 44 broadband seismological stations deployed in the western Himalaya in different periods. Out of 44 stations, 15 stations are operated during 2002 to 2003 in the NW Himalaya and Ladakh (Rai et al., 2006), 10 stations are operated during 2005 to 2008 in the Gangetic Plain (Borah et al., 2015) and remaining 19 stations are operated during 2005 to 2008 and 2011 to 2012 in the Kumaon-Garhwal Himalaya (Mahesh et al., 2013). The stations locations are shown in Figure 1.

Each station consists of a Guralp CMG-3T or 3ESP sensor with time tagging using Global Position System (GPS) and a refraction technology data logger continuously recording waveforms at 20 samples per second for the stations in the NW Himalaya and Ladakh and 50 samples per second for the other stations. For consistency, the waveforms are decimated to 20 samples per second. Earlier this data set is used to map the Moho discontinuity of the study region (Rai et al., 2006; Caldwell et al., 2013; Oreshin et al., 2008). The inferred Moho depth varies from ~40 to 75 km from the Delhi region to Ladakh in the Tibetan Himalaya.

METHODOLOGY

We use the well known seismological technique of the Receiver Function to map the seismic discontinuities in the upper mantle. This technique utilizes the waves converted (P to S) at velocity discontinuities to study the nature of the Earth's structure directly beneath the receiver. The arrival time and amplitude of the converted phase provide us the information related to depth location, width and possible causal mechanisms of the discontinuity. We select good teleseismic earthquakes having high signal to noise ratio (S/N) with magnitude greater than 5.5 and within the distance range of 30 to 90°. Further, we calculate the Receiver Functions at each station using time domain deconvolution method of Ligorja and Ammon (1999). Since our interest is to map the discontinuities in the deep depth in the upper mantle (200 to 800 km), we filter the

waveforms in a low frequency band with a Gaussian width of 1.0 corresponding to a frequency of less than 0.5 Hz. The depth resolution for Receiver Function at Gaussian width factor of 1.0 is ~1.9 km (Sheriff and Geldart, 1995). We carefully examine the Receiver Functions at each station and finally select 2088 Receiver functions with good Signal to Noise ratio for our analysis.

We use "Common Depth Point" (CDP) stacking technique of Dueker and Sheehan (1997) to map the 3-D structure of the upper mantle. The following steps are involved in the CDP stacking approach,

- i. Computation of geographical locations of the piercing points of all P to S conversions for each source-receiver pair at 2 km depth increments from 200 to 800 km, using TauP toolkit (Crotwell et al., 1999) with respect to a reference model. The crustal part of this reference model is obtained from the Receiver Function modeling of each station (unpublished data) and further deep in the model, we add the IASP91 velocity model (Kennet and Engdahl, 1991).
- ii. Calculation of the travel times of P to S converted phase (T_{pds}) from various depths using the formula,

$$T_{pds} = \int_{-d}^0 \left(\sqrt{V_S(z)^{-2} - p^2} - \sqrt{V_P(z)^{-2} - p^2} \right) dz \quad (1)$$

Where p is the rayparameter for P wave, d represents the depth of the discontinuity and $V_P(z)$ and $V_S(z)$ are the P and S wave velocities at depth z .

- iii. Dividing the study area into rectangular blocks of fixed width as 0.5° in latitude and varying length 4-6° in longitude depending on their piercing points at each depth. Piercing point is the location at depth, where the P-to-S conversion occurs. To produce the depth image of discontinuity, the amplitudes from individual receiver functions piercing a particular area are summed (stacked) using:

$$A(d) = \frac{1}{N} \sum_{i=1}^N A_i(T_{pds}) \quad (2)$$

Where $A(d)$ is the stacking amplitude for a candidate discontinuity at depth d , N is the number of receiver function piercing particular depth d . T_{pds} is the Pds move out time of the corresponding receiver function for a discontinuity computed using the equation (1). $A_i(T_{pds})$ is amplitude of the i^{th} receiver function.

We use bootstrap resampling technique (Efron and Tibshirani, 1986) to ascertain the uncertainties that results from variation and/or noise in the Receiver Functions. We select 95% of the piercing points in rectangle box and run the 50 iterations of the CDP stack with group of the points randomly selected from the full pool (with duplication, so that the number of points for each iteration is same as the number of unique points). The mean depth of discontinuity

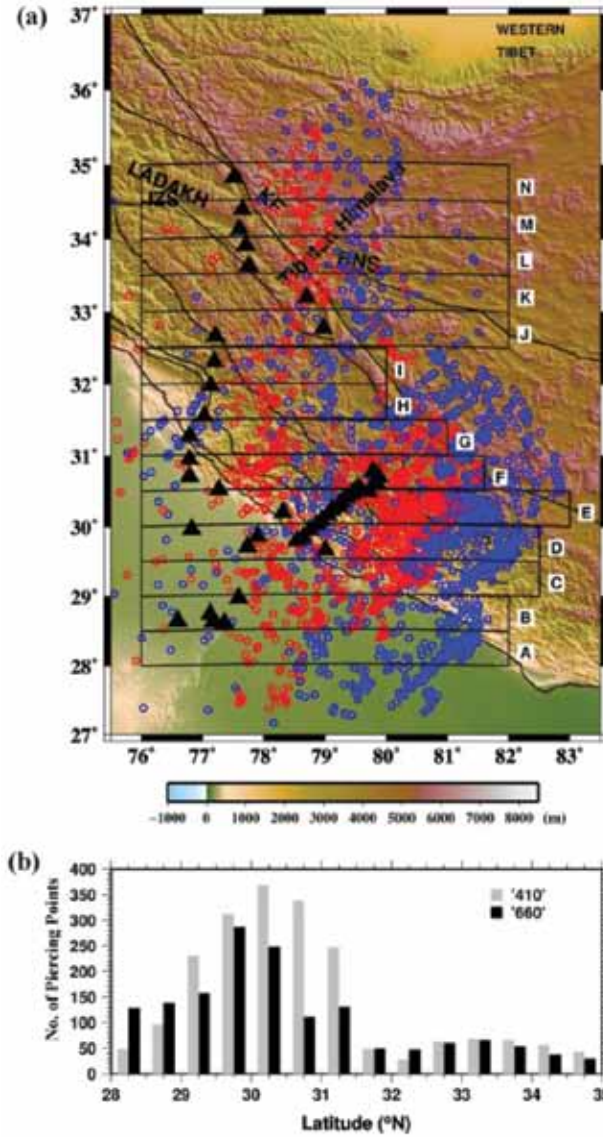


Figure 2. (a) Distribution of piercing points of P to S converted phases at 410 (red circles) and 660 km (blue circles) depth. Triangles represent seismic stations. Rectangular boxes (A to N) show the node for which Receiver Functions are stacked and present as its mid-point. The geological structures are same as Figure 1. (b) Number of piercing points of 410 (gray color) and 660 (black) km discontinuities used for each block.

on each rectangle box from those iterations is calculated using the following formula,

$$\bar{D} = \frac{1}{N} \sum_{i=1}^N D_i \quad (3)$$

where N is the number of bootstrap, D_i is the depth of the 410 and 660 km discontinuities corresponding to maximum stacking amplitude in the depth ranges of 410 ± 25 and 660 ± 25 km from the i^{th} bootstrap. Standard deviation of the mean depths, σ_{410} and σ_{660} are calculated using:

$$\sigma_d = \frac{1}{N-1} \sum_{i=1}^N (D_i - \bar{D})^2 \quad (4)$$

where d is the 410 or 660 km discontinuity. Further, the mantle transition zone thickness is estimated by depth differences of the 660 km and the 410 km discontinuity in the rectangular block. The standard deviation for the mantle transition zone (MTZ) thickness is:

$$\sigma_{\text{MTZ}} = \sqrt{\sigma_{410}^2 + \sigma_{660}^2} \quad (5)$$

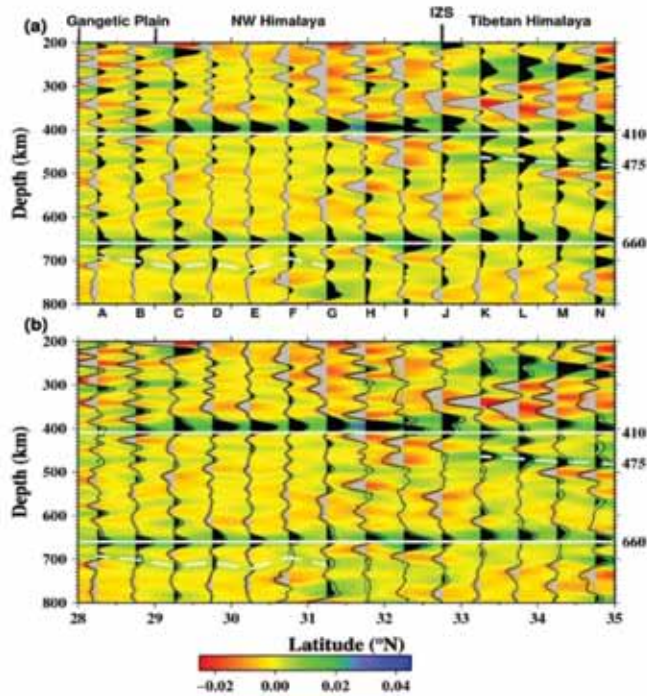


Figure 3. The stacked Receiver Functions from the Gangetic Plain to Ladakh-Karakoram i.e in the Tibetan Himalaya without bootstrap technique (a) and with bootstrap resampling (b). The color scale indicates size of the amplitude.

RESULTS AND DISCUSSION

The geographical distribution of piercing points at P410s km (red circles) and P660s km (blue circles) are illustrated in Figure 2a and the number of points in each rectangular block corresponding to mean latitude is shown in Figure 2b. We reduce the length of four blocks (F to I), to the south of the Indus Zangpo Suture, to avoid the piercing points at P660s falling in Tibetan Himalaya (see Figure 2b). We have fairly large number of piercing points in the NW Himalaya region and moderately good number of points for the Tibetan Himalaya region. Figure 3 shows the stacked Receiver Functions with depth, without bootstrap procedure (Figure 3a) and with bootstrap procedure (Figure 3b) at each sampled block of 0.5° in latitude. In both the cases the main features are comparable. Figure 3b shows the smooth image and we use it for further discussion/interpretation. The variation of representative depths of 410 and 660 discontinuities and the thickness of mantle transition zone are shown in Figure 4 with error bars.

410 km Discontinuity

In the Gangetic Plain the 410 discontinuity is observed at ~ 406 km being gradually uplifted to ~ 393 km in the NW Himalaya and reaches to ~ 402 km to the south of Indus

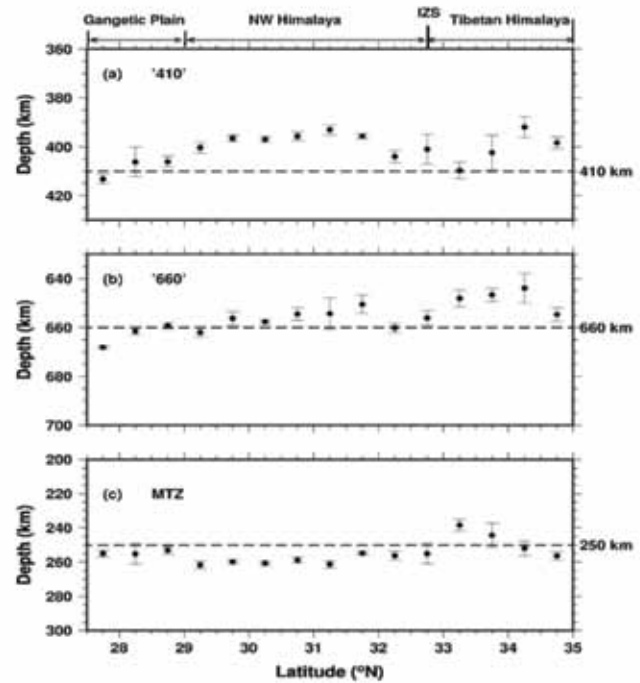


Figure 4. Depth of (a) 410 km discontinuity, (b) 660 km discontinuity and (c) thickness of the mantle transition zone calculated at each block shown in Figure 2.

Zangpo Suture (Figure 4a). However, it shows complex nature (nearly double peak for I, J, L, M and N; Figure 3b) at Indus Zangpo Suture and further north where it reaches to ~ 392 - 400 km in Ladakh, i.e Tibetan Himalaya. This complex signature is observed in the data without bootstrap as well (Figure 3a) therefore, we assume that the 410 discontinuity is of complex nature beneath this region. Similar observation is reported by Wittlinger et al., (2004) in the southern part of western Tibet to the north of our study region. The observed systematic elevation of the 410 discontinuity beneath the NW Himalaya may be the presence of thickened high velocity layer at shallow mantle in this region, reported in the earlier studies (e.g., Ritzwoller et al., 2002; Priestley et al., 2006; Oreshin et al., 2008). However this discontinuity appears slightly deeper beneath northern Tibet and with possible presence of hotter material in the upper mantle (Kind et al., 2002; Wittlinger et al., 2004).

475 km Discontinuity

A significant sharp northward dipping high velocity interface in the depth range of 460-490 km is observed to the north of Indus Zangpo Suture (Figure 3b), beneath the Tibetan Himalaya, which is not observed beneath Gangetic plains and Himalaya. In the Himalaya-Tibetan belt, the

crustal thickness varies between 70 and 80 km (Rai et al., 2006). The multiples with respect to the Moho conversion (around 8 – 10 s) can be observed around 25 to 30 s, which generally corresponds to ~250-300 km depth. The presence of multiples in the depth range of 460 to 490 km (i.e., 46 – 49 s) requires a strong conversion in the Receiver Functions in the time range of ~13 to 17 s. Although, we observe some peaks in this time range, however these peaks are weak, rather than strong amplitudes, and thus can be the multiples of mid-crustal conversions (~4.5 to 6 s) present in this complex Himalaya-Tibet region. Further, this depth range is shallower than ~520 km global discontinuity. Since this depth range is shallower than the 520 km global discontinuity and greater than shallower multiples of shallow depth conversions, it may be interpreted as relic of the subducted oceanic slab as observed in the tomographic images (Ritzwoller et al., 2002; Priestley et al., 2006) and the sinking slab may be responsible for the disturbed 410 km discontinuity present in this region. Similar observation was reported by Rai et al., (2009) in the Ladakh-Karakoram region and Wittlinger et al., (2004) in the southern part of western Tibet, whereas it is not seen in the central Tibet (Kind et al., 2002).

660 km Discontinuity

We observe a sharp 660 km discontinuity throughout the study region (Figure 3b) instead of complex 660 km discontinuity as reported by Rai et al., (2009). The depth of this discontinuity beneath Gangetic Plain is observed around ~660 km, whereas, it varies from ~650 to 662 km beneath the NW Himalaya and elevated to ~644 to 654 km in the Tibetan Himalaya, to the north of Indus Zangpo Suture (Figure 4b). The uplift of 660 km in the Tibetan Himalaya may be possibly due to the presence high velocity ~475 km discontinuity. A weak positive discontinuity at a depth of 670-700 km is observed from Gangetic plain to Indus Zangpo Suture but the consistency is missing in the Tibetan Himalaya (Figure 3b). The discontinuity at 655-661 km is a result of phase change from garnet to ilmenite and the discontinuity at 670-700 km could be the result of transformation from ilmenite to pervoskite (Rai et al., 2009).

Mantle Transition Zone

Our results show that the mantle transition zone thickness is at ~254 km for the Gangetic Plain, whereas it varies in the range of ~255 to 262 km beneath the NW Himalaya (Figure 4c). It decreases to ~239-244 km immediately to the north of Indus Zangpo Suture and increases to 251-256 km further north beneath the Tibetan Himalaya (Figure 4c). We observe the mantle transition zone thickness is more beneath the Gangetic Plain and NW Himalaya than the

Tibetan Himalaya. The thickened mantle transition zone in Gangetic plain and Himalaya is suggestive of presence of colder material than the Tibetan Himalaya. Also similar observation is presented using travel time residuals by Oreshin et al., (2008). Rai et al., (2009) also reported ~10 km more thickened mantle transition zone in the Gangetic Plain compared to India.

CONCLUSIONS

In the present study, we map the mantle transition zone of the western Himalaya. These values are comparable with the earlier results of mantle transition zone study of the Indian subcontinent, from Kanyakumari to Karakoram (Rai et al., 2009). They used 1957 receiver functions with Gaussian width 0.6 and stacked at bin latitude of 1.0° which facilitated a smooth picture of the study region. We adopted the same methodology of Rai et al., (2009) using 2088 Receiver Functions of Gaussian width 1.0 with a stacked bin of 0.5° latitude, thus obtaining reasonably constrained values. Our results show a sharp and gradually elevated 410 discontinuity from Gangetic Plain to the NW Himalaya upto the Indus Zangpo Suture, further complex in the Tibetan Himalaya. We also observed a sharp 660 km discontinuity in the entire study region and uplifted in the Tibetan Himalaya. The elevated 410 km discontinuity may be underthrusting of the Indian lithosphere slab in the shallower mantle (upto a depth of 300 km) as seen in the tomographic images in the study region. The observed northward dipping high velocity interface at ~475 km may be the signature of broken Tethys slab and may be responsible for the complex (double peak) 410 and elevated 660 km discontinuities in the Tibetan Himalaya (Rai et al., 2009). The thickened mantle transition zone in the NW Himalaya by about ~12 km than Tibetan Himalaya indicates a colder NW Himalaya by about ~100 C (Oreshin et al., 2008). A weak positive discontinuity at a depth range of 670-700 km is observed from Ganges basin to NW Himalaya but the consistency is missing further in the Tibetan Himalaya.

ACKNOWLEDGEMENTS

The field program was supported by Department of Science & Technology, Govt. of India. We are very thankful to the members of Seismic Tomography group of CSIR-NGRI, for their support during seismological stations deployment. NK is supported by research fellowship from the Ministry of Social and Justice Empowerment, Govt. of India. Figures are made with Generic Mapping Tools. Support from CSIR Research projects MLP-6505-28(SKG) and INDEX-0204 are acknowledged. Authors are also thankful to Prof. B.V.S. Murthy and Chief Editor for useful suggestions and appropriate editing of the manuscript.

Compliance with ethical standards

The authors declare that they have no conflict of interest and adhere to copyright norms.

REFERENCES

- Agee, C., 1993. Petrology of the mantle transition zone, *Ann. Rev. Earth Planet. Sci.*, v.21, pp: 19-41.
- Argand, E., 1924. La tectonique de l'Asie, *Int. Geol. Cong. Resp. Sess.*, v.13, pp: 170-372.
- Borah, K., Nagaraju, K., Rai, S.S., and Prakasam, K.S., 2015. Sediment thickness beneath the Indo-Gangetic Plain and Siwalik Himalaya inferred from Receiver Function, *J. Asian Earth Sci.*, v.99, pp: 41-56.
- Caldwell, W.B., Klemperer, S.L., Rai, S.S., and Lawrence, J.F., 2009. Partial melt in the upper-middle crust of the northwest Himalaya revealed by Rayleigh wave dispersion, *Tectonophysics*, v.477, pp: 58-65.
- Caldwell, W.B., Klemperer, S.L., Lawrence, J.F., Rai, S.S., and Ashish, 2013. Characterizing the Main Himalayan Thrust in the Garhwal Himalaya, India with receiver function CCP stacking, *Earth Planet. Sci. Lett.*, v.367, pp: 15-27.
- Crotwell, H.P., Owens, T.J., and Ritsema, J., 1999. The TauP Toolkit: Flexible seismic travel time and raypath utilities, *Seismol. Res. Lett.*, v.70, pp: 154-170.
- Devi, E.U., Kumar, P., and Kumar, M.R., 2011. Imaging the Indian lithosphere beneath the eastern Himalayan region, *Geophys. J. Int.*, v.187, pp: 631-641.
- Dueker, K.G., and Sheehan, A.F., 1997. Mantle discontinuity structure from midpoint stacks of converted P to S waves across the Yellowstone hotspot track, *J. Geophys. Res.*, v.102, pp: 8313-8327.
- Efron, B., and Tibshirani, R., 1986. Statistical data analysis in the computer age, *Sci.*, v.253, pp: 390-395.
- Hirn, A., Jiang, M., Sapin, M., Diaz, J., Nercessian, A., Lu, Q.T., Lepine, J.C., Shi, D.N., Sachpazi, M., Pandey, M.R., Ma, K., and Gallart, J., 1995. Seismic anisotropy as an indicator of mantle flow beneath the Himalayas and Tibet, *Nature*, v.375, pp: 571-574.
- Kennet, B., and Engdahl, E., 1991. Travel times for global earth location and phase identification, *Geophys. J. int.*, v.105, pp: 429-465.
- Kind, R., Yuan, X., Saul, J., Nelson, D., Sobolev, S.V., Mechie, J., Zhao, W., Kosarev, G., Ni, J., Achauer, U., and Jiang, M., 2002. Seismic images of crust and upper mantle beneath Tibet: evidence for Eurasian plate subduction, *Sci.*, v.298, pp: 1219-1221.
- Klemperer, S.L., 2006. Crustal flow in Tibet: geophysical evidence for the physical state of Tibetan lithosphere and inferred patterns of active flow, in *channel Flow, Ductile Extrusion and Exhumation in Continental Collision Zones*, *Geol. Soc. Lond. special publications*, v.268, pp: 39-70.
- Kumar, P., Yuan, X., Kind, R., and Ni, J., 2006. Imaging the colliding India and Asian lithospheric plates beneath Tibet, *J. Geophys. Res.*, doi: 10.1111/j.1365-246x.2008.03777x., v.111.
- Li, Q., Van Der Hilst, R.D., and Toksoz, M.N., 2006. Constraining P velocity variations in the upper mantle beneath Southeast Asia, *Phys. Earth Planet. Inter.*, v.154, pp: 180-195.
- Ligorria, J.P., and Ammon, C., 1999. Iterative deconvolution and receiver-function estimation, *Bull. Seismol. Soc. Am.*, v.89, pp: 1395-1400.
- Mahesh, P., Rai, S.S., Sivaram, K., Ajay, P., Sandeep, G., Sarma, P.R., and Gaur, V.K., 2013. One-Dimensional reference velocity model and precise locations of earthquake Hypocenters in the Kumaon-Garhwal Himalaya, *Bull. Seismol. Soc. Am.*, v.103, pp: 328-339.
- Mattayer, M., 1986. Intracontinental subduction, crust-mantle decollement and crustal stacking wedge in the Himalayas and other collisional belts, In: Coward, M.P., Ries, A.C. (Eds.), *Collision Tectonics*, *Geol. Soc. Lond. Spec. Pub.*, v.19, pp: 37-50.
- Molnar, P., 1988. A review of geophysical constraints on the deep structure of the Tibetan Plateau, the Himalaya and the Karakoram and their tectonic implications, *Phil. Trans. R. Soc. Lond. Ser.*, v.326, pp: 33-88.
- Nábělek, J., Hetenyi, G., Vergne, J., Sapkota, S., Kafle, B., Jiang, M., Su, H., Chen, J., Huang, B., and the Hi-CLIMB Team, 2009. Underplating in the Himalaya-Tibet collision zone revealed by the Hi-CLIMB experiment, *Sci.*, v.325, pp: 1371-1374.
- Ni, J., and Barazangi, M., 1984. Seismotectonics of the Himalayan collision zone: geometry of the underthrusting Indian plate beneath the Himalaya, *J. Geophys. Res.*, v.89, pp: 1147-1163.
- Oreshin, S.S., Kiiselev, S., Vinnik, L., Prakasam, K.S., Rai, S.S., Makeyeva, L., and Savvin, Y., 2008. Crust and mantle beneath western Himalaya, Ladakh and western Tibet from integrated seismic data, *Earth Planet. Sci. Lett.*, v.271, pp: 75-87.
- Patriat, P., and Achache, J., 1984. India-Asia collision chronology has implications for crustal shortening and driving mechanism of plates, *Nature*, v.311, pp:615-621.
- Priestley, K., Dabayle, E., McKenzie, D., and Pilidou, S., 2006. Upper mantle structure of eastern Asia from multimode surface waveform tomography, *J. Geophys. Res.*, doi:10.1029/2005JB004082., v.111.
- Rai, S.S., Priestley, K., Gaur, V.K., Mitra, S., Singh, M.P., and Searle, M.P., 2006. Configuration of the Indian Moho beneath the NW Himalaya and Ladakh, *Geophys. Res. Lett.*, doi: 10.1029/2006GL026076., v.33.
- Rai, S.S., Prakasam, K.S., and Gaur, V.K., 2009. Seismic imaging of the mantle discontinuities beneath India: from Archean cratons to Himalayan subduction zone, in Gupta, A., Dasgupta, S. (Eds.), *Physics and chemistry of the Earth Interior*, Springer New York, pp: 153-161.
- Replumaz, A., Karson, H., Van Der Hilst, R.D., Besse, J., and Tappanier, P., 2004. 4-D evolution of SE Asia's mantle from

Imaging of seismic discontinuities of the upper mantle in the western Himalaya through Receiver Function analysis

- geological reconstruction and seismic tomography, *Earth Planet. Sci. Lett.*, v.221, pp: 103-115.
- Ritzwoller, M.H., Shapiro, N.M., Barmin, M.P., and Levshin, A.L., 2002. Global surface wave diffraction tomography, *J. Geophys. Res.*, doi:10.1029/2002JB001777., v.107.
- Schulte-Pelkum, V., Monsalve, G., Sheehan, A., Pandey, M.R., Sapkota, S., Bilham, R., and Wu, F., 2005. Imaging the Indian subcontinent beneath the Himalaya, *Nature*, v.435, pp: 1222-1225.
- Sheriff, R.E., and Geldart, L.P., 1995. *Exploration seismology; History, Theory and Data Acquisition*, Cambridge University Press, Cambridge, pp: 592+ xv.
- Singh, A., Singh, C., and Kennet, B.L.N., 2015. A review of crust and upper mantle structure beneath the India subcontinent, *Tectonophysics*, v.644, pp: 1-21.
- Tilman, E, Ni, J., and Team, I.I.S., 2003. Seismic imaging of the Downwelling Indian lithosphere beneath central Tibet, *Sci.*, v.300, pp: 1424-1427.
- Van der Voo, R., Spakman, W., and Bijwaard, H., 1999. Tethyan subducted slab under India, *Earth Planet. Sci. Lett.*, v.171, pp: 7-20.
- Wittlinger, G., Vergne, J., Tapponier, P., Farra, V., Poupinet, G., Jiang, M., Su, H, Herquel, G., and Paul, A., 2004. Teleseismic imaging of subducting lithosphere and Moho offsets beneath western Tibet, *Earth Planet. Sci. Lett.*, v.221, pp: 117-130.
- Zhang, H., Zhao, Z., and Xu, Q., 2012. Crustal and upper mantle velocity structure beneath Central Tibet by P-wave teleseismic tomography, *Geophys. J. Int.*, v.190, pp: 1325-1334.
- Zhao, W., Mechie, J., Brown, L.D., Guo, J., Haines, S., Heam, T., Kemplerer, S.L., Ma, Y.S., Meissner, R., Nelson, K.D., Ni, J., Pananont, P., Rapine, R., Ross, A., and Saul, J., 2001. Crustal structure of central Tibet as evidence from project INDEPTH wide-angle seismic data, *Geophys. J. Int.*, v.145, pp: 486-498.
- Zhou, H.W., and Murphy, M., 2005. Tomographic evidence for whole scale underthrusting of India beneath the entire Tibetan plateau, *J. Asian Earth Sci.*, v.25, pp: 445-457.

Microscopic Evidences for the Impact Origin of Ramgarh Structure, Rajasthan, India

Satyanarayan Rana* and Vinod Agrawal

Department of Geology, Faculty of Earth Sciences, Mohanlal Sukhadia University, Udaipur 313001, India

*Corresponding Author: snrana1984@gmail.com

ABSTRACT

An impact crater on the Earth is a depression that is formed by the high velocity impact of an extraterrestrial object like meteorite. Impacts produced on Earth are highly exposed to obliteration by various geological agents. This demands the use of certain diagnostic criteria for the identification and confirmation of impact structures on Earth, the most important of these are crater morphology, geophysical anomalies, evidences for shock metamorphism and the presence of meteoritic material. Microscopic features like Planar deformation features (PDFs) and Planar fractures (PFs) in quartz grains are uniquely diagnostic of an impact event and are the robust evidences of the shock metamorphism due to an impact. A crater-like structure at Ramgarh, Rajasthan, India has been a contentious subject amongst the geoscientists for its origin. Evidences presented for the impact origin of Ramgarh structure so far are insufficient, equivocal and controversial. In this communication, we have reported the microscopic shock alteration evidences from the Ramgarh structure in the form of Planar Fractures and Planar Deformation Features in quartz grains.

Key words: Impact craters, Ramgarh structure, Shock Metamorphism and Planar Deformation Features.

INTRODUCTION

Studies by geologists on the impact structures led to an understanding that the collision of extra-terrestrial objects have significantly modified the Earth's surface, causing disturbances in its crust, and changed its geological history (Shoemaker 1977; Grieve, 1987, 1991; Nicolaysen and Reimold, 1990). However, Earth suffers from active erosion, volcanic resurfacing and tectonic activity, which tend to erase the impact features from the rock record. Therefore, the unambiguous identification of impact structures require their recognition based on certain diagnostic shock-metamorphic effects that are uniquely indicative of an impact (Grieve, 1991; Stöffler and Langenhorst, 1994; Grieve, 1998; Montanari and Koeberl, 2000; Koeberl, 2002; Langenhorst, 2002; Therriault et al., 2002). Shock-metamorphic effects have been critical to the identification of terrestrial impact structures because of their uniqueness and ease of identification. Ramgarh Structure in western India is a crater like feature impressed on the Neoproterozoic sediments of Vindhyan Supergroup. The origin of this spectacular feature has been a debated subject since its inception in the Geological literature and different workers have proposed their respective views towards its possible origin. Based on detailed geological mapping and structural analysis of the area, the structure was considered as a product of structural or tectonic deformation and named as Ramgarh Dome or oblong anticline (Prasad, 1984; Ramasamy, 1987). However, majority of the workers stand with meteoritic impact theory for its origin based on its near circular morphology, possible shatter cones, IRS-IA Image analysis, shear fracturing,

granulation, anomalous birefringence in quartz grains, closely spaced-fractures and multiple-joint striated surfaces in quartzites, presence of Ni-Fe rich rounded micro glassy objects, glassy (microtektites) spherules, severely fractured quartz grains with corroded margins and microprobe analysis of magnetic spherules (Balasundaram and Dube, 1973; Crawford, 1972; Ahmad et al., 1974; Murali and Lulla, 1992; Master and Pandit, 1999; Sisodia et al., 2008; Mishra et al., 2008). Though, Ramgarh structure closely resembles the other terrestrial impact craters, the evidences presented so far for its impact origin are scanty, equivocal, non-diagnostic and controversial. In the present paper, we have reported microscopic planar features in quartz grains resulted due shock metamorphism in the study area, an evidence supporting the impact origin of the Ramgarh structure.

Study Area

Ramgarh Structure (25° 20' N: 76° 37' E) is situated in Baran district of Rajasthan, 110 kms ENE of Kota city (Figure 1). The structure resembles Meteor crater of Arizona, USA in terms of shape and is obvious in topographic maps and satellite imageries (Sisodia et al., 2003) (Figure 2). This circular structure covers an area of 16 Sq.km with a diameter of about 4 km and rising about 250 m above the ground level. The Ramgarh structure is located in the central part of the Neoproterozoic Vindhyan basin of Rajasthan. On a regional scale the area in and around Ramgarh structure comprises the rocks belonging to Bhandar Group of Vindhyan Supergroup (Ramasamy, 1987; Sharma, 1973) (Figure 3). The outer flanks of the

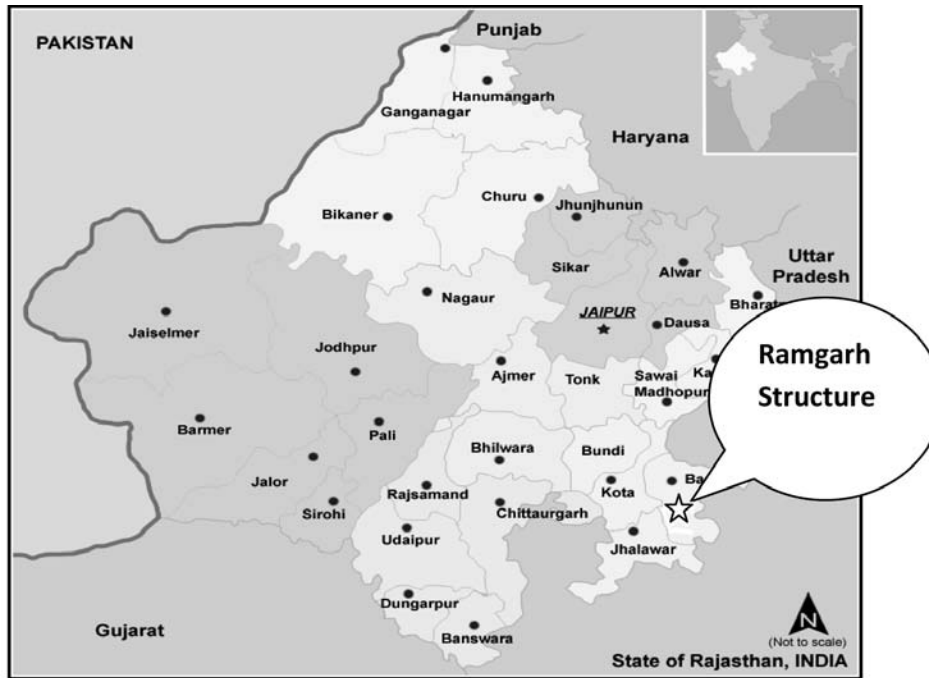


Figure 1. Location of Ramgarh structure (marked as Star) in the detailed map of the Rajasthan.



Figure 2. (a) Ramgarh Structure can be seen from a distance of 5-7 Km, (b) Google earth image of Ramgarh structure.

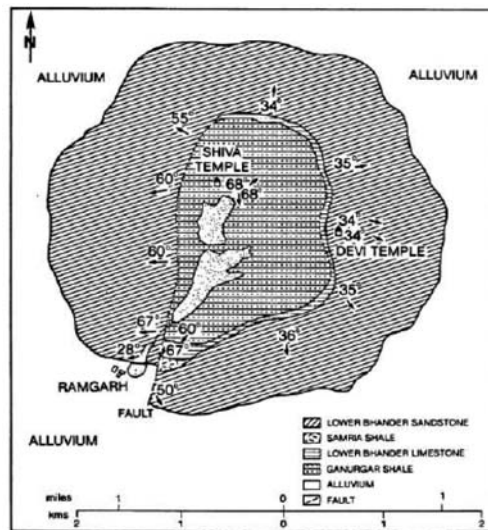


Figure 3. Geological map of Ramgarh Structure (Sharma, 1973).

Table 1. Shock-produced diagnostic deformation effects (after Montanari and Koeberl, 2000).

Pressure (GPa)	Features	Target Characteristics	Remarks
2-45	Shatter Cones	Best developed in homogeneous fine-grained,	Conical fracture surfaces with subordinate striations radiating from a focal point.
5-45	Planar Fractures (PFs) and Planar Deformation Features (PDFs)	found in many rock-forming minerals (e.g., quartz, feldspar, olivine and Zircon)	Sets of extremely straight, sharply defined parallel lamellae; may be in multiple sets with specific crystallographic orientations.
30-40	Diaplectic glass	Most important in quartz and feldspar (e.g., maskelynite from plagioclase)	Isotropization through solid-state transformation under preservation of crystal habit as well as primary defects and sometimes planar features
15-20	High-pressure Polymorphs	Quartz polymorphs most common: coesite, Stishovite.	Recognizable by crystal parameters, confirmed usually with XRD or NMR.
>15	Impact diamonds	From carbon (graphite) present in target rocks	Usually very small but occasionally up to mm-size; inherits graphite crystal shape.
45-70	Mineral Melts	Rock-forming minerals	Impact melts are either glassy (fusion glasses) or crystalline; of macroscopically homogeneous, but microscopically often heterogeneous composition.

rim are constituted of sandstone with quaquaversal dips. The inner flanks of the rim have relatively steeper slope (Sisodia et al., 2008).

METHODS

Circular geological structures of regional extent like that one present at Ramgarh, which is located in geological setting with no other probable mechanism for creating near-circular feature may be the result of a meteoritic impact and hence may be an impact crater. Only the presence of diagnostic shock metamorphic effects is considered as an unambiguous evidence for an impact event (Table 1). In complex craters, the central uplift usually consists of dense basement rocks and contains severely shocked material and this region should be examined in detail for the presence shock metamorphic signatures that confirm an impact event. This uplift is often more resistant to erosion than the remaining crater rocks, and thus possess the higher potential of preserving the shocked material (Grieve and Pilkington, 1996). In the present study diagnostic microscopic features in the form of planar Fractures (PFs) and Planar Deformation Features (PDFs) developed due to shock metamorphism are reported from the Ramgarh structure.

Shock waves are capable of generating a variety of unusual microscopic planar features in common rock forming minerals like quartz and feldspar. These features typically occur as sets of parallel deformation planes within individual crystals. The recognition and interpretation of these features, particularly those in quartz has played a crucial role in identifying new impact structures.

Distinctive planar features in quartz have been one of the most widely applied criteria for recognizing impact structures (Engelhardt and Bertsch, 1969; Stöffler and Langenhorst, 1994; Grieve et al., 1996). Its abundance in crustal rocks, stability over long periods of geologic time, resistance to alteration by weathering makes it an ideal mineral for the same. It is an optically simple (uniaxial) mineral to study and to analyze on the Universal Stage.

Planar fractures are parallel sets of multiple planar cracks or cleavage like features in the quartz grain developed by the low level shock waves (< 10 GPa) which generally do not cross the grain boundaries. They are relatively widely spaced (> 5–20 μm) and thin (typically 3–10 μm), but thicker than PDFs (>20 μm). Planar deformation features (PDFs) are the distinctive and long-studied shock produced microstructures. These PFs, which appear identical to cleavage, occur typically in multiple sets, usually 2–3 sets per grain (French and Koeberl, 2010) (Figure 4). Extensive geological and experimental studies have established that these features develop at pressures of approximately 10–30 GPa, far higher than pressures produced by non-impact processes in crustal rocks.

In contrast to planar fractures, with which they may occur, PDFs are not open cracks. Instead, they occur as multiple sets of closed, extremely narrow, parallel planar regions. Individual PDFs are both narrow (typically <2–3 μm) and more closely spaced (typically 2–10 μm) than planar fractures (Engelhardt and Bertsch, 1969; Stöffler and Langenhorst, 1994; Langenhorst, 2002). Though, earlier workers have described Planar Deformation Fractures (PDFs) in quartz grains from the Ramgarh structure, but their authenticity is still doubtful.

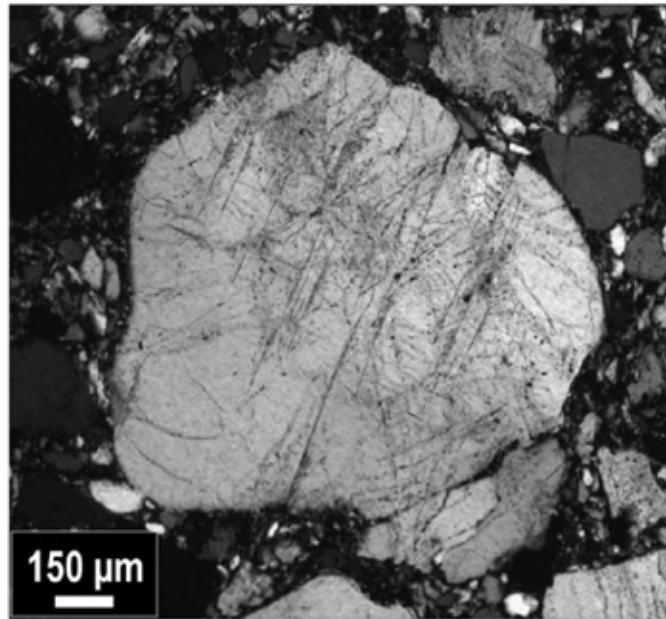


Figure 4. Planar fractures (PFs) developed in a brecciated quartzite from the central uplift of the Aorunga (Chad) impact structure. (French and Koeberl, 2010).

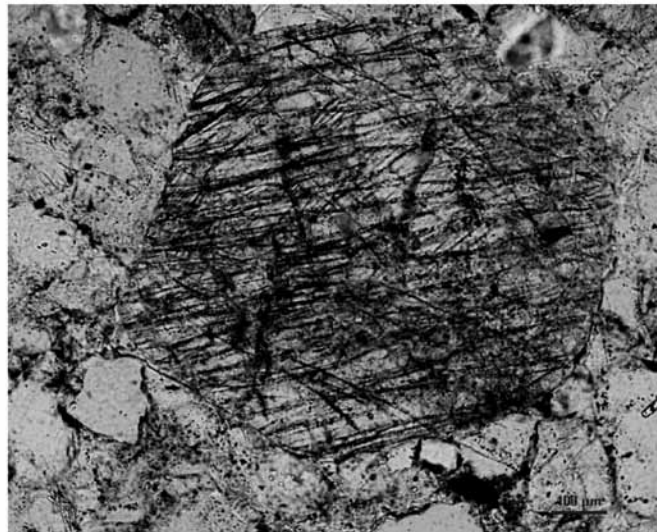


Figure 5. Photomicrograph of Planar fractures (PFs) developed in a quartz grain of sandstone from the central uplift of the Ramgarh Structure. Three sets of well-developed parallel narrow open fractures, filled with dark material (PPL View, 10X). Bar scale is 100 μ m.

Petrographic Studies

Petrographic observation of the sandstones collected from the centrally uplifted region by the authors have revealed the presence of shocked quartz grains marked by the significantly developed Planar fractures (PFs) as well as Planar Deformation Features (PDFs).

Seven thin sections of sandstones that were examined are showing shocked quartz grains with well-developed

parallel set of narrow open fractures. Three sets of planar fractures have been noticed which are not crossing grain boundaries. These fractures are widely spaced ($> 5\text{--}20\ \mu\text{m}$) and are oriented at specific angles to the c-axis of the host quartz (Figure 5). The planes consist of open fractures, filled with some dark material which may be ferruginous. The fractures are relatively thin (typically $3\text{--}10\ \mu\text{m}$), but relatively thicker than PDFs. The development of intense, widespread, and closely spaced planar fractures is strongly

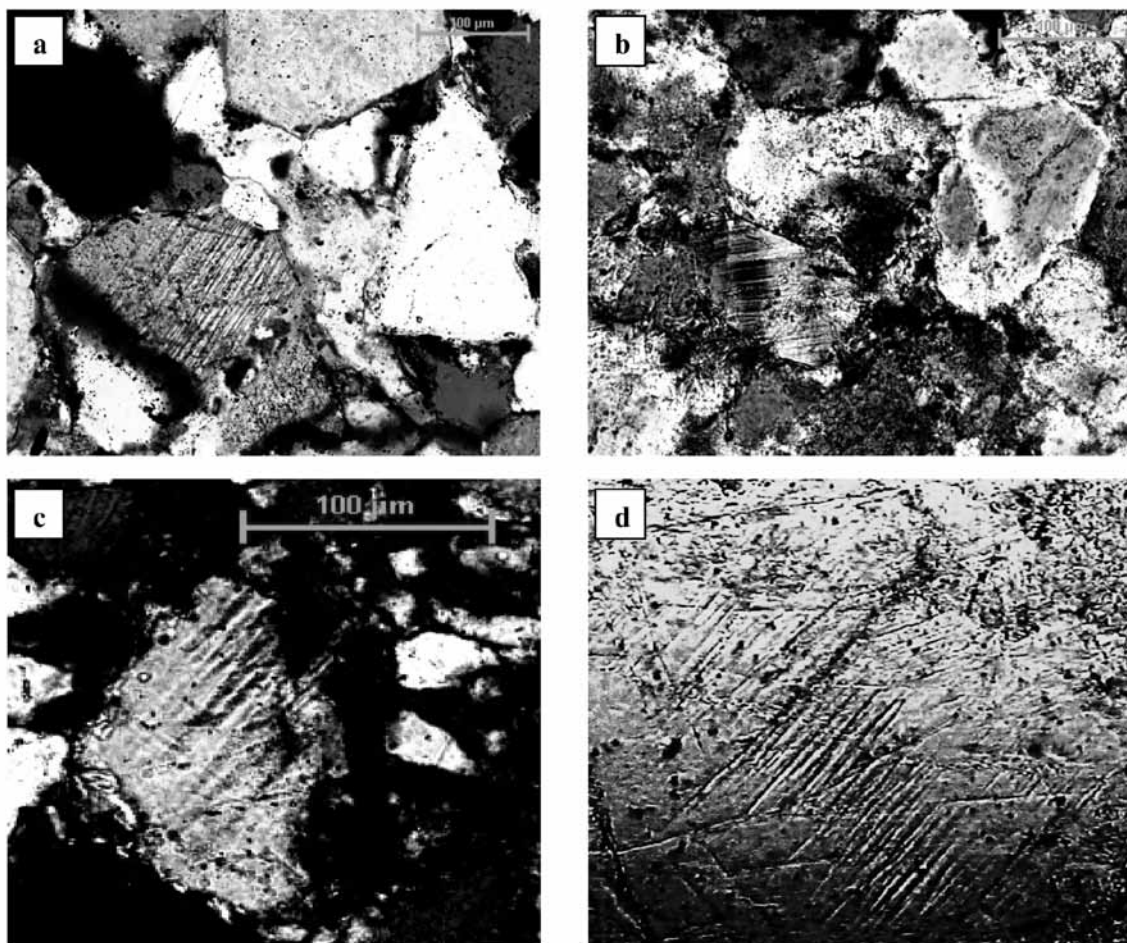


Figure 6. Photomicrographs of shock metamorphic features in quartz grains from Ramgarh Structure. (a) Decorated planar deformation features (PDFs) in a quartz grain from a sample of sandstone in the central uplift (crossed polarizers, 20X). (b) Planar deformation features in a large quartz grain (crossed polarizers, 20X). (c) Faint but obviously developed two sets of PDFs in another quartz grain (XPL, 20X); (d) Quartz grain with two sets of PDFs (PPL, 20X). The bar scale is 100 μm in all the photographs.

suggestive of shock, and such fractures are frequently accompanied in impact structures by other features clearly formed at higher shock pressures.

Several quartz grains (8-10 grains per thin section) with PDFs have been identified in the 10 thin sections of sandstones. The thickness of individual PDF lamellae is 1-3 μm , and the spacing between individual planes ranges from about 2 -5 μm . The PDFs are sharp, straight and confined within the grain boundary which are visible under high magnification in both plane polarised light and under crossed polars. Many of these PDFs are decorated with planar fluid inclusion trails (Figure 6a). In some quartz grains, PDFs are faintly developed but can be easily identified (Figure 6c). All the examined samples have revealed the presence of shocked quartz grains (10-12 grains per sections). These are recognizably distinct from endogenic planar micro deformation features or the Metamorphic Deformation Lamellae (MDLs) which are characterized by clearly irregular and non-

planar character and lack of parallelism. Also MDLs are characteristically widely spaced than PDFs (>5 μm). Since PDFs are characteristically produced in quartz under high shock pressures (>10GPa) and their occurrence along with Planar fractures at Ramgarh definitely indicate that PDF-containing Ramgarh sandstones have undergone intense shock metamorphism. However, the density of the PDFs in quartz grains of these sandstones is low because the porous sedimentary rocks respond differently to the shock waves. Shock waves passing through the porous sediments generate more heat mainly because more of the shock-wave energy is absorbed by the numerous grain interfaces and pore spaces in the sediment (Kieffer, 1971; Kieffer and Simonds, 1980; Stöffler, 1984). As a result, extensive melting will occur at lower shock pressures in sediments than in crystalline rocks. Therefore, the density of quartz PDFs in shock altered sedimentary rocks like sandstones is very low, either because they did not form or because they were immediately destroyed by post shock melting.

CONCLUSIONS

During the course of present work detailed petrographic studies of the sandstones around the Ramgarh structure were carried out. Microscopic examination revealed the presence of Planar Fractures and Planar Deformation Features indicating shock metamorphism. Well-developed parallel set of narrow open fractures are noticed in the quartz grains exhibiting shock features. Owing to these diagnostic observations indicating shock metamorphism due to meteorite impact we infer an impact origin of Ramgarh structure.

ACKNOWLEDGEMENTS

This field study has been conducted as a part of BSR Fellowship funded by the UGC. Authors are thankful to Dr. G. Suresh, GSI, Hyderabad for his kind help in petrographic studies. Authors wish to record their deep sense of gratitude to Dr. Harsh Bhu, Professor and Head, Department of Geology, Mohanlal Sukhadia University, Udaipur, Rajasthan for helpful review of the manuscript. Sincere thanks are due to Shri Pawan Kumar Gautam, Geologist, GSI, Lucknow for his valuable suggestions in the preparation of manuscript. Constructive suggestions from the Editor of the Journal are gratefully acknowledged. Authors are grateful to Dr.V.V.Seshasai for constructive review and editing. We thank the Chief Editor for his support. At last, but not the least, we would also like to thank people at Ramgarh for their cooperation during the fieldwork.

Compliance with ethical standards

The authors declare that they have no conflict of interest and adhere to copyright norms.

REFERENCES

Ahmad, N., Bhardwaj, B.D., Sajid, H.A., and Hasnain., 1974. Ramgarh meteoritic crater., *Curr. Sci.*, Bangalore, v.43, no.18, pp: 598.

Balasundaram, M.S., and Dube, A., 1973. Ramgarh structure., *Nature*, v.242, pp: 40.

Crawford, A.R., 1972. Possible impact structure in India., *Nature*, v.237, pp: 96.

Engelhardt, W. V., and Bertsch, W., 1969. Shock Induced Planar Deformation Structures in Quartz from the Ries Crater, Germany, *Contr. Mineral and Petrol.*, v.20, pp: 203.

French, B. M., and Koeberl, C., 2010. The convincing identification of terrestrial meteorite impact structures: What works, what doesn't, and why, *Earth-Science Reviews*, v.98, pp: 123–170.

Grieve, R. A. F., 1987. Terrestrial Impact Structures. *Annual Review of Earth and Planetary Science Letters.*, v.15, pp: 245-270.

Grieve, R. A. F., 1991. Terrestrial Impact: the record in the rocks., *Meteoritics*, v.26, pp: 175-194.

Grieve, R. A. F., and Pilkington, M., 1996. The signature of terrestrial impacts. *ASGO Journal Australian Geology and Geophysics*, v.16, pp: 399-420.

Grieve, R. A. F., 1998. Extraterrestrial impacts on earth: the evidence and the consequences. In: Grady, M.M., Hutchison, R., McCall, G.J.H., Rothery, D. (Eds.), *Meteorites: Flux with Time and Impact Effects*. Geological Society, London, Special Publication, v.140, pp: 105–131.

Kieffer, S.W., 1971. Shock metamorphism of the Coconino Sandstone at Meteor Crater, Arizona. *Journal of Geophysical Research*, v.76, pp: 5449–5473.

Kieffer, S.W., and Simonds, C.H., 1980. The role of volatiles and lithology in the impact cratering process. *Reviews of Geophysics and Space Physics*, v.18, pp: 143–181.

Koeberl, C., 2002. Mineralogical and Geochemical Aspects of Impact Craters. *Mineralogical Magazine*, v.66, pp: 745-768.

Langenhorst, F., 2002. Shock metamorphism of some minerals: Basic introduction and microstructural observations. *Bulletin of the Czech Geological Survey*, v.77, pp: 265-268.

Master, S., and Pandit, M.K., 1999. New evidence for an impact origin of the Ramgarh structure., *Meteoritics and Planetary Science (suppl.)*, v.34, pp: A79.

Mishra, S., Lashkari, G., Panda, D., Dube, A., Sisodia, M. S., Newsom, H. E., and Sengupta, D., 2008. Geochemical evidence for the meteorite impact origin of Ramgarh structure, 39th Conference, Lunar and Planetary Science, Texas, LPI Contribution, no.1391, pp: 1499.

Montanari, A., and Koeberl, C., 2000. *Impact Stratigraphy: The Italian Record*. Lecture Notes in Earth Sciences, Springer Verlag, New York, v.93, pp: 364.

Murali, A.V., and Lulla, K.P., 1992. Ramgarh crater, Rajasthan, India: study of multispectral images obtained by Indian remote sensing satellite (IRS-IA), *Geocarto International*, v.7, pp: 75-80.

Nicolaysen, L. O., and Reimold, W. U., 1990. Cryptoexplosions and Catastrophes in the Geological Record, with a Special Focus on the Vredefort Structure. *Tectonophysics*, v.171, pp: 1-422.

Prasad, B., 1984. Geology, sedimentation and palaeo-geography of the Vindhyan Supergroup, Southeastern Rajasthan, *Mem. Geol. Surv. India*, v.116, pp: 72.

Ramasamy, S.M., 1987. Evolution of Ramgarh dome, Rajasthan, India. *Rec. Geol. Surv. Ind.*, v.113, Pt. 7, pp: 13-22.

Shoemaker, E. M., 1977. Astronomically observable crater-forming projectiles. In *Impact and Explosion Cratering* (D. J. Roddy, R. O. Pepin, and R. B. Merrill, Eds.), Pergamon, Elmsford, N. Y., pp: 617-628.

- Sharma, H. S., 1973. Ramgarh structure, India., *Nature*, v.242, no.5392, pp: 39-40.
- Sisodia, M.S., and Lashkari, G., 2003. Ramgarh structure, Rajasthan, India: meteorite impact evidences, Workshop on Impact Cratering, LPI, USA, 8008.
- Sisodia, M.S., Lashkari, G.L., and Bhandari, N., 2008. Impact origin of Ramgarh structure, Rajasthan: some new evidences, *Jour. Geol. Soc. Ind.*, v.67, pp: 423-431.

- Stöffler, D., 1984. Glasses formed by hypervelocity impact. *Journal of Non-Crystalline Solids*, v. 67, pp: 465–502.
- Stoffler, D., and Langenhorst, F., 1994. Shock Metamorphism of quartz grains in nature and experiment : basic observation and theory., *Meteoritics*, v.29, pp: 155-181.
- Therriault, A. M., Grieve, R. A. F., and Pilkington, M., 2002. The recognition of terrestrial impact structures, *Bulletin of the Czech Geological Survey*, v.77, no.4, pp: 253–263.

Petrology and geochemistry of the troctolite and ultramafic from the Paleoproterozoic Kandra Ophiolite Complex, Eastern Dharwar Craton, SE India

V.V. Sessa Sai

Geological Survey of India, Southern Region, Bandlaguda, Hyderabad-India-500068

E-mail : seshu1967@gmail.com

ABSTRACT

Field and petrological studies indicate the presence of two spatially associated high Mg lithounits; troctolite and ultramafic within the southern gabbros of the Paleoproterozoic Kandra Ophiolite Complex (KOC), Eastern Dharwar Craton, SE India. Petrographic studies indicated that troctolite is essentially composed of olivine and plagioclase with sub-ordinate augite, while magnetite and ilmenite are noticed as accessory oxides. Mineral chemistry studies by EPMA reveal that olivine in troctolite is forsterite ($Fe_{0.63.14}$) plagioclase is labradorite ($An_{69.96}$) and the Fe-Ti oxide ilmenite in troctolite analysed TiO_2 -53.08 %, FeO^T -44.22%. Major oxides of troctolite indicated SiO_2 - 43.10%, TiO_2 - 0.29%, Al_2O_3 -15.81%, FeO - 10.44%, Fe_2O_3 - 5.56%, CaO -7.92% and MgO - 13.08%. Petrographically, ultramafic is essentially composed of magnesio hornblende with subordinate chlorite, while ilmenite is the accessory oxide phase. Mineral chemistry studies by EPMA of the ultramafic indicate that the magnesio hornblende analysed SiO_2 - 43.71%, Al_2O_3 -14.61%, FeO - 15.35% and MgO - 9.94%, while chlorite analysed SiO_2 - 27.02%, Al_2O_3 -22.6%, FeO - 19.75% and MgO - 19.7%. Ilmenite in the ultramafic analysed FeO - 45.14%, TiO_2 - 53.44%. Major oxides of ultramafic indicated SiO_2 - 28.6%, TiO_2 - 0.65 %, Al_2O_3 - 17.22 %, FeO - 6.84 %, Fe_2O_3 - 6.88%, CaO - 0.41% and MgO - 26.84%. HFSE depletion is noticed in both these high Mg lithounits; (Zr- 42.17 ppm, Nb-2.65ppm and Y-5.35ppm) in troctolite and (Zr- 40.13ppm, Nb-2.47ppm and Y-3.16 ppm) in ultramafic. Rare Earth Element (REE) geochemical studies indicate that these spatially co-existing troctolite and ultramafic show an overall depleted but contrasting REE patterns. Troctolite exhibits a low magnitude positive Eu anomaly while the ultramafic exhibit a negative Eu anomaly indicating co-magmatic origin of the mafic-ultramafic lithounits in the southern gabbros of KOC.

Key words: Troctolite, ultramafic, Kandra ophiolite, Eastern Dharwar Craton and India.

INTRODUCTION

The extrusive basic igneous rocks at the Kandra area were initially studied by Roy (1944) who designated them as "Kandra volcanics". Subsequently Subramanyam (1966) studied the rocks representing the "Kandra volcanics" and the associated granite intrusives and opined that these rocks were emplaced during the time gap between close of Archaean Dharwar and deposition of Proterozoic Cuddapah rocks. Nagaraja Rao et al., (GSI, 1990) carried out Geological mapping around Kandra area and established the stratigraphy in the area and redesignated the Kandra volcanics as Kandra Igneous Complex (KIC). Rao (1992) during the field studies observed that Kandra area in the Nellore schist belt (NSB) consists of para and ortho metamorphics, basic igneous rocks belonging to two different periods of intrusion migmatites, granites and pegmatites and hence proposed that the term "Kandra volcanics" be restricted to amygdaloidal amphibolites and ortho amphibolites. Leelanandam (1990), based on geological setup of the rocks exposed around Kandra area and their disposition in the regional geological and

structural setup was the first to suggest the "possible" ophiolitic nature of Kandra volcanics. Based on the geological setting and available the ages of the granitic rocks around the Kandra area in southern part of NSB, an age of ~1500 Ma was suggested for emplacement of Kandra dolerites (Rao et al., 2004). Extensive field and petrological studies (Sessa Sai, 2005) indicated the presence of parallel sheeted dolerite dykes with profound chilled margins in the area to ENE of Kandra. Further by identifying the presence of veins of oceanic plagiogranite in a sheeted dyke near Gollapalle area to the NE of Kandra the oceanic crust nature of Ultramafic-mafic suite at Kandra was confirmed; hence KIC was designated as Kandra Ophiolite Complex (KOC; Sessa Sai, 2009). Vijaya Kumar (2010) carried out geochronological studies and assigned a U-Pb age of 1.85 Ga to the oceanic crust of Kandra in SE India. Saha (2011) studied the structural aspects and interpreted the dismembered nature of the Paleoproterozoic KOC. The accretionary nature of the Palaeoproterozoic oceanic crust at Kandra along the SE India and its tectonic significance was discussed by Vijaya Kumar et al., (2010); Saha, (2011); Saha and Mazumder, (2012).

Geological Set Up

KOC occurs as a discordant mafic-ultramafic Complex in the southern part of NSB in Eastern Dharwar Craton (EDC). Situated close to the eastern margin of the Proterozoic Cuddapah Basin at its southern end (Figure 1a), the WNW-ESE trending KOC is exposed over a length of 18 kms with a maximum width of 5 km in its central portion around Kandra (Figure 1). Field studies indicate the "discordant relationship" of KOC with the amphibolite and mica schist of NSB (Sessa Sai, 2005). KOC is made predominantly of two magmatic components (i) the northern dolerite and diabase dykes that represent the hypabyssal part and (ii) the southern cumulus gabbro and olivine gabbro that represent the plutonic part of KOC. KOC is characterised by absence of a significant volcanic component. Caught up patches of quartz arenites and conglomerate are widely noticed in northern dykes, while field studies indicate that at the westernmost part of KOC the dolerite dykes are intrusive into the conglomerate-quartzite sequence (Sessa Sai, 2005). N-S to NNE-SSW trending younger dolerites are noticed as intrusive into the northern dykes that are characterised by enclaves of conglomerate and quartz arenite. The sheared southern contact of the KOC and its disposition of KOC along a major fault indicate the tectonic contact of the KOC with NSB (Leelanandam, 1990; Sessa Sai, 2009). Through this communication the petrological, mineral chemistry and geochemical details of the spatially associated troctolite and ultramafic are presented in a succinct manner. Both the troctolite and ultramafic rocks are spatially associated with the southern gabbros of KOC. EPMA analyses of samples from the troctolite and ultramafic was carried out by CEMECA Sx100 Electron Probe Micro Analyzer at the EPMA Laboratory, Geological Survey of India, Hyderabad. The operating conditions were 15 kV accelerating voltage, 1–2 micron beam diameter and 12 nA current.

Troctolite

Petrographic studies indicate that troctolite is essentially composed of olivine and plagioclase with sub-ordinate augite, while magnetite and ilmenite are noticed as accessory oxide phases. Plagioclase is unaltered and exhibits characteristic lamellar twinning. Olivine in plane polarized light is colorless with high relief. In crossed nicols olivine exhibit high birefringence. The interspaces between the euhedral plagioclase laths are occupied by subhedral to anhedral grains of olivine. Development of cumulus texture, a magmatic texture indicating fractional crystallisation is noticed in troctolite. Reaction coronas between olivine and plagioclase are observed in troctolite (Figure 2a). Mineral chemistry studies by EPMA reveal that the olivine in troctolite is forsterite ($\text{Fo}_{63.14}$) plagioclase is labradorite (An-

69.96), close to the bytownite field. The Fe-Ti oxide ilmenite analysed TiO_2 -53.08 %, FeO^T -44.22%. Olivine-plagioclase rich troctolite has been reported from the Sikhote-Alin ophiolite from the terrain located at the southern far east of Russia (Vysotskiy and Khanchuk, 2016). Geochemical studies reveal that the troctolite of KOC analysed (in %); SiO_2 -43.10, TiO_2 -0.29, Al_2O_3 -15.81, FeO -10.44, Fe_2O_3 - 5.56, CaO -7.92 and MgO -13.08 (Table-1). Trace element geochemistry (ppm) indicate depleted HFSE in troctolite; Zr- 42.17, Nb-2.65 and Y-5.35. Rare Earth Element (REE) geochemical studies indicate that the troctolite exhibits an overall depleted REE pattern with a positive Eu anomaly (Figure 3) indicating fractionation of the plagioclase from the melt. EPMA analyses of the mineral phases from the troctolite of KOC is furnished in Table-2.

Ultramafic

Petrographic studies indicate that the ultramafic is essentially composed of greenish amphibole with subordinate chlorite and accessory ilmenite. Amphibole exhibits optical characters of magnesio-hornblende and is pleochroic in shades of pale green. Minor displacement is noticed at places along the cleavage planes of the amphibole (Figure 2b). Chlorite is pale greenish in color and occurs as randomly oriented grains. Ilmenite under reflected light is grayish and anisotropic. Geochemically ultramafic analysed SiO_2 - 28.6, TiO_2 -0.65, Al_2O_3 -17.22, FeO - 6.84, Fe_2O_3 - 6.88, CaO - 0.41 and MgO - 26.84. (Table-1). Mineral chemistry studies by EPMA indicated that the amphibole analysed SiO_2 - 43.71, Al_2O_3 -14.61, FeO - 15.35 and MgO - 9.94 indicating tschermakite composition, while chlorite analysed SiO_2 -27.02, Al_2O_3 -22.6, FeO -9.75, MgO - 19.7. Ilmenite analysed FeO -44.22 and TiO_2 -53.08. Rare Earth Element (REE) geochemical studies indicate that the ultramafic exhibits a depleted REE pattern with a significant negative Eu anomaly (Figure 3). EPMA analyses of the mineral phases from the ultramafic of KOC is furnished in Table-2.

DISCUSSION

Recent field studies indicated that the troctolite and ultramafic bands occur as N35°W-S35°E bands near to the vicinity of Δ 183 ($14^\circ 24' : 79^\circ 47' 10''$) to the north of Arimanapadu in southern high ground of KOC. It is observed that both these spatially associated high Mg lithounits are confined to the southern gabbros; the plutonic part of the KOC. Ultramafic slivers have been reported at Kandra in the form of talc-chlorite schists (Leelanandam, 2006). Reaction coronas between olivine and plagioclase are noticed in some gabbroic rocks wherein the low pressure conditions during corona formation is well constrained by the conditions during

Petrology and geochemistry of the troctolite and ultramafic from the Paleoproterozoic Kandra Ophiolite Complex, Eastern Dharwar Craton, SE India

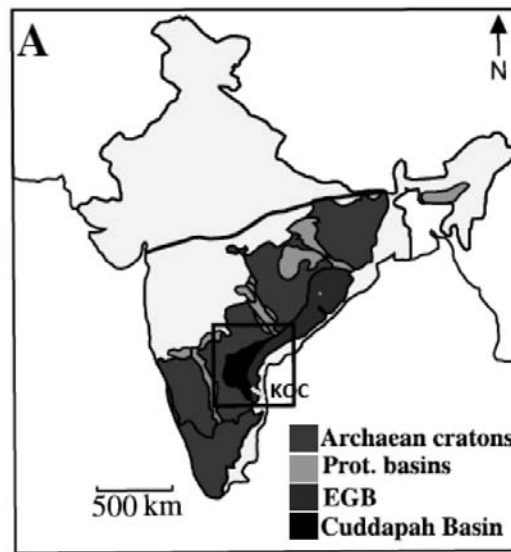


Figure 1a. Simplified Geological Map of India showing the Precambrian terrane in SE India. Note the location of KOC to the east of southern end of eastern margin of Proterozoic Cuddapah basin.

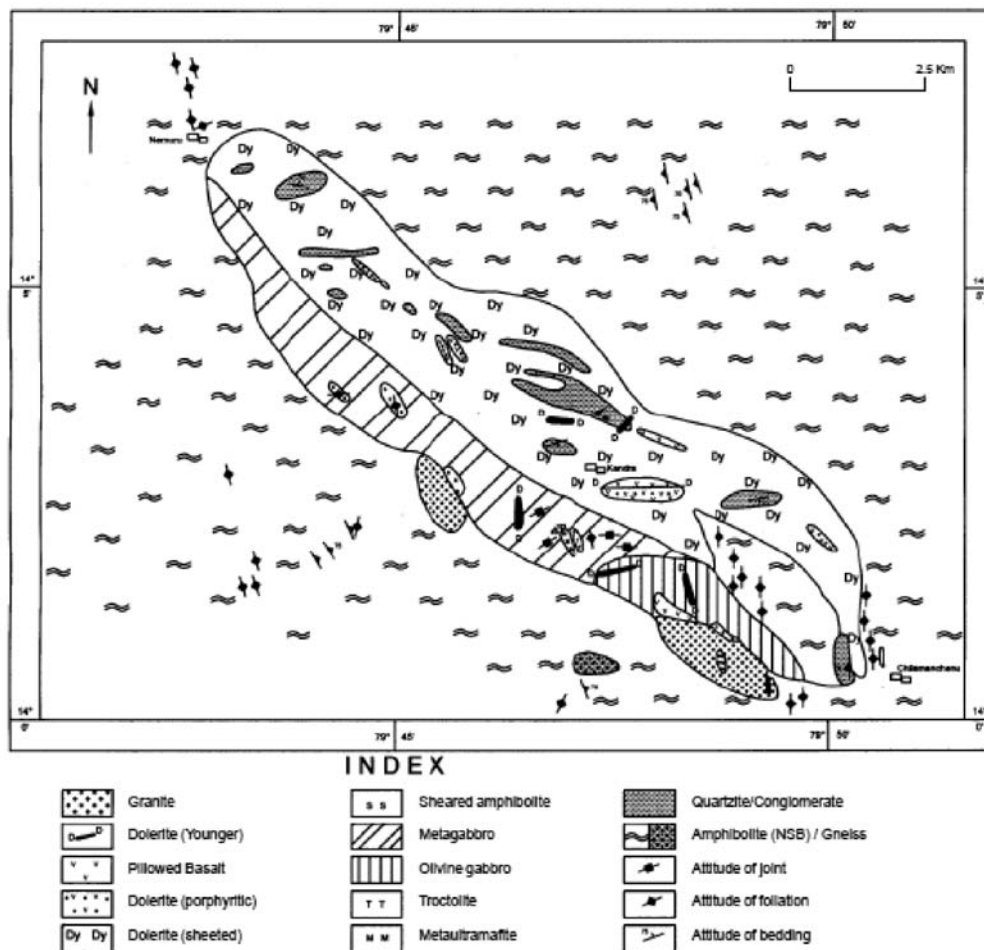


Figure 1b. Geological map of Kandra ophiolite complex, Nellore schist belt (Sesha Sai, 2009; modified after Nagaraja Rao et al., 1990)

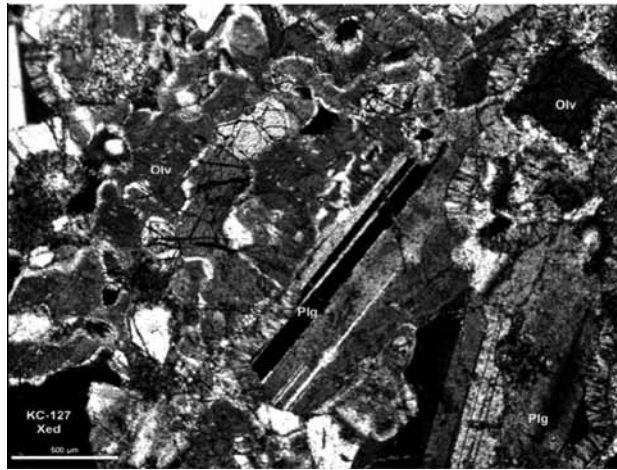


Figure 2a. Photomicrograph of olivine and plagioclase in the troctolite.

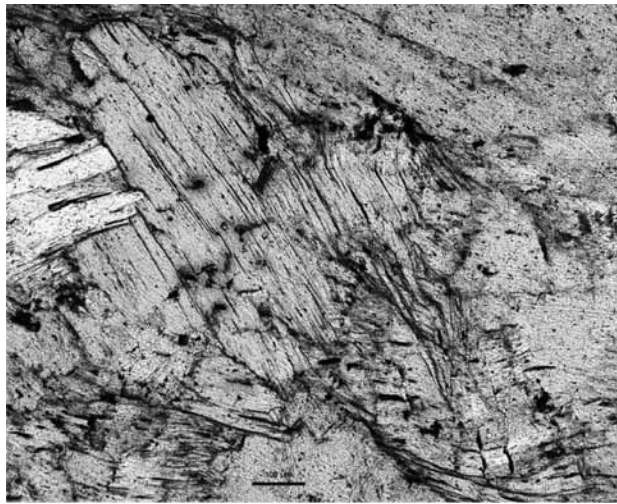


Figure 2b. Photomicrograph showing cleavage with minor displacement in magnesio hornblende.

Table 1. Geochemical analyses of Troctolite and ultramafic from KOC, EDC, India.

Major oxide (%)	KC-127 Troctolite	KC-125B Ultramafic	Trace Element (ppm)	KC-127 Troctolite	KC-125B Ultramafic
SiO ₂	43.10	28.6	Th	0.95	2.17
TiO ₂	0.29	0.65	U	<0.5	<0.5
Al ₂ O ₃	15.81	17.22	Zr	42.17	40.13
Fe ₂ O ₃	5.56	6.88	Nb	2.65	2.47
FeO	10.44	6.84	Be	<0.3	<0.3
MnO	0.19	0.1	Y	5.65	3.16
CaO	7.92	0.41	Cs	<0.2	<0.2
MgO	13.08	26.84	Hf	1.09	1.06
Na ₂ O	1.65	0.01	La	4.48	2.02
K ₂ O	0.20	0.01	Ce	9.07	5.66
P ₂ O ₅	0.04	0.08	Nd	4.61	2.55
Cr ₂ O ₃	0.1	0.01	Sm	1.08	0.65
LOI	0.37	11.34	Eu	0.65	0.09
TOTAL	98.66	98.99	Gd	1.01	0.68
Mg. No.	55.61	80.62	Dy	1.02	0.63

Petrology and geochemistry of the troctolite and ultramafic from the
Paleoproterozoic Kandra Ophiolite Complex, Eastern Dharwar Craton, SE India

Table 2. EPMA analyses of the mineral phases from the troctolite and ultramafic of KOC.

Oxide	Mineral chemistry of the olivine, plagioclase and ilmenite from the troctolite of KOC						Mineral chemistry of the amphibole, chlorite and ilmenite from the ultramafic of KOC			
	Core	Rim	Core	Rim	Ilmenite (6 oxygens)	(Amphibole) Tschermakite (23 oxygens)	Ilmenite (6 oxygens)			
SiO ₂	36.32	53.38	50.17	51.02	0.02	0.02	43.71	44.29	0.01	0.02
Al ₂ O ₃	0.005	0.80	31.72	31.02	0.01	0.00	14.61	14.77	0.02	0.00
TiO ₂	0.00	0.00	0.06	0.03	52.74	53.08	0.45	0.32	53.44	54.12
MnO	0.37	0.39	0.00	0.00	0.55	0.57	0.17	0.19	0.92	0.92
MgO	31.14	25.44	0.00	0.00	1.81	1.74	9.94	10.01	0.38	0.36
FeO	32.04	19.72	0.12	0.04	43.86	44.22	15.35	15.81	45.14	44.51
Na ₂ O	0.03	0.05	3.56	3.82	0.18	0.27	1.84	2.01	0.01	0.02
K ₂ O	0.00	0.02	0.01	0.02	0.00	0.00	0.27	0.31	0.00	0.00
CaO	0.01	0.07	14.34	14.02	0.01	0.00	11.16	11.21	0.00	0.00
Cr ₂ O ₃	0.02	0.00	0.00	0.00	0.08	0.05	0.07	0.07	0.05	0.02
P ₂ O ₅	0.01	0.02	0.01	0.01	0.01	0.00	0.06	0.00	0.00	0.01
Total	99.84	99.89	99.99	99.98	99.27	99.95	97.63	98.99	99.97	99.98
Si	0.994	1.311	9.156	9.295	0.001	0.001	6.456	6.459	0.001	0.001
Ti	0.000	0.000	0.000	0.000	1.995	1.997	0.050	0.035	2.017	2.036
Al	0.000	0.023	6.823	6.660	0.001	0.000	2.543	2.538	0.001	0.000
Cr	0.000	0.000	0.000	0.000	0.003	0.002	0.008	0.008	0.002	0.000
Fe(ii)	0.733	0.405	0.018	0.006	1.845	1.849	1.896	1.928	1.894	1.861
Mn	0.009	0.008	0.000	0.000	0.023	0.024	0.021	0.023	0.039	0.039
Mg	1.270	0.931	0.000	0.000	0.136	0.130	2.189	2.176	0.028	0.027
Ni	0.000	0.000	0.000	0.000	0.001	0.000	0.000	0.000	0.000	0.000
Ca	0.000	0.002	2.804	2.736	0.000	0.000	1.766	1.751	0.000	0.001
Na	0.000	0.000	1.260	1.349	0.000	0.000	0.527	0.568	0.000	0.000
K	0.000	0.000	0.002	0.005	0.000	0.000	0.051	0.051	0.000	0.000
TOTAL	3.006	2.680	20.063	20.052	4.003	4.002	15.507	15.546	3.982	3.964
	Core	Rim	Core	Rim	Ilmenite (6 oxygens)	(Amphibole) Tschermakite (23 oxygens)	Ilmenite (6 oxygens)			
	Olivine (4 oxygens)		Plagioclase (8 oxygens)							

crystallisation of the magma as the coronas must have formed during initial igneous cooling (Turnet and Stuwe, 1992). However, presence of primary igneous texture is noticed in the troctolite in the form of development of cumulus plagioclase. Studies from the Ligurian Ophiolites of Italy (Renna and Tribuzio, 2011) indicated that the troctolite rich in olivine is crystallised from the infiltrating melts showing the geochemical signatures of mid oceanic rich basalt (MORB). REE geochemical studies indicate that spatially co-existing troctolite and ultramafic show depleted REE patterns. However, troctolite exhibits a low magnitudes positive Eu anomaly indicating plagioclase fractionation from the melt giving rise to the troctolite, while in contrast the ultramafic exhibit negative Eu anomaly (Figure 3) indicating subsequent crystallisation and co-magmatic relationship with the troctolite (Sesha Sai, 2015). The observation that the Fe-Ti oxide nature of the troctolite in the southern gabbro complex of the KOC through the present study attains significance since it corroborates with

the occurrence of the Fe-Ti oxide of the gabbros associated with the oceanic crust (Robinson, et al., 2000).

Eastern Gondwana Correlations

KOC is situated in the southern part of the Neoarchean NSB (Ravikant, 2010). Magmatic evolution of some Archean greenstone belts may be related subduction-related Proterozoic ophiolites (Furnes et al., 2014). 1.85 Ga KOC of eastern Gondwana signifies events of arc-continent collisions resulting in assembly of Paleoproterozoic supercontinent Columbia (Vijay Kumar et al. 2010). Island arc basalt-type geochemical signatures are characteristic of mafic rocks of Palaeoproterozoic Kandra (Vijay Kumar et al., 2015). A significant cluster of Paleoproterozoic ophiolites has been inferred to occur along the margins of Australia, Antarctica and India (Moores, 2002, Vijay Kumar et al., 2010, Santosh, 2012). Palaeoproterozoic perhaps witnessed the Nuna supercontinent assembly 1.9–1.8 Ga (Reddy and

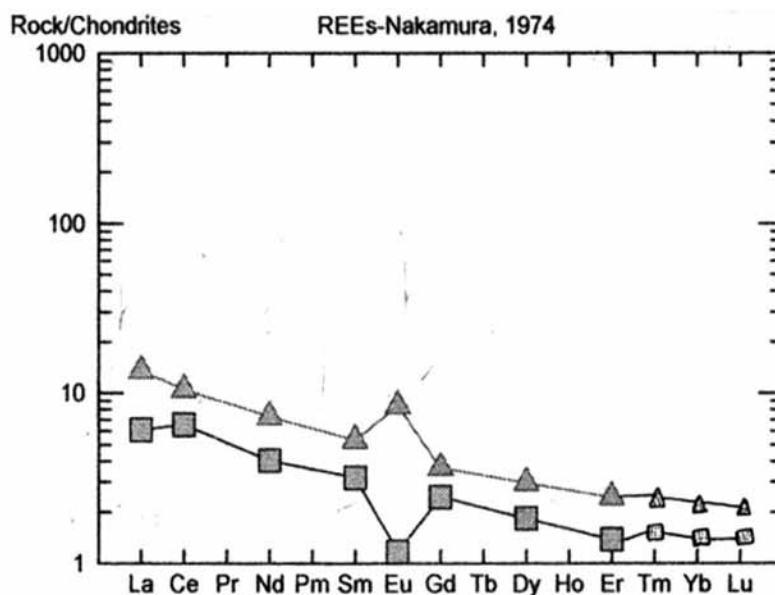


Figure 3. Chondrite normalised REE pattern for troctolite (▲) and ultramafic (■) of KOC.

Evans, 2009). In this context KOC in SE India attains geological significance to correlate the Paleoproterozoic subduction related processes in eastern Gondwana.

CONCLUSIONS

Field studies revealed the existence of two mafic-ultramafic lithounits; troctolite and ultramafic in southern part of KOC. Field disposition attains significance since both these lithounits are confined to the southern gabbros of the KOC; that represent the plutonic component of the Kandra oceanic crust. Incidentally it is observed that the conglomerate-arenite caught patches are confined to the northern dyke Complex, the hypabyssal part of the KOC. Petrographic studies indicate cumulus plagioclase in the troctolite, a feature indicating fractionation of the Ca rich plagioclase from the melt. The high Mg nature of troctolite (13.08 % MgO) and ultramafic (26.84 % MgO) along with the HFSE depletion in both these lithounits indicate the mantle source. REE geochemical studies reveal a depleted but contrasting chondrite normalised REE patterns; a positive Eu anomaly in troctolite and a negative Eu anomaly in ultramafic, indicating a magmatic origin for the mafic-ultramafic suite of rocks from the Paleoproterozoic Kandra Ophiolite Complex, EDC, SE India.

ACKNOWLEDGEMENTS

Shri.S.Kannan, ADG (Retd.), GSI, is profusely thanked for according permission to publish the work. Prof. C. Leelanandam and Dr. T.R.K. Chetty are gratefully acknowledged for helpful discussion and encouragement

to publish this paper. Shri. S.T.Narahari, GSI, Hyderabad is thanked for EPMA facility while Dr. S. Bhattacharjee and Dr. Vikash Tripathy are thanked for constructive suggestions. Dr.P.R.Reddy, Chief Editor, IGU is thankfully acknowledged for valuable support.

Compliance with Ethical Standards

The authors declare that they have no conflict of interest and adhere to copyright norms.

REFERENCES

- Furnes Herald, Maarten de Wit and Yildirim Dilek., 2014. Four billion years of ophiolites reveal secular trends in oceanic crust formation. *Geoscience Frontiers*, v.5, no.4, pp: 571–603.
- Leelanandam, C., 1990. The Kandra volcanic in Andhra Pradesh: A possible ophiolite, *Current Science*, v.59, pp: 785-888.
- Leelanandam C., Burke K., Ashwal L. D., Webb S. J., 2006. Proterozoic mountain building in Peninsular India: an analysis based primarily on alkaline rock distribution. *Geological Magazine*, v.43, pp: 195-212.
- Moore, E.M., 2002. Pre - 1 Ga (pre-Rodinian) ophiolites; their tectonic and environmental implications, *Geological Society of America Bulletin*, v.114, pp: 80-95.
- Nagaraja Rao, B. K., Katti, P.M., and Roop Kumar, D., 1990. *Geology of Kandra Igneous Complex, Nellore district, A.P.* Unpub. Prog. Rep. G.S.I. FS 1989-90.
- Nakamura N., 1974. Determination of REE, Ba, Fe, Mg, Na and K in carbonaceous and ordinary chondrites. *Geochim. Cosmochim. Acta* v.38, pp: 757-775.

Petrology and geochemistry of the troctolite and ultramafic from the
Paleoproterozoic Kandra Ophiolite Complex, Eastern Dharwar Craton, SE India

- Rao, A.T., 1992. The Kandra Igneous Complex from the Precambrian Nellore schist belt, Andhra Pradesh. *Jour. Appl. Geochem.*, v.6, no.1, pp: 1-14.
- Rao, A.T., Chalamiah, K., Srinivasa Rao, D., Devavarma, D., and Dhananjaya Rao, E.N., 2004. Dolerites from Kandra Volcanic Region, Nellore schist belt, A.P. *Jour. Appl. Geochem.*, v.6 no.1 pp: 1-14.
- Ravikant, V., 2010. Palaeoproterozoic (1.9 Ga) extension and breakup along the eastern margin of the Eastern Dharwar Craton, SE India: New Sm–Nd isochron age constraints from anorogenic mafic magmatism in the Neoproterozoic Nellore greenstone belt. *Jour. Asian Earth Sci.*, v.12, pp: 67-81.
- Reddy S. M., and Evans D. A. D., 2009. Palaeoproterozoic supercontinents and global evolution: correlations from core to atmosphere. In S. M., Mazumder R., Evans, D. A. D. And Collins, A. S edited Geological Society Special Publication, Palaeoproterozoic Supercontinents and Global Evolution., no.323, pp: 1-26.
- Renna M.R., and Tribuzio, R., 2011. Olivine-rich Troctolites from Ligurian Ophiolites (Italy): Evidence for Impregnation of Replacive Mantle Conduits by MORB-type Melts. *Journal of Petrology*. doi: 10.1093/petrology/egr029
- Robinson, P.T., Dick, H.J.B., and Narlad, J.H., 2000. ODP Leg Shipboard part. Lower oceanic crust formed an ultra-slow spreading ridge, Oceanic Drilling Program Hole 735 B, South west Indian Ridge, Geological Society of America, Special paper, pp: 75-86.
- Roy, B.C., 1944. The Nellore mica belt, *Geol. Surv. India. Bull. Econ. Geologist.*, no.11 pp: 156.
- Saha Dilip, 2011. Dismembered ophiolites in Paleoproterozoic nappe complexes of Kandra and Gurrampkonda, South India. *Journal of Asian Earth Sciences*, 10 August , v.42, no.3, pp: 158-175.
- Saha, D., and Mazumder, R., 2012. An overview of the Palaeoproterozoic geology of Peninsular India, and key stratigraphic and tectonic Geological Society of London, Special Publications, v-365, pp: 5-29.
- Santosh M., 2012. India's Palaeoproterozoic legacy. Mazumder, R. & Saha, D. (eds) 2012. Palaeoproterozoic of India. Geological Society, London, Special Publications, v.365, pp: 263-288.
- Sesha Sai, V.V., 2005. Petrographic, petrochemical and mineral chemistry studies of Kandra Igneous Complex, Nellore schist belt, Andhra Pradesh. *Rec. GSI*, v.138, Part-5, pp: 229-233.
- Sesha Sai, V.V., 2009. Sheeted dykes in Kandra Ophiolite Complex, Nellore schist belt, Andhra Pradesh-Vestiges of Precambrian Oceanic crust. *Jour.Geol.Soc.Ind.*, v.74, pp: 509-514.
- Sesha Sai, V.V., 2015. Geochemical evidence for magmatic origin of the Paleoproterozoic Kandra mafic-ultramafic suite, SE India - Implications from REE studies of troctolite and ultramafic. 25th Goldschmidt conference, Abstract 1769.
- Turner and Stüwe Kurt, 1992. Low-pressure corona textures between olivine and plagioclase in unmetamorphosed gabbros from Black Hill, South Australia. *Mineralogical Magazine*, December 1992, v.56, pp: 503-509.
- Subramanyam, P., 1966. Studies on Kandra volcanics of Nellore district, A.P. (Abstract). Seminar on mafic and ultramafic rocks of India, Osmania University, Hyderabad. pp: 45-46.
- Vijaya Kumar, K., Ernst, W.G., Leelanandam, C., Wooden, J.L., Grove, M.J., 2010. First Paleoproterozoic ophiolite from Gondwana: geochronologic–geochemical documentation of ancient oceanic crust from Kandra, SE India. *Tectonophysics*. v.487, pp: 22-32.
- Vijaya Kumar, K., Rathna, K., and Leelanandam, C., 2015. Proterozoic subduction-related and continental rift-zone mafic magmas from the Eastern Ghats Belt, SE India: geochemical characteristics and mantle sources. *Current Science*, v.108, no.2, pp: 1-14.
- Vysotskiy, S.V., and Khanchuk, A.I., 2016. Different-depth gabbro-ultrabasic associations in the Sikhote-Alin ophiolites (Russian Far East). *Russian Geology and Geophysics* v.57, no.1, pp: 1-14.

The effect of 10.7 cm solar flux on the monsoon rainfall over India

S. K. Midya¹, S. Goswami² and K. Sengupta¹

¹ Department of Atmospheric Science, University of Calcutta, 51/2 Hazra Road, Kolkata- 700019

² Department of Chemistry, Dinabandhu Mahavidyalaya, Bongaon, North 24 Parganas- 743235

*Corresponding author: goswami_subbasis@yahoo.com

ABSTRACT

The present study attempts to find a probable correlation between the solar cycle and Monsoon Rainfall in India, using the S-Component of the 10.7cm Solar Radio Flux, measured at Ottawa by Remote Sensing Techniques, which varies in response to the Solar Activity, as the representative of the activity of the Sun. Results show a possibility of the Solar activity playing a role in determining the amount of rainfall over a particular region. The general trend is increase in rainfall amount with increase in the solar activity. A possible explanation is suggested for all the observations.

Key words: Solar activity, Solar Flux, Monsoon Rainfall, Monsoon Depressions (MD), Monsoon Low (ML), Mid Tropospheric Cyclone (MTC), Sea Surface Temperature (SST) and Southern Oscillation Index (SOI).

INTRODUCTION

In India over 70% of the annual rainfall is recorded during South West Monsoon. Generally speaking, the monsoon winds reach the extreme south of Indian peninsula near around 1st of June. Thereafter it gets divided into two branches. The Arabian Sea branch moves northwards. The Bay of Bengal branch moves northwards up to the central Bay of Bengal and rapidly spreads over most of Assam by the 1st week of June. On reaching the southern periphery of the Himalayas, it gets deflected westwards and progresses towards the Gangetic Plains. By mid July, the Monsoon reaches Kashmir and remaining country but as a much feeble current. The normal stay of monsoon over India is for about 100 days beginning from 1st June. But unlike the onset, withdrawal of Monsoons is a gradual process. It withdraws from North West (NW) India by the beginning of September and from the rest of the country by first fortnight of October.

Indian summer monsoon, exhibits a wide spectrum of variability, on daily, sub-seasonal, inter-annual, decadal and centennial time scales. Major synoptic systems associated with south-west monsoon are Monsoon Depressions (MD) and Monsoon Lows (ML) which form over North Bay of Bengal, north of 18°N and adjoining land areas and move west-north-westwards towards northwest India during the four summer monsoon months of June to September. Another important synoptic system of the Asian summer monsoon is the Mid Tropospheric Cyclone (MTC). These synoptic scale weather systems are embedded in the large scale monsoon circulation which has significant control on the temporal and spatial distribution of the rainfall associated with them and also on their motion.

The important teleconnections are El Nino/Southern Oscillation (ENSO), Indian Ocean and Atlantic Ocean Sea Surface Temperature (SST), Indian Ocean Oscillation and land surface conditions. The global teleconnections of Indian summer monsoon rainfall variability has been studied extensively. It has been found that in the south Asian region two of the major precipitation maxima associated with areas of intensive convective activity are located near the Bay of Bengal and in the vicinity of Philippines. The variations of monthly mean outgoing longwave radiation in the two regions are poorly correlated, particularly in the decade of 1980s. (Wang and Fan, 1999). Monsoon rainfall variations and teleconnections over south and east Asia have been studied by Kripalani and Kulkarni (2001). Role of Indian Ocean in the ENSO-Indian summer teleconnection in the NCEP climate forecast system has been studied by Achuthavarier et al., 2011. The influence of Sea Surface Temperature (SST) on Indian subdivisional monthly rainfall, namely spatial and temporal influences are investigated by Maity and Nagesh Kumar (2007).

Earlier Studies

The relationship between El Nino events and Indian monsoon has been studied by many researchers since 1980 based on same methodology and same correlation. (Sikka, 1980; Pant and Parthasarathy, 1981; Keshavamurthy, 1982; Rasmusson and Carpenter, 1983; Barnett, 1983; Mooley and Parthasarathy, 1984; Webster and Yang, 1992; Krishna Kumar et al., 1999; Krishnamurthy and Goswami, 2000; Pai, 2003; Kane, 2005; Krishna Kumar et al., 2006; Rajeevan and Pai, 2007). One of the most important results is that there is an inverse relationship between the El Nino

events and Indian Summer Monsoon Rainfall (ISMR). The Indian summer monsoon is weaker than normal during the El Nino years, and that the relationship is opposite for La Nina. Sikka (1980), Pant and Parthasarathy (1981), Rasmusson and Carpenter (1983) have shown that there is an increased propensity of droughts during El Nino and of excess rainfall during La Nina.

Most of severe droughts over India occurred in association with the El Nino events. However, there is no one-to-one relationship between them. Different scenarios involving shifts in the Walker and Hadley circulations have been put forward to explain the occurrence or nonoccurrence of drought during El Nino years (e.g., Ju and Slingo, 1995; Goswami, 1998; Slingo and Annamalai, 2000; Lau and Wu, 2001).

Plenty of results are available on the space-time variability of the Southern Oscillation (SO). A possible relationship between the Southern Oscillation and ISMR was first demonstrated by Walker, (1924). Several of the predictor parameters used by Walker for long range forecasts of ISMR were some measures of the Southern Oscillation (SO).

In 1980s, more studies were taken up to explore the relationship of ISMR with Southern Oscillation. Association between ISMR and the Southern Oscillation Index (SOI) has also been studied (Pant and Parthasarathy, 1981; Parthasarathy and Pant, 1985). The SOI used is the difference of normalized sea level pressure between Tahiti (central Pacific) and Darwin (northern Australia), two stations located in the core regions of the circulation systems associated with the Southern Oscillation. The SOI values of different months and standard seasons show opposite tendencies during the deficient and excess years of ISMR. In 1990s, SOI and Darwin pressure tendency were used as the predictors in long range forecast models (Gowariker et al., 1989, 1991). However, this parameter was not used as a predictor due to weakening of its statistical correlation with ISMR in the forecast models used by Indian Meteorological Division (IMD) in the later years (Rajeevan et al., 2006).

The role of the sea surface temperature over the Arabian Sea on the southwest monsoon over India has been a subject of debate for a long time (Pisharoty, 1965; Saha and Bhavadekar, 1973; Shukla and Misra, 1977; Weare, 1979; Joseph and Pillai, 1984). Observational studies on the relationship between the Indian Ocean Sea Surface Temperature (SST) and the Indian monsoon mostly focused on the correlative aspect of the relationships (Saha, 1970; Cadet and Diehl, 1984; Joseph et al., 1994; Clark et al., 2000; Rajeevan et al., 2002). It is important to note that seasonal variations of the SST over this region are very large, but the inter-annual variations are very weak. The relationship between the Arabian Sea SST

and monsoon rainfall had been reexamined by removing the large amplitude high frequency noise and very low-frequency long-term trends (Rao and Goswami, 1988). They found that there exists a homogenous region in the south-eastern Arabian sea where the March-April (MA) SST anomalies significantly correlate with the seasonal (June to September) rainfall over India. The relationship of SSTs over south Indian Ocean with ISMR has been addressed (Verma, 1990). The importance of SST anomalies over the equatorial Indian Ocean, which influenced ISMR adversely during the 1987 El-Nino has been emphasized (Krishnamurti et al., 1989). The study suggests a strong correlation between ISMR and Pacific SST anomalies than with Indian Ocean SST anomalies (Shukla and Paolino, 1983).

Solar Activity and Rainfall

The influence of solar activity on climate has been a matter of debate for a long time. That solar activity affects the North Atlantic Oscillations (NAO) was also shown by Kodera and Kuroda (2002). They showed that during solar maximum phases, the NAO covers the northern hemisphere and extends to the stratosphere by contrast to the minima phases when it remains confined to the Atlantic sector and the troposphere. That solar activity plays an important role in influencing the precipitation on land and annual precipitation in Beijing is closely related to the variation of sunspot number has been observed by Zhao et al., (2004). It has been found that Indian rainfall is strongly correlated with the sunspot activity and overall trend is that during the period of low sunspot activity occurrence of rainfall is high compared to the period of high sunspot activity. (Hiremath, 2006). Recent study of the solar influence on the monsoon rainfall over Tamilnadu shows negative correlations between occurrences of sunspot number and rainfall activities (Selvaraj and Aditya, 2012). That the climate is influenced by the solar activity and all India rainfall is maximum when the sunspot numbers are minimum i.e. an anti correlation exists between rainfall and sunspot numbers (Selvaraj et al., 2013).

The activity of the Sun is expressed through various solar indices. Directly observed solar features e.g. sunspots, plagues, flares are highly reflected by these solar indices. Solar indices measure solar emissions at different wavelengths e.g. the 2800 MHz radio flux, the 530.3 nm Fe XIV coronal line intensities, the total solar irradiance. The best known and longest activity indices is the 10.7cm (2800 MHz) solar radio flux measured daily by the National Research Council of Canada since 1947. It is observed that variable component of solar parameters play a significant role on different atmospheric phenomena (Saha et al., 2011; Midya et al., 1999).

It has been reported that during the period 1700-1985, more El Ninos (63%) occurred in coastal Peru during the sunspot minima or in descending phase than in maxima or the ascending phase (37%) (Mendoza et al., 1991). The signature of solar activity variability in meteorological parameters has been studied (Tsiropoula, 2003). The Sun's output varies on a wide range of time scales from minutes to the billion year time scale of solar evolution. They appear quasi-periodically and can be divided into short (transient episodes solar activity like ares or Coronal Mass Ejections), intermediate term variations (16-month cycle discovered recently), long-term variations (11-year solar cycle, the 22-year Hale cycle of magnetic activity, the 80 to 90-year Gleissberg cycle, the 180 to 200 year de Vries cycle).

Walker (1924) reported the effect of sunspots on rainfall taking into account representative stations for the whole world. It has been concluded that for peninsular and northwest India, the apparent positive correlation between Rainfall in India and Sunspot activities, as reported by Walker and others does not hold good during recent sunspot cycles (Satakopan, 1946). A study on possible association between Indian Monsoon Rainfall and solar activity is made by Bhattacharyya and Narasimha (2005). Recent advances in reconstruction of the past climate with fine temporal resolution clarified the relationship between the solar cycles and the monsoon rainfall in South Oman with multiple time scales from decadal to millennial (Neff et al., 2001; Burns et al., 2002; Fleitmann et al., 2003). The direct cause of higher rainfall in South Oman was explained by stronger northward surface winds (Burns et al., 2002; Fleitmann et al., 2003). However, the mechanism of how the change in solar activity produces a regional circulation change remains unexplained.

A variation of $\delta^{18}\text{O}$ in stalagmites is related to the precipitation amount during the monsoon season. The relationship between the precipitation in South Oman and solar activity can be understood using modern meteorological datasets spanning from surface to 10 hPa. An equivalent relationship was first provided between the solar activity and the Indian Ocean monsoon found by paleoclimate studies. Next, an investigation was made on the processes whereby solar activity produces such effect. (Kodera, 2004)

Monsoon has been an intriguing puzzle since long. A number of climate records show correlations between solar cycles and climate, but the absolute changes in solar intensity over the range of decades to millennia are small and the influence of solar flux on climate is not well established. (Neff et al., 2001, Bhattacharyya and Narasimha, 2005).

It has now been established that a strong contribution to the total solar radiation occurred at 10.7 cm. Covington also showed that the 10.7 cm Solar Flux correlates with indices of solar activity such as Sunspot Number, Total Sunspot Area (Covington, 1948).

Determination of the strength of solar radio emission in a 100MHz-wide band centered on 2800 MHz (corresponding to a wavelength of 10.7 cm) averaged over an hour is made by 10.7 cm solar flux measurement. It is emitted primarily from the coronal plasma trapped in magnetic field over the active region, expressed in solar flux units (sfu, 1 sfu = $10^{-22} \text{ Wm}^{-2}\text{Hz}^{-1}$) and is a basic indicator of solar activity. It can vary from values below 50 to values above 300. Typically values in excess of 200 occur in periods of peak solar cycle. It comprises a time-varying mix of up to three principal emission mechanisms which may be differently distributed over the solar disk and may vary independently with time. It is used as a proxy for other solar emissions which are more difficult to obtain. (Tapping, 2013). The advantage of using the 10.7 cm index over others is that, the measurement of 10.7 cm Flux is completely objective and can be done in any weather.

In this study the Slowly Varying Component of 10.7cm Flux is computed since it is expected that while the Basic component remains steady over the years, the Variable component that depends directly on solar activity may be associated with the variability of different weather systems or Circulations.

Methods and Analysis

The area-weighted average of the daily rainfall at more than 300 rain-gauge stations spread across India is often used as an index of monsoon activity, and its cumulative value for monsoon period (June–September) is called the all-India summer monsoon rainfall (ISMR). Data for the monthly average for the period 1947-2006 has been taken from the website of Indian Institute of Tropical Meteorology (IITM, Pune). Whole Indian region has been divided into seven homogeneous regions namely North Mountainous India (NM India), North-East India (NE India), North Central India (NC India), North West India (NW India), North Peninsular India (NP India), South Peninsular India (SP India) and East Peninsular India (EP India).

The daily data for the relative sunspot number and 10.7 cm solar flux, adjusted to 1 AU (March – May) are taken from the official website of the US National Oceanic and Atmospheric Administration (NOAA), <http://www.ngdc.noaa.gov/ngdc.html> for the above-mentioned period.

The variable component of 10.7 cm solar flux is calculated by plotting the relative sunspot number against the 10.7 cm solar flux shown in Figure 1.

Calibration curve is drawn considering 10.7 cm solar radio flux and relative sunspot number data for large number of days and from that calibration curve, variable component is calculated for our required monsoon period.

Extrapolating to zero sunspot area, the line of the most probable relation between 10.7 cm solar flux and relative sunspot number, the basic component is obtained

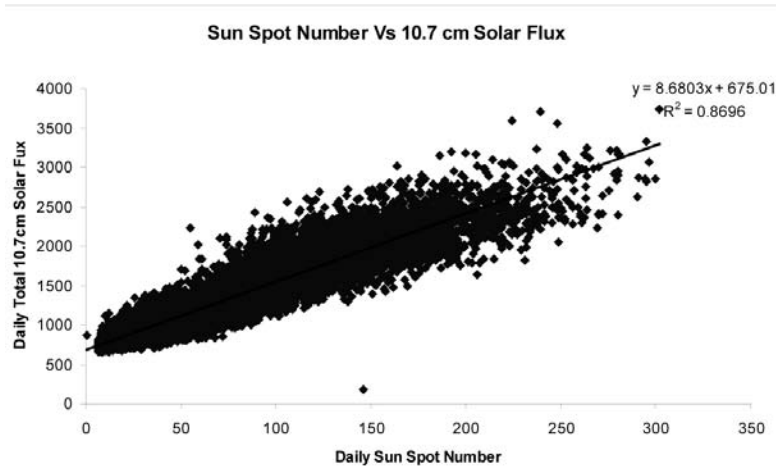


Figure 1. Variation of Daily sunspot against daily 10.7 cm solar Flux.

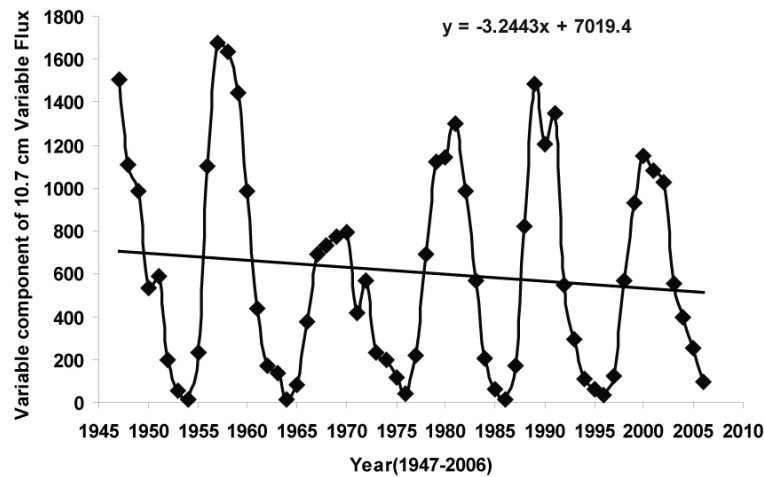


Figure 2. Variation of variable component of 10.7 cm solar flux during monsoon period for the period 1947-2006 (data only for monsoon months).

and it is the quiet sun emission. The emission above the base level is called the variable component of 10.7 cm solar flux which is computed from daily value of 10.7 cm solar flux adjusted to 1 AU. The time series analysis of monsoon rainfall over the above mentioned period has been performed along with time series analysis of variable components of 10.7 cm solar flux to evaluate the effect of solar activity over precipitation.

RESULTS AND DISCUSSION

Variation of 10.7 cm variable flux and rainfall during Monsoon period:

Figure 2 shows the trend of variation of variable components of 10.7 cm solar flux during monsoon (June-September) period.

Figures 3(a-h) show the trends of monsoon rainfall over All India, NM India, NE India, NC India, NW India,

NP India, SP India and EP India respectively. Thus, it is found that both F10.7 and Summer Monsoon Rainfall show an approximate sinusoidal pattern of the same nature but overall, there appears to be a decreasing trend for both emission of 10.7 cm Solar Flux as well as the Monsoon Rainfall for all the regions during the chosen period of study.

Rainfall is a complicated phenomena. There are different factors which are related to rainfall. Heavy rainfall occurs near the equator and decreases with the increase in the latitude i.e. towards polar regions. Rainfall tends to be heavier near coastlines as main source of moisture for rainfall is evaporation from oceans. Rainfall is influenced by pressure and temperature variation in a particular area. Presence of mountains produce orographic rainfall. So point to point regression is quite unexpected. In some cases, the trend is not so significant, but it is clear that there is an overall decreasing trend in all cases.

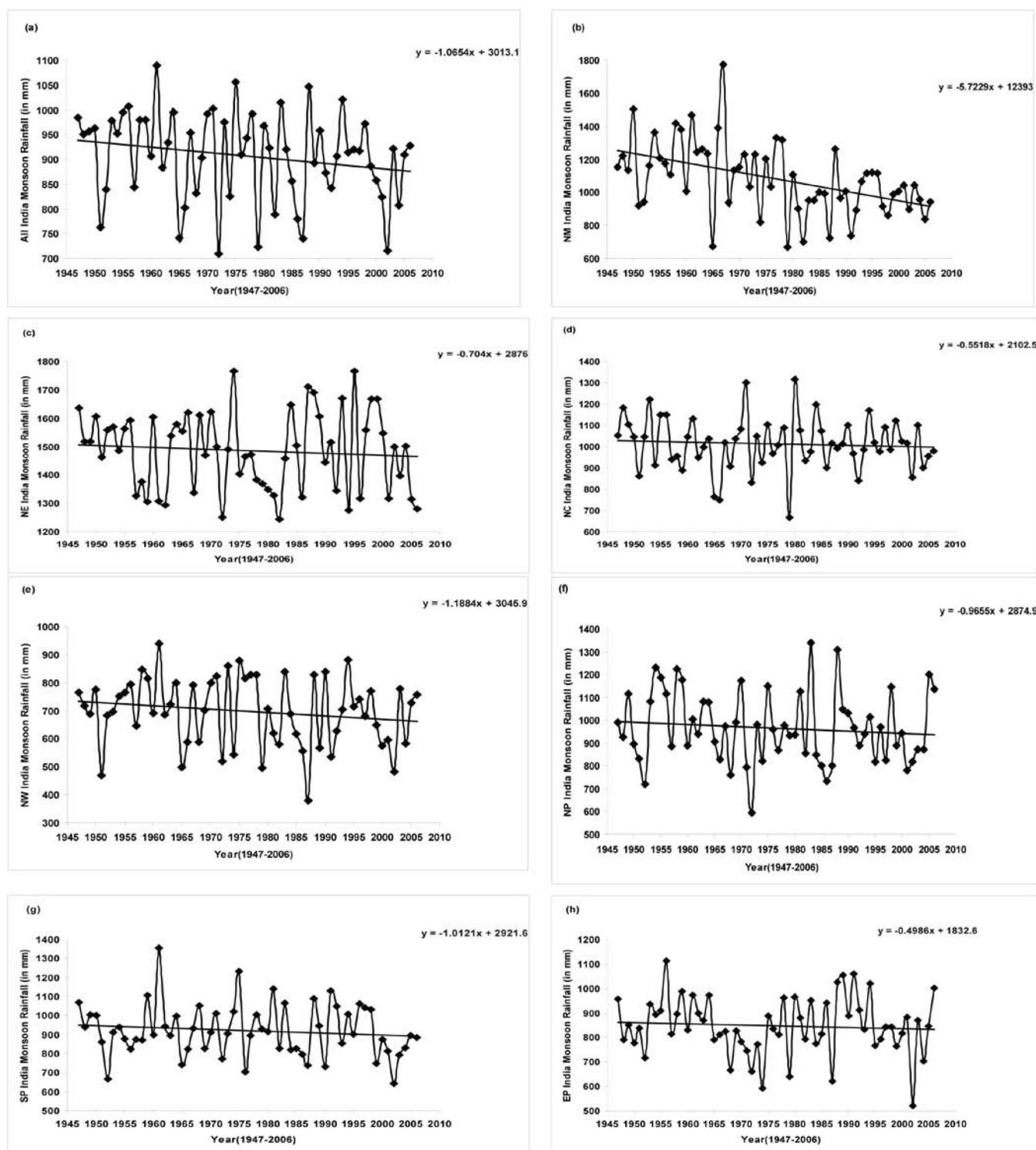


Figure 3. Trends of monsoon rainfall over (a) All India, (b) NM India, (c) NE India, (d) NC India, (e) NW India, (f) NP India, (g) SP India and (h) EP India for the period 1947-2006.

With the increase of magnetospheric activities, decrease of cosmic ray is quite expected. It may affect the decrease of cloud formation. Again, if cloud formation is significant,

rainfall may not occur in large scale due to the decrease of other rain forming constituents. In our analysis increase of rainfall is due to large availability of rain producing elements.

CONCLUSIONS

In an earlier communication, it is shown that variable component of 10.7 cm solar flux has a significant effect on different atmospheric phenomena (Saha et al., 2011; Midya and Saha, 2011)

Bhalme and Mooley found a highly significant (approximately 22 years) solar cycle in flood area index and weak quasi periodicity of 2.7 to 3.0 years (Quasi Biennial Oscillation, QBO) in drought area index for India for monsoon season (Bhalme and Mooley 1980, 1981).

From Cross-spectrum analysis they showed that the approximate 22 years cycle in the flood area index is related to double sunspot cycle.

It is quite expected that variable component of 10.7 cm solar flux plays a significant role for the production of water molecules in the vapour state and hence rainfall rate will be affected with variation of variable component of 10.7 cm solar flux.

Our result shows that rainfall trend (both monsoon and total) decreases with the decrease of variable component of 10.7 cm solar flux. This fairly agrees with our explanation.

ACKNOWLEDGEMENTS

We acknowledge with thanks to Indian Institute of Tropical Meteorology (IITM, Pune) for rainfall Data and NOAA National Geophysical data centre for Solar data. We are also thankful to unknown reviewers for valuable suggestions and comments. We thank Dr.Nandini Nagarajan for constructive evaluation of the manuscript. We also thank Dr. MRK Prabhakar Rao and Chief Editor for editing the manuscript.

Compliance with Ethical Standards

The authors declare that they have no conflict of interest and adhere to copyright norms.

REFERENCES

- Achuthavarier, D., Krishnamurthy, V., Kirtman, B.P., and Huang, B., 2011. Role of Indian Ocean in the ENSO-Indian summer monsoon teleconnection in the NCEP Climate Forecast System, COLA Technical Report 309 (February 2011).
- Barnett, T. P., 1983. Interaction of the Monsoon and Pacific Trade Wind System at Interannual Time Scales Part I: The Equatorial Zone, *Mon. Wea. Rev.*, v.111, no.4, pp: 756-773.
- Bhalme, H. N., and Mooley, D. A., 1980. Large scale droughts/floods and monsoon circulation, *Mon.Wea.Rev.*,v.108, pp: 1197-1211.
- Bhalme, H. N., and Mooley, D. A., 1981. Cyclic fluctuations in the flood area and relationship with the double (Hole) sunspot cycle, *J.Climatol.Appl.Meteor.*,v.20, pp: 1041-1048.
- Bhattacharyya, S., and Narasimha, R., 2005. Possible association between Indian monsoon rainfall and solar activity, *Geophys. Res. Lett.*, L05813. Doi:10.1029/2004GL021044, v.32.
- Burns, S. J., Fleitmann, M., Mudelsee, U., Neff, A., Matter, A., and Mangini, A. A., 2002. A780-year annually resolved record of Indian Ocean monsoon precipitation from a speleothem from south Oman, *J. Geophys. Res.*, doi:10.1029/2001JD001281., v.107, no.D20, pp: 4434.
- Cadet, D., and Diehl, B., 1984. Interannual variability of surface fields over the Indian Ocean during recent decades, *Monthly Weather Review*, v.112, pp: 1921-1935.
- Clark, C. O., Cole, J. E., and Webster, P. J., 2000. Indian Ocean SST and Indian summer rainfall: Predictive relationships and their decadal variability, *J. Climate*, v.13, pp: 2503-2519.
- Covington, A. E., 1948. Solar radio noise observations at 10.7 cm, *Proc IRE*, v.36, pp: 454-457.
- Fleitmann, D., Burns, S. J., Mudelsee, M., Neff, U., Kramers, A., Mangini, A., and Matter, A., 2003. Holocene forcing of the Indian monsoon recorded in a stalagmite from southern Oman, *Science*, v.300, pp: 1737- 1739.
- Goswami, B. N., 1998. Interannual variations of Indian summer monsoon in a GCM: External conditions versus internal feedbacks, *J. Climate*, v.11, pp: 501-522.
- Gowariker, V., Thapliyal, V., Sarker, R. P., Mandel, G. S., and Sikka, D. R., 1989. Parametric and power regression models: New approach to long range forecasting of monsoon rain in India, *Mausam*, v.40, pp: 115-122.
- Gowariker, V., Thapliyal, V., Kulshrestha, S. M., Mandel, G. S., SenRoy, N., and Sikka, D. R., 1991. A power regression model for long range forecast of southwest monsoon rainfall over India, *Mausam*, v.42, pp: 125-130.
- Hiremath, K. M., 2006. The Influence of Solar Activity on the Rainfall over India:Cycle-to-Cycle Variations, *J. Astrophys. Astr.*, v.27, pp: 367-372.
- Joseph, P. V., and Pillai, P. V., 1984. Air-sea interaction on a seasonal scale over north Indian Ocean, Part-I: Interannual variations of sea surface temperature and Indian summer monsoon rainfall, *Mausam*, v.35, pp: 323-330.
- Joseph, P. V., Eischeid, J. K., and Pyle, R. J., 1994. Interannual variability of the onset of the Indian summer monsoon and its association with atmospheric features, El Nino, and sea surface temperature anomalies, *J. Climate*, v.7, pp: 81-105.
- Ju, J., and Slingo, J., 1995. The Asian summer Monsoon and ENSO, *Quart. J. Roy. Meteor. Soc.*, v.121, pp: 1133-1168.
- Kane, R. P., 2005. Unstable ENSO Relationship with Indian regional rainfall, *Int. J. Climatol.*, v.26, no.6, pp: 771-783.
- Keshavamurthy, R. N., 1982. Response of the Atmosphere to Sea Surface Temperature Anomalies over the Equatorial Pacific and the Teleconnections of the Southern Oscillation, *J. Atmos. Sci.*, v.39, pp: 1241-1259.
- Kodera, K., 2004. Solar influence on the Indian Ocean Monsoon through dynamical processes, *Geophys. Res. Lettters*, L24209, doi: 10.1029/2004 GL020928, v.31.

- Kodera, K. K., and Kuroda, Y., 2002. Dynamical response to the solar cycle, *J. Geophys. Res.*, doi : 10.1029/2002JD002224., v.107, no.D24, pp: 4749.
- Kripalani, R.H., and Kulkarni, A., 2001. Monsoon Rainfall Variations and Teleconnections Over South and East Asia, *Int. J. Climatol.*, v.21, pp: 603-616.
- Krishna Kumar, K., Rajagopalan, B., and Cane, M. A., 1999. On the weakening relationship between the Indian Monsoon and ENSO, *Science*, v.284, pp: 2156-2159.
- Krishna Kumar, K., Rajagopalan, B., Hoerling, M., Bates, G., and Cane, M., 2006. Unraveling the Mystery of Indian Monsoon Failure during El Nino, *Science*, doi:10.1126/science.1131152., v.314, pp: 115-119.
- Krishnamurti, T. N., Bedi, H. S., and Subramaniam, M., 1989. The summer monsoon of 1987, *J. Climate*, v.2, pp: 321-340.
- Krishnamurthy, V., and Goswami, B. N., 2000. Indian monsoon-ENSO relationship on Interdecadal time scale, *J. Climate*, v.13, pp: 579-595.
- Lau, K.M., and Wu, H.T., 2001. Principal modes of rainfall-SST variability of the Asian summer monsoon: A reassessment of the monsoon-ENSO relationship, *J. Climate*, v.14, pp: 2880-2895.
- Maity, R., and Nagesh Kumar, D., 2007. Hydroclimatic teleconnection between global sea surface temperature and rainfall over India at subdivisional monthly scale, *Hydrol. Process.*, DOI:10.1002/hyp.6300., v.21, pp: 1802-1813.
- Mendoza, B., Pe'rez-Enri'quez, R., and Alvarez-Madrigal, M., 1991. Analysis of solar activity conditions during periods of El-Nino events, *Ann. Geophys.*, v.9, pp: 50-54.
- Midya, S. K., Chattopadhyay, R., and Pal, C. M., 1999. The Effect of Relative Sunspot Numbers, Solar Flare Numbers and Variable Components of 10.7 cm Solar Flux on the Seasonal Variation of 6300A line at Calcutta, *Earth Moon and Planets (Netherlands)*, v.77, pp: 93-97.
- Midya, S. K., and Saha, U., 2011. Rate of Change of Total Column Ozone and Monsoon Rainfall – A co-variation with the Variable Component of 10.7 cm Solar Flux during pre-monsoon period, *Mausam*, v.62, no.1, pp: 91-96.
- Mooley, D. A., and Parthasarathy, B., 1984. Indian summer monsoon and El Nino, *Pure and Applied Geophys.*, v.121, pp: 339-352.
- Neff, U., Burns S. J., Mangini, A., Mudelsee, M., Fleitmann, D., and Matter, A., 2001. Strong coherence between solar variability and the monsoon in Oman between 9 and 6 kyr ago, *Nature*, v.411, pp: 290– 293.
- Pai, D.S., 2003. Teleconnections of Indian summer monsoon with global surface air temperature anomalies, *Mausam*, v.54, pp: 407-418.
- Pant, G. B., and Parthasarathy, B., 1981. Some aspects of an association between the southern oscillation and Indian summer monsoon, *Arch. Meteorol. Geophys. Bioklimaetol.*, v.1329, pp: 245-252.
- Parthasarathy, B., and Pant, G. B., 1985. Seasonal relationship between Indian summer monsoon rainfall and Southern Oscillation, *J. Climatol.* v.5, pp: 369-378.
- Pisharoty, P. R., 1965. Evaporation from the Arabian sea and the Indian southwest Monsoon, *Proceedings of International Indian Ocean Expedition (IIOE)*, P.R.Pisharoty (Eds), pp: 43-54.
- Rajeevan, M., and Pai, D. S., 2007. On the El Nino-Indian Monsoon predictive relationships, *Geophys. Res. Letters*, L04704, doi: 10.1029/2006GL028916., v.34.
- Rajeevan, M., Pai, D. S., Anil Kumar, R., And Lal, B., 2006. New Statistical models for long-range forecasting of southwest monsoon rainfall over India, *Climate Dynamics*, doi: 10.1007/s00382-006-019706., v.28, pp: 813-828.
- Rajeevan, M., Pai, D. S., and Thapliyal, V., 2002. Predictive relationships between Indian Ocean sea surface temperatures and Indian summer monsoon rainfall, *Mausam*, v.53 pp: 337-348.
- Rao, K. G., and Goswami, B. N., 1988. Inter-decadal variations of sea surface temperature over the Arabian Sea and the Indian monsoon- a new perspective, *Mon. Wea. Rev.*, v.116, pp: 558-568.
- Rasmusson, E. M., and Carpenter, T. H., 1983. The relationship between Eastern Equatorial Pacific sea surface temperatures and rainfall over India and Sri Lanka, *Mon. Wea. Rev.*, v.1, pp: 517-528.
- Saha, K., 1970. Zonal anomaly of sea surface temperature in equatorial Indian Ocean and its possible effect upon monsoon circulation, *Tellus*, v.22, pp: 403-409.
- Saha, S., and Bavadekar, S. N., 1973. Water vapour budget and precipitation over the Arabian sea during the northern summer, *Quart. J. Royal. Met. Soc.*, v.99, pp: 273-278.
- Saha, U., Midya, S. K., and Das, G. K., 2011. The Effect of the Variable Component of 10.7 cm Solar flux on the Thunderstorm frequency over Kolkata and its Relation with Ozone Depletion Mechanism, *The Pacific Journal of Science and Technology (Akamai)*, v.12, no.1, pp: 591-597.
- Satakopan, V., Jun 1946. Sunspots and monsoon rainfall in India, *Current Science*, v.109, no.6, pp: 151-153.
- Selvaraj, R. S., and Aditya, R., 2012. The solar influence on the monsoon rainfall over Tamilnadu, *J. Ind. Geophys. Union*, v.16, no.3, pp: 107-111.
- Selvaraj, R.S., Umarani, P. R., and Mahalakshmi, N., 2013. Correlative study on Solar activity and all India rainfall: Cycle to Cycle Analysis, *J. Ind. Geophys. Union*, v.17, no.1, pp: 59-63.
- Shukla, J., and Misra, B. M., 1977. Relationships between sea surface temperature and wind speed over the central Arabian sea and monsoon rainfall over India, *Mon. Wea. Rev.*, v.105, pp: 998-1002.
- Shukla, J., and Paolino, D. A., 1983. The Southern Oscillation and long range forecasting of summer monsoon rainfall over India, *Mon. Wea. Rev.*, v.111, pp: 1830-1837.

The effect of 10.7 cm solar flux on the monsoon rainfall over India

- Sikka, D. R., 1980. Some aspects of the large scale fluctuations of summer monsoon rainfall over India in relation to fluctuations in the planetary and regional scale circulation parameters, *Proc. Indian Acad. Sci.(Earth Planet Science)*, v.89, pp: 179-195.
- Slingo, J.M., and Annamalai, H., 2000. The El Nino of the century and the response of the Indian summer monsoon, *Mon. Wea. Rev.*, v.128, pp: 1778-1797.
- Tapping, K.F., 2013. The 10.7 cm solar radio flux (F10.7), *Space Weather*, doi:10.1002/swe.20064, v.11, pp: 394-406.
- Tsiropoula, G., 2003. Signatures of solar activity variability in meteorological Parameters, *Journal of Atmospheric and Solar-Terrestrial Physics*, v.65, pp: 469- 482.
- Verma, R. K., 1990. Recent monsoon variability in the global climate perspective, *Mausam*, v.41, pp: 315-320.
- Walker, G. T., 1924. Correlation in seasonal variation of weather, IX: A further study of world weather, *Memoirs of India Met Dept*, v.24, pp: 275-332.
- Wang, B., and Fan, Z., 1999. Choice of South Asian summer Monsoon Indices, *Bulletin of American Meteorological Society*, v.80, no.4, pp: 629-638.
- Weare, B.C., 1979. A statistical study of the relationship between surface temperature and the Indian monsoon, *J. Atmos. Science.*, v.36, pp: 2279-2291.
- Webster, P. J., and Yang, S., 1992. Monsoon and ENSO: Selectively interactive Systems, *Quart. J.Roy. Met. Soc.*, v.118, pp: 877-926.
- Zhao, J., Han, Yan-Ben and Li, Zhi-An, 2004. The Effect of Solar Activity on the Annual Precipitation in the Beijing Area, *Chin. J. Astron. Astrophys.*, v.4, no.2, pp: 189-197.

Chaotic analysis of daily and weekly rainfall timeseries over Chennai

S. Tamil Selvi*¹ and R. Samuel Selvaraj²

¹Research centre, Department of Physics, Bharathiar University, Coimbatore, Tamil Nadu, India

²Department of Physics, Presidency College, Chennai, Tamil Nadu, India

*Corresponding Author : tssekar9773@gmail.com

ABSTRACT

In this work the reconstruction of phase space and G-P algorithm (correlation dimension) are used to study the chaotic characteristics of daily and weekly rainfall at Chennai, Tamil Nadu. The results show that the daily and weekly rainfall series have a low dimensional chaos. This is also verified using Lyapunov exponent method, which is used to confirm the presence of chaos. The maximum Lyapunov exponent is used to calculate the predictability time. The essential number of parameters in the embedding dimension for the two series were calculated to be 2. The sufficient number of parameters were calculated to be 4 and 6 respectively. The presence of large number of zeros in the high resolution time series may result in underestimation of the dimension, still correlation dimension is the elementary test for the chaos identification. The embedding dimension calculated from the correlation dimension gives the underlining number of parameters to be used in the forecast model.

Key words: correlation dimension, daily and weekly rainfall, low dimensional chaos, Lyapunov exponent method and embedding dimension.

INTRODUCTION

Time series data, such as rainfall, are very complex to model and study. The difficulty lies in the large range of variability displayed, both in time and space. The variables are mostly inter-related and they are stochastic and unpredictable. Nonlinear dynamics is a rapidly growing field with a new set of tools to analyse such complex processes. Investigation of the presence of low dimensional chaotic behaviour in rainfall dynamics has been of much interest lately. India Meteorological Department (IMD) has been using the power regression and parametric models for long range forecast of monsoon rainfall. These models are used for long range forecast over India, as a whole and for the four clusters of meteorological subdivisions. The statistical models have innate limitations as an alternate technique for the forecast of monsoon rainfall is desirable. Such a model has not been developed so far forecasting techniques for individual states and meteorological subdivisions (Rajeevan, Michaeland and McPhaden, 2004). The Indian rainfall, especially the summer monsoon system has been analysed extensively. The winter monsoon or the northeast monsoon is very less investigated, due its complexity. This paper explores the possible number of variables that may govern the dynamics in the rainfall series during northeast monsoon season over Chennai city.

In any system, if the underlying dynamics is governed by a deterministic equation, the system exhibits a nonlinear chaotic nature which could be random (Kantz, Holger, and Schreiber, 2004). The randomness in most of the natural systems can be attributed to this reason. Initially, most of

the forecast techniques used linear stochastic approach (Harms, Archie and Campbell, 1967; Klemes, 1978; Salas et al., 1981) mainly due to lack of other computational methods. For a multivariate dynamical system like monsoon an approach of Phase space reconstruction can be used to study its dynamics (Packard and Norman, et al., 1980) (Grassberger, Peter, and Itamar Procaccia, 1983). The phase space method enables one to obtain information about the behaviour of the system without explicit knowledge of the dynamical system or its actual solutions (Satyan, 1988). The possible short term prediction in an intermittent time series which is actually deterministic can be found using chaotic analysis. The likelihood of long term prediction can also be analysed. This simplifies the complexities in modelling the natural systems and produces accurate prediction (Williams and Garnett, 1997).

Several nonlinear methods, such as the method of time delays (Takens and Floris, 1981), correlation dimension, Lyapunov spectrum (Sano, Masaki and Sawada, 1985), mutual information (Fraser, Andrew and Harry, 1986) and False nearest neighbour method (Kennel, Brown and Abarbanel, 1992). Cao's method have been widely used for identifying the behaviour and to analyse the properties of the systems (Cao and Liangyue, 1997). It is reported that the number of dimensions that governs a particular process can be identified through nonlinear chaotic analysis which is computationally easier (Sivakumar, 2000). The Correlation dimension method is most widely used and it can be treated as a method for substantiating the presence of chaos in the system. The presence of chaos on different time scale of the time series data is analysed. The rainfall for a period

of 43 years (1971-2013) have been analysed with two time scales, i.e., dailyseries and weekly series.

Study Area

Chennai city, situated on the shores of the Bay of Bengal, is the capital of Tamil Nadu and the fourth largest metropolis in India. The Chennai regional Metropolis (with the latitude between 12°50'49" and 13°17'24", and the longitude between 79°59'53" and 80°20'12") is located on the Coramandal coast in South India and the land is a flat coastal plain. Chennai has a tropical climate and there is not much temperature variation among different seasons. The annual rainfall recorded over Chennai is 122 cm. Occasional flooding takes place after intense rainfall events. Most of this annual rainfall is recorded during northeast monsoon season. The weather is hot and humid, for most part of the year.

Data and Methodology

A data set of daily rainfall of Chennai city for a period of 43 years (1971-2013) was obtained from Regional Meteorological Centre, Chennai. This long term data is considered due to the presence of 55% zeros in the daily rainfall. The city records most of its rainfall only during the northeast monsoon season (October to December). The data set was arranged considering only October, November and December daily rainfall values from 1971-2013. A total of 3907 data points were used.

Chaotic analysis of Time series

Reconstruction of the phase space

For a scalar time series x_t , where $t = 1, 2, \dots, N$, the phase space can be reconstructed using the method of delays. The basic idea in the method of delays is that the evolution of any single variable of a system is determined by the other variables with which it interacts. Information about the relevant variables, is thus implicitly contained in the history of any single variable. On the basis of this an "equivalent" phase space can be reconstructed by assigning

an element of the time series x_t and its successive delays as coordinates of a new vector time series

$$Y_t = \{x_t, x_{t-\tau}, x_{t-2\tau}, \dots, x_{t-(m-1)\tau}\}$$

Where $t = 1, 2, \dots, N-(m-1)\tau/\Delta t$, m is the dimension of the vector Y_t , also called the embedding and τ is a delay time taken to be some suitable multiple of the sampling time Δt (Packard and Norman, et al., 1980). Take a scalar time series x_1, x_2, \dots, x_n in system phase space as an example. Supposing its dimension d is 1, its dimension of embedding phase space should be three. If $m=4$ x_1, x_2, x_3, x_4 forms the first vector Y_1 of a four dimensional state space and then moving right on step, x_2, x_3, x_4, x_5 forms the second vector Y_2 . Thus in the same way $Y_1, Y_2, Y_3, \dots, Y_l$ forms the time series of reconstructed phase space.

Correlation Dimension analysis:

In order to identify the Chaos in the system, it is first embedded into an m -dimensional pseudo phase space spanned by the time series and its time-shifted values so that a point in the space is described by

$$X(t) = \{x(t), x(t+\tau), \dots, x_{[t+(m-1)\tau]}\},$$

Where $x(t)$ is the time series and τ is the fixed time delay. The next step involves the calculation of the cumulative correlation function (Henderson and Wells, 1988).

$$C(l) = \frac{1}{N^2} \sum_{i,j=1}^N H(l - r_{ij})$$

Where r_{ij} is the Euclidean distance between the i^{th} and j^{th} points, N is the total number of points, l is a distance variable and H is the Heaviside function with $H(x) = 0$ if $x \leq 0$ and $H(x) = 1$ if $x > 0$. Next we calculate the slope $d(m)$ of the linear part of the $\ln C(l)$ vs. $\ln(l)$ curve by fitting a least square line. By repeating the process for $m = 1, 2, 3, 4, 5, \dots$ we obtain successive estimates of the attractor dimension. If the slope converges to a limiting value $d_\infty = d(M) = d(M+1) = \dots$, then d_∞ is the true correlation dimension of the attractor and the corresponding embedding dimension M is a measure of the number of variable sufficient to model the dynamics. A non-integer value of d_∞ indicates

Table 1. Statistics of rainfall data for different temporal scales at Chennai city

Parameters	Daily rainfall(mm)	Weekly rainfall(mm)
Number of data	3906	558
Mean	9.028	63.19
Standard deviation	23.741	89.714
Coefficient of Variation	2.63	1.42
maximum value	346.6	604.5
Minimum value	0.0	0.0
Percentage of zeros	55 %	17%

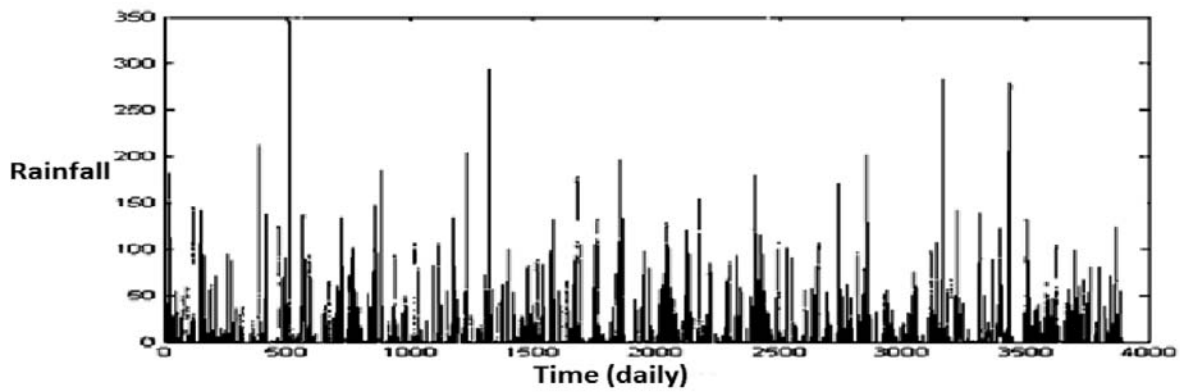


Figure 1a. Time series plot of Chennai Daily rainfall (mm).

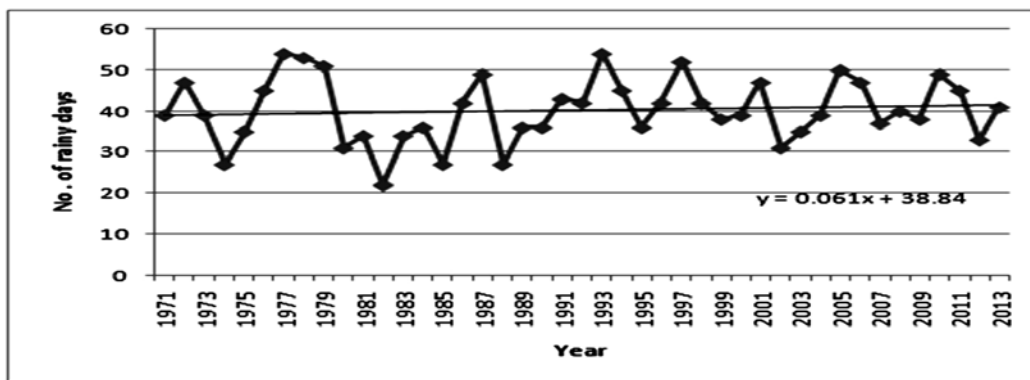


Figure 1b. A plot for the number of rainy days from 1971-2013.

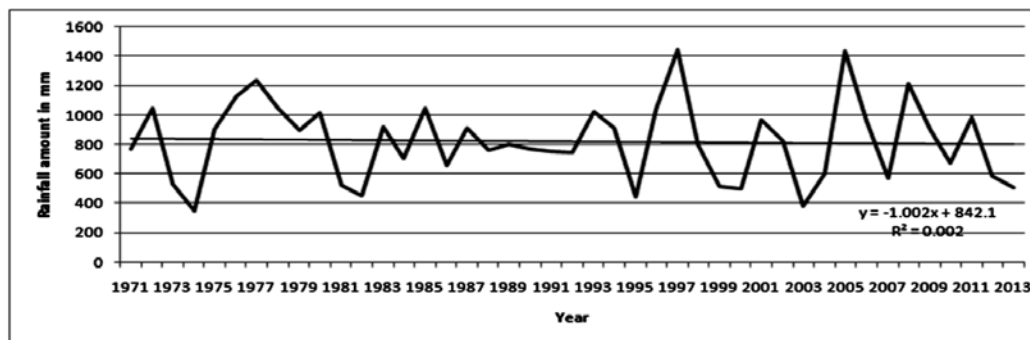


Figure 1c. A plot for the amount of rainfall received from 1971-2013.

the presence of a strange attractor, a term coined by Ruelle and Takens (Ruelle, David and Takens,1971), signifying deterministic but chaotic dynamics. It is interesting to note that there will be no saturation of slopes for a purely random time series.

In order to investigate the existence of chaotic behaviour in the rainfall dynamics on different time scales, we applied the method sketched above to 43 year time series of Chennai city's northeast monsoon rainfall. The data were grouped into two sets, a daily series and weekly series. Table 1 gives some of the important statistics of the rainfall series.

Analysis of Chennai daily rainfall series

Chennai daily rainfall time series data are used for analysis. The number of data point is 3907 daily total with 45% of nonzero values in it. Figure 1a shows the time series plot for the daily rainfall data. Even though there are prominent peaks observed in the plot, the irregular behaviour of the series does not indicate whether the series is deterministic, stochastic or chaotic. In order to analyse the daily rainfall data, a graph is plotted by considering the number of rainy days in each year (Figure 1b) and another plot is made for the total amount of rainfall received in each year (Figure 1c).

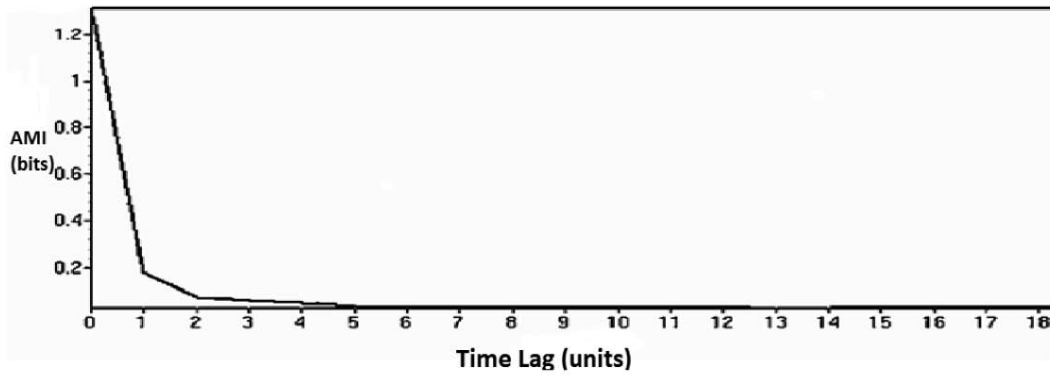


Figure 2. Average mutual information for estimating time delay calculation.

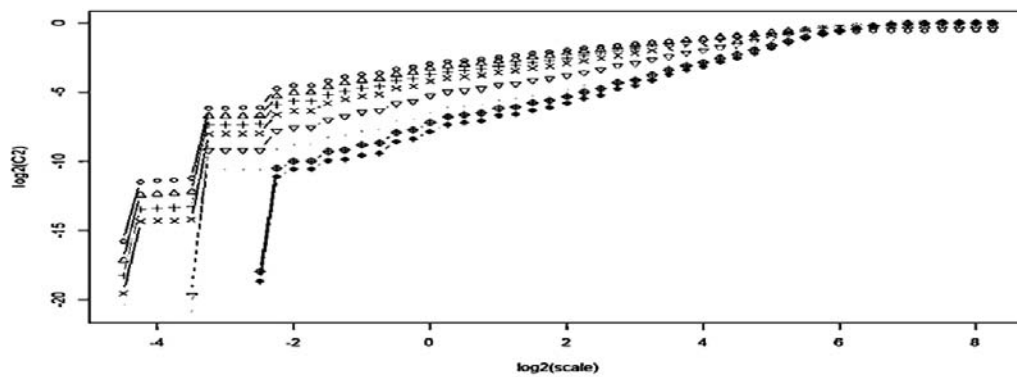


Figure 3. Correlation sum for daily rainfall series for different embedding dimension ($m=1$ to $m=10$).

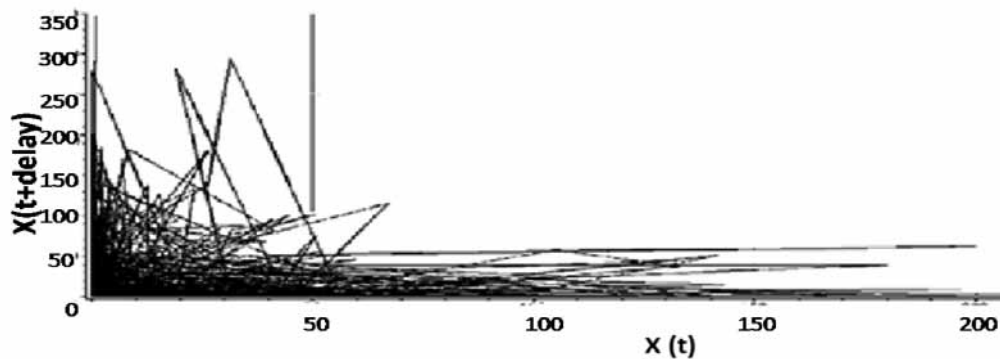


Figure 4. Reconstructed phase space for Chennai daily rainfall.

The trendline in the plot clearly shows that the number of rainy days increases (increasing trend) and at the same time the intensity (amount) of rainfall decreases (decreasing trend). Chennai has experienced particularly heavy rains roughly once every 10 years—1969, 1976, 1985, 1996, 1998, 2005 and 2015.

Further investigation is done using the correlation dimension. The time delay was calculated using the Average Mutual Information (AMI) function using the Visual recurrence analysis (VRA). The delay coordinate for Chennai daily rainfall series was 8.

Figure 2 shows the AMI chart for the daily series. The correlation sum and the correlation exponent were calculated using the R statistical software. Figure 3 shows the correlation sum for daily rainfall data for a time delay of 8. The correlation exponent increases with increase in embedding dimension up to a certain value and saturates further. The saturation value of the correlation dimension $d_c = 0.487$. This indicates the presence of a low dimension attractor in Chennai daily rainfall series. The dimension of a reconstructed phase space can be estimated from Takens (1981) embedding theorem. It was calculated to be 1.974.

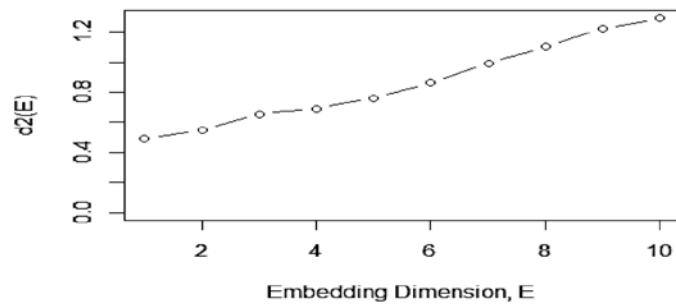


Figure 5. Relation between correlation dimension and Embedding dimension for Chennai daily rainfall series.

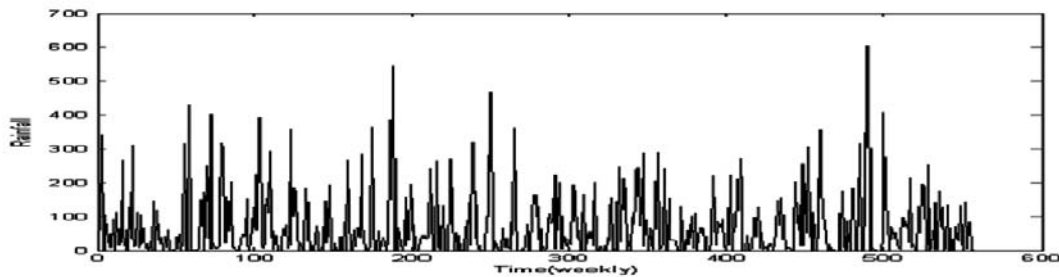


Figure 6. Time series plot of Chennai weekly rainfall.

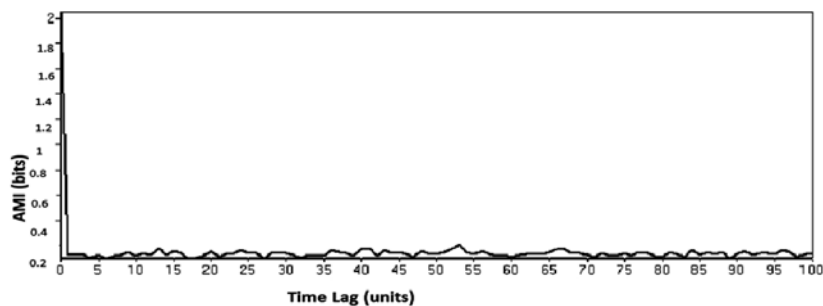


Figure 7. Time lag by average mutual information function for weekly rainfall.

A reconstructed space phase for the daily rainfall series is in two dimension with $m=2$, time delay $\tau= 1$ is shown in Figure 4. The projection of attractor on the plane $\{X_i, X_{i+1}\}$ is shown here. It can be inferred from the figure that the projection does not show a clear well defined attractor. Also it is not scattered over the entire region of phase space. The Figure 4 suggests that the dynamics of Chennai city rainfall exhibits intermediate level of complexity.

The estimation of embedding dimension, m , was further verified by the False Nearest Neighbour (FNN) method using Visual Recurrence Analysis (VRA). The value from FNN method was estimated to be $m=1$. The saturation value of the correlation exponent presented in Figure 5 occurs at $m= 4$. This value of saturation provides the upper bound of phase space sufficient to describe the dynamics of the attractor. According to the theory of non-linear dynamics, the dimension of the phase space is equal to number of variables present in the evolution of the system. Thus in the analysis of the Chennai daily

rainfall series, the low dimensional attractor in it can be modelled with minimum number of essential variables equal to 2 and number of sufficient variables is 8. Thus on a small temporal scale the rainfall dynamics shows persistence.

Analysis of Chennai weekly rainfall series:

Chaotic analysis was performed using the time series for the weekly rainfall data. The data from Thursday to Wednesday (meteorological week in use in IMD) were aggregated to form the weekly data. Figure 6 shows the weekly rainfall data record.

The total number of samples is 558 with 83 % of non-zero values in it. The average mutual information function for the weekly time data is shown in the Figure 7. It is clear from the figure that there is a complete loss of information after two weeks indicating it is an optimal time delay.

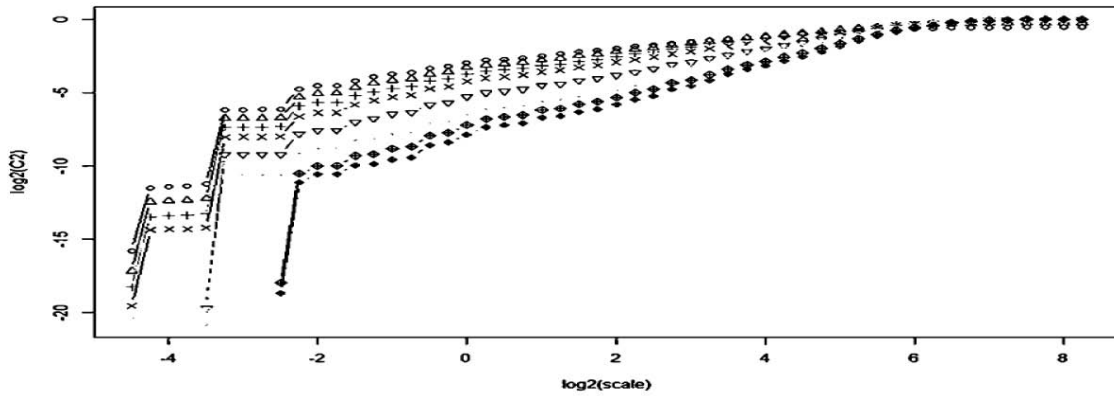


Figure 8. Correlation sum graph for the weekly rainfall.

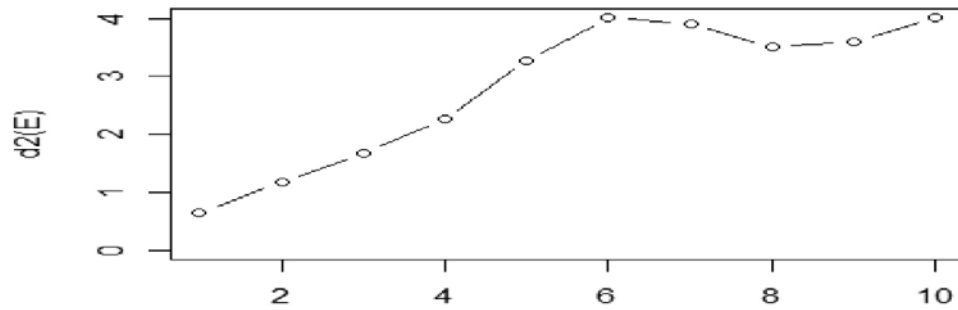


Figure 9. Relation between embedding dimension and correlation integral for weekly rainfall.

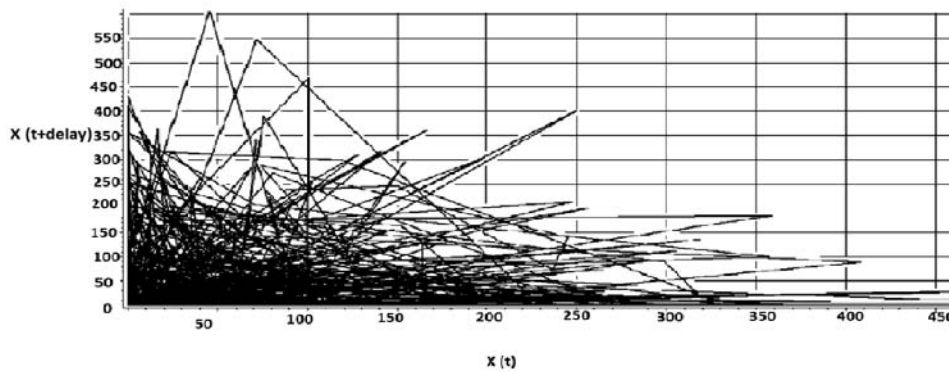


Figure 10. Phase space reconstruction for weekly rainfall.

The correlation sum for the weekly rainfall data is shown in Figure 8. The relationship between the correlation exponent and the embedding dimension for the reconstructed phase space is shown in Figure 9. The correlation exponent increases with increase in the embedding dimension up to a certain value and saturates at $d_c = 0.655$. Thus the sufficient embedding dimension for describing the system as per Taken's (1981) theorem was found to be 2.31.

The saturation value of the correlation exponent presented in Figure 9 occurs at $m = 6$. This value of saturation provides the upper bound of phase space

sufficient to describe the dynamics of the attractor. According to the theory of non-linear dynamics the dimension of the phase space is equal to the number of variables present in the evolution of the system.

Thus in the analysis of the Chennai daily rainfall series, the low dimensional attractor in it can be modelled with minimum number of essential variables equal to 2 and number of sufficient variables is 8. Thus on a small temporal scale the rainfall dynamics shows persistence. The essential number of variables required for the evolution of the system is same for both daily and the weekly rainfall, unlike the 8 parameter model used by Guhathakurta et al., (1999).

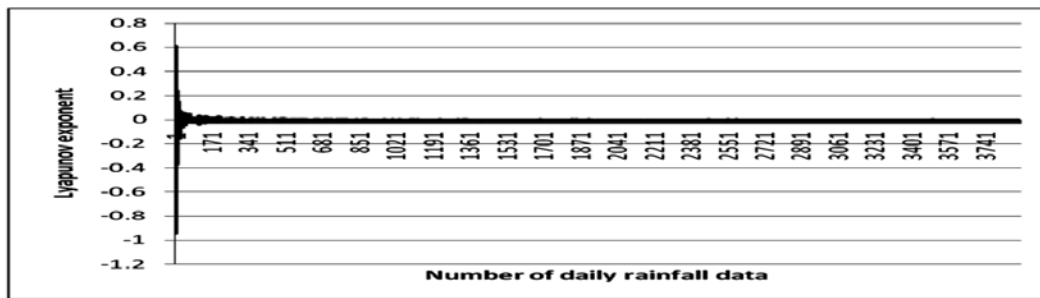


Figure 11a. Maximal Lyapunov exponent for the daily rainfall.

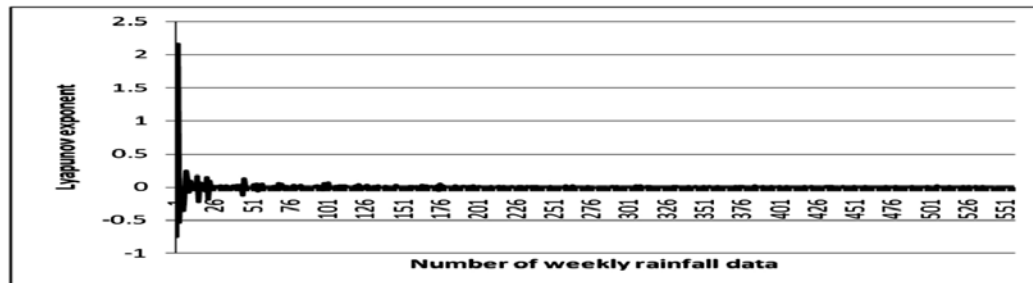


Figure 11b. Maximal Lyapunov exponent for the weekly rainfall.

In order to study monsoon rainfall, two parameters are sufficient to model the station rainfall. The two dimensional reconstructed phase space plot is shown in Figure 10. In comparison to the phase space plot of the daily series, the weekly series shows quite a good spread over the phase region and the presence of number of zeros that influenced daily rainfall has considerably reduced in the weekly rainfall.

Lyapunov exponent

The Lyapunov exponent is a measure of the rate of attraction to or repulsion from a fixed point in the phase space. One of the most prominent evidences of chaotic behavior of a chaotic system is the existence of positive Lyapunov exponent. A positive Lyapunov exponent indicates divergence of trajectories in one direction, or alternatively, expansion of an initial volume in this direction, and a negative Lyapunov exponent indicates convergence of trajectories or contraction of volume along another direction. This average rate of divergence can be estimated by the method of Wolf et al., (1985) and the Rosenstein et al., (1993) algorithm. The maximum Lyapunov exponent calculated for the daily and weekly rainfall timeseries using Rosenstein algorithm are 0.613417/day and 2.163982/week respectively as shown in Figure 11a and 11b. The Lyapunov time is defined as the inverse of the maximum Lyapunov exponent.

DISCUSSIONS

1997 monsoon holds the record with the highest average rainfall. The year 2005 made another record of maximum annual rainfall (Ramakrishnan, 2006). Figures 1b and 1c clearly show that the number of rainy days slightly increases (increasing trend) while the intensity (amount) of rainfall slightly decreases (decreasing trend). We can conclude that, Chennai has experienced particularly heavy rains roughly once every 10 years—1969, 1976, 1985, 1997, 2005, 2015. Y.E.A. Raj, former Deputy Director General of Meteorology, Regional Meteorological Centre, Chennai, pointed out that El Nino has a positive effect on winter monsoon but the phenomenon is not the only factor deciding a bountiful monsoon. "Even without El Nino, we had a good northeast monsoon many a time. The year 2005 received 79% excess rainfall, but it was not attributed to El Nino effect." 1997 was an El Nino year that saw vigorous rains in Chennai.

The correlation exponent value and the embedding dimension essential for describing the system and the sufficient number of embedding dimension giving the evolution of the system are presented in table 2. The coefficient of variation for the daily and weekly time series data are shown in the table 1. For the two series the correlation exponent value increases up to a certain embedding dimension values beyond which it saturates. This is an indication of some low dimension chaos in

Table 2. Correlation dimension result for the rainfall data on different temporal scales.

Parameters	Daily rainfall	Weekly rainfall
Correlation dimension	0.487	0.655
Delay time	8	2
Essential embedding dimension	1.97 ~ 2	2.31 ~ 2
Sufficient embedding dimension	4	6

the system. The correlation exponent value for the daily and weekly series are 0.487 and 0.655 respectively. The corresponding embedding dimension value for the two series is 1.97 and 2.31 (Table 2). This value gives the number of essential variables required to study the Chennai rainfall dynamics as 2 and the sufficient number of variables involved in the evolution of the system is 4 for daily series and 6 for weekly series.

The irregularity of the values in the time series can be represented by correlation dimension. A series with high(low) variability in values provides a higher(lower) dimension, which in turn, indicates higher(lower) complexity in the dynamic of the process. From the above results the variability of the rainfall for the two series is not seen explicitly. In nature the temporal accretion of the rainfall often decreases the variability. The values of the coefficient of variation in Table 2 also support the above point.

The phase space trajectory alone does not imply a chaotic system, hence, the need for further investigation arises. An indicator of nonlinearity in dynamical or time series data is the Lyapunov exponent. A positive Lyapunov value is an indicator of chaos. Chaotic system is strongly sensitive to initial value. The Lyapunov exponent predictability time gives the forecasting period up to which we can get reliable forecast. The maximum Lyapunov exponent is calculated for the daily and weekly rainfall time series as 0.613417 and 2.163982 respectively. This implies that the system is unstable and chaotic. The Lyapunov time is defined as the inverse of the maximum Lyapunov exponent. For the above system, the value of Lyapunov time is 1.630 and 0.462 for the daily and weekly rainfall respectively. This indicates the prediction time after which the system starts to behave in a chaotic manner.

CONCLUSIONS

Using the correlation dimension value, the rainfall dynamics of the Chennai city rainfall was examined for two temporal scales, daily and weekly. The principal assumption was that the influence of the presence of zeros in the rainfall series will be minimised if a different temporal scale is chosen. The result provided evidence that the rainfall dynamics can be characterised by deterministic chaos. The correlation dimension value for the daily and weekly rainfall series were 0.487 and 0.655 respectively. This suggests that

there is a low dimension chaos prevailing in the dynamics of the system. Also the essential number of variables for the evolution of the system is 2 for both the temporal scales and the sufficient number of the variables required for the evolution of the system is 4 and 6 respectively. Thus the correlation dimension method serves as a basic step in chaos identification. The selection of number of parameters to model the rainfall dynamics in India is always a debatable issue. The correlation dimension method helps to identify the exact number of variables involved in the evolution of the system. An important limitation in the present analysis is the presence of large number of zeros. This may result in the underestimation of the correlation dimension. Thus the presence of chaos is confirmed by one of the non-linear test such as Lyapunov exponent method, to strengthen the current result. Therefore, we conclude that daily and weekly forecast can be prepared for short to medium time scale, due to its intrinsic complexity. From the analysis results, we arrive at a conclusion that the dynamical behaviour of Chennai daily and weekly rainfall has a low-dimensional chaos and hence, long term prediction is nearly impossible.

ACKNOWLEDGMENTS

Thanks are due to Dr. T.V. Lakshmi Kumar and Dr.O.P.Singh for constructive suggestions and objective reviewing. They also thank Dr.Nandini Nagarajan for apt editing of the manuscript.

Compliance with Ethical Standards

The authors declare that they have no conflict of interest and adhere to copyright norms.

REFERENCES

- Cao, and Liangyue, 1997. "Practical method for determining the minimum embedding dimension of a scalar time series." *Physica D: Nonlinear Phenomena* 110.1, pp: 43-50.
- Fraser, Andrew M., and Harry L. Swinney, 1986. "Independent coordinates for strange attractors from mutual information." *Physical review A* 33.2, pp: 1134.
- Grassberger, Peter, and Itamar Procaccia, 1983. "Characterization of strange attractors." *Physical review letters* 50.5, pp: 346.

- Guhathakurta, P., Rajeevan M., and Thapliyal V., 1999. "Long Range Forecasting Indian Summer Monsoon Rainfall by a Hybrid Principal Component Neural Network Model." *Meteorology and atmospheric physics* 71.3-4, pp: 255-266.
- Harms, Archie A., and Thomas H., Campbell, 1967. "An extension to the Thomas-Fiering Model for the sequential generation of streamflow." *Water Resources Research* 3.3, pp: 653-661.
- Henderson, H.W., and Wells, R., 1988. Obtaining attractor dimensions from meteorological data. *Adv. Geophys*, v.30, pp: 205-237.
- Kantz, Holger, and Thomas Schreiber, 2004. *Nonlinear time series analysis*. Cambridge university press, v.7.
- Kennel, M., Brown, R., and Abarbanel H., 1992. "Determining embedding dimension for phase-space reconstruction using a geometrical construction". *Physical Review A*, v.45, no.6 pp: 3403-3411.
- Klemes, V., 1978. "Physically based stochastic hydrologic analysis." *Advances in hydroscience* 11, pp: 285-356.
- Packard, and Norman H., et al., 1980. "Geometry from a time series." *Physical review letters* 45.9, pp: 712.
- Rajeevan, M., Michael J., and McPhaden, 2004. "Tropical Pacific upper ocean heat content variations and Indian summer monsoon rainfall." *Geophysical research letters* 31.18.
- Ramakrishnan, T., 2006. Entering 2006, city reservoirs filled to the brim, Jan. 3, 2006- Retrieved from "The Hindu".
- Rosenstein, M. T., Collins J. J., and De Luca, C. J., 1993. "A practical method for calculating largest Lyapunov exponents from small data sets." *Physica D*, v.65, pp: 117-134.
- Ruelle, David, and Floris Takens, 1971. "On the nature of turbulence." *Communications in mathematical physics* 20.3, pp: 167-192.
- Salas, Jose D., Ricardo A., and Smith, 1981. "Physical basis of stochastic models of annual flows." *Water Resources Research* 17.2, pp: 428-430.
- Sano, Masaki, and Yasuji Sawada, 1985. "Measurement of the Lyapunov spectrum from a chaotic time series." *Physical review letters* 55.10, pp: 1082.
- Satyan, V., 1988. "Is there an attractor for the Indian summer monsoon?" *Proceedings of the Indian Academy of Sciences-Earth and Planetary Sciences* 97.1, pp: 49-52.
- Sivakumar B., 2000. "Chaos theory in hydrology: Important issues and interpretations". *J. Hydrol.*, v.227, pp: 1-20.
- Takens and Floris, 1981. "Detecting strange attractors in turbulence." *Dynamical systems and turbulence*, Warwick 1980. Springer Berlin Heidelberg, pp: 366-381.
- Williams and Garnett P., 1997. *Chaos theory tamed*. Joseph Henry Press.
- Wolf A., Swift, J.B., Swinney, H. L., and Vastano, J.A., 1985. "Determining Lyapunov exponents from a short time series." *Physica D*, v.16, pp: 285-317.

Characteristics of pre-monsoon convective activity over two contrasting environments from microwave radiometer data – A case study

P.P. Leena*, S. Sakharam, V. Anilkumar, S.K. Das and G. Pandithurai

Indian Institute of Tropical Meteorology, Pune, India 411008

*Corresponding Author: leena@tropmet.res.in

ABSTRACT

In the present study, microwave radiometer observations were used to understand the thermodynamic state of the atmosphere before, during and after the thunderstorm events occurred over two contrasting environments i.e. Pune and Mahabaleshwar. Initially thermodynamic state of atmosphere was analyzed using single cases from each site. Analysis of temporal variability of atmospheric parameters and associated thermodynamic indices of individual events showed significant positive differences between Pune and Mahabaleshwar in surface fields like temperature before thunderstorm, while surface relative humidity (RH) records indicated negative differences. Differences in various thermodynamic indices showed that strength of instability is higher over Pune compared to that over Mahabaleshwar.

Later composite analysis along with difference of the mean was verified so as to confirm the results quantitatively. Among the represented thermodynamic indices lifted index, humidity index and showalter index showed a negative difference, whereas total index, k-index and convective temperature showed positive difference before and during the storm. However, no significant changes were observed after the thunderstorm activity. Analysis suggested that there is a regional difference in thermodynamic features during the evolution of thunderstorm and also a possibility of thunderstorm potential over Pune compared to Mahabaleshwar. This work also shows the robustness of ground based microwave radiometry for the study of convective events.

Key words: Thunderstorm, Thermodynamic state, Western Ghats and Microwave Radiometer.

INTRODUCTION

Severe convective activities during pre-monsoon season include thunderstorm events, which are mainly associated with heavy precipitation, lightning, strong winds, hailstorms etc. These convective systems are considered as micro-scale or meso-scale phenomena, which will have time scale of the order of less than an hour and length scale limited to 10 km. Even though it has short time span, prediction of these convective systems is very important. Though many approaches of study are in practice using several modes of observations, most of the dynamical and thermodynamical features of thunderstorms in the literature are based on the mid-latitude systems. Over continental tropics, observations of the genesis of storms are rare. Thus, understanding of storm-time thermodynamic structure, especially in tropical regions is very important.

There are several techniques established for the study of thunderstorms. However, temporal evolutions of these convective events are not well understood, especially over tropics. The possible reason for this may be difficulty in obtaining the vertical structure of the storms or difficulty to forecast the events as the time span of these convective systems is only about 20–30 min. It is well known that short period forecasting of the future location of convective storms has been historically based on the first

technique i.e. extrapolation of radar reflectivity echoes. But, generally forecasting using these techniques is not good as their accuracy decreases rapidly due to short life time of individual convective systems. Hence, various studies (Browning 1980; Wilson and Mueller 1993 etc.) suggested that techniques for forecasting initiation, growth as well as dissipation of convective storms are required to produce a forecast beyond 20 minutes. Apart from this, Numerical Weather Prediction (NWP) models have the limitation in representing these storms and vertical structure since the vertical structure is decided by the interaction between the environmental shear and microphysical interactions. Apart from this, during the recent years, many statistical techniques (for e.g. Reap 1994; Lambert et al., 2005 etc.) were developed to forecast thunderstorm. Rajeevan et al., (2012) developed a statistical model based on binary logistic regression for predicting probability of lightning occurrence over southeast India using the perfect prognostic method (PPM).

Though there are several techniques or models, all these were mainly used for the prediction of the severe convective activities with less information on evolution of thermodynamic state of atmosphere. It is well known that in order to study the temporal evolution of these convective events we need continuous observations, which in turn will help in severe convective event prediction. Recently,

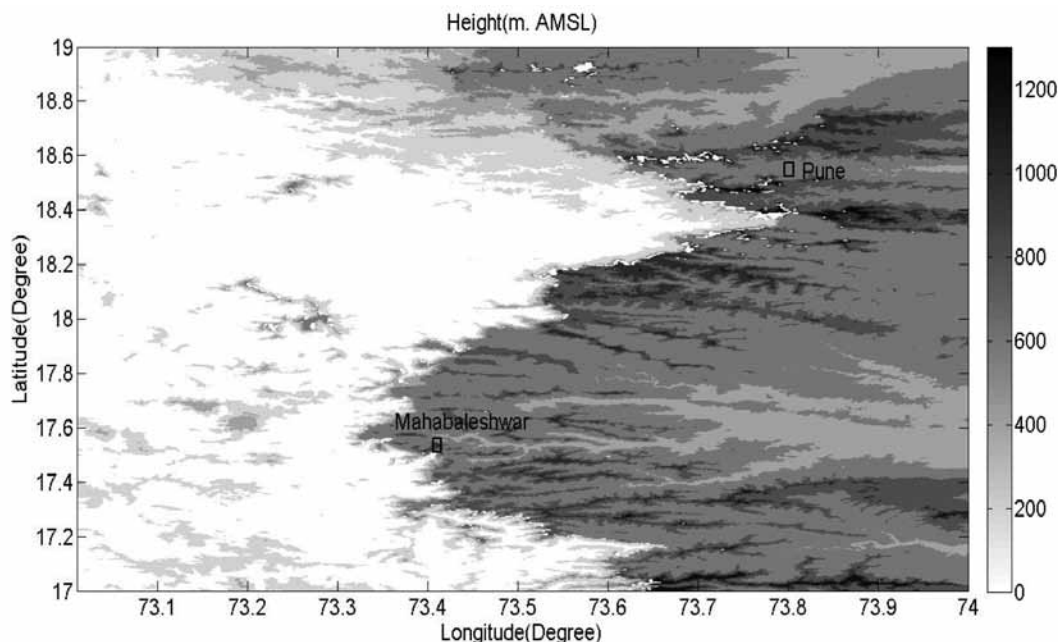


Figure 1. Topography map showing the study region (region highlighted).

the availability of microwave radiometric profilers (MWRP or MWR) provided unique opportunity to monitor the thermodynamic state continuously at a location (Ware et al., 2003; Chan, 2009; Rajeevan et al., 2010; Madhulatha et al., 2013). Considering its fine resolution, Chan (2009) has used MWRP in nowcasting of intense convective weather over Hong Kong. Importance of the MWRP derived indices was explored by Chan and Hon (2011) by describing the usage of these indices in nowcasting. Madhulatha et al., (2013) have demonstrated the use of ground-based microwave radiometer for studying severe convective activity over Southeast Indian region. They showed that there are sharp changes in the thermodynamic parameters associated with the storms. Recently, Ware et al., (2014) have also suggested that early stage of convection can be detected in temperature and humidity parameters derived from ground based MWR.

Thus, all these studies using MWR have not only reported the robustness of this observation but also its capability in studying severe convective activity. They have also shown that these data sets provide a unique, real time assessment of the pre-convective atmosphere. Considering this, in the present work thermodynamic state of atmosphere during severe convective activity has been studied using microwave radiometer measurements over two contrasting environments i.e. high and low altitude sites. The main objective of the study is to bring out the pre-monsoon convective event characteristics mainly using radiometer observations and secondly to verify whether they show any regional difference. Unfortunately, during pre-monsoon period the radiometer did not work over

the mentioned stations simultaneously. Hence the results presented in the following are derived using available limited cases of severe convective activity. Though the results are convincing and satisfy the objective to maximum extent the same are yet to be established quantitatively. It is believed that this information not only is useful to see the behavior of severe convective events over high and low altitude sites but also can contribute in nowcasting of thunderstorm as well as in developing weather forecast models.

STUDY REGION

To address the above mentioned objective, we have considered pre-monsoon thunderstorm activities occurred at high and low altitude stations with contrasting environment viz., Mahabaleshwar (or Maha) and Pune respectively. Topography map of the study region generated from SRTM (Shuttle Radar Topography Mission) data (Farr et al., 2007) is shown here in Figure 1. Both the sites are located in the Western Ghats, in which Mahabaleshwar (17.56 °N, 73.4 °E) is at an altitude of 1348m above mean sea level (AMSL). The low altitude station, Pune (18.5°N, 73.86°E) is at an elevation of 570 m AMSL and situated at the lee side (eastern) of Western Ghats in a Valley.

SYNOPTIC CONDITION

It is well known that March-April-May (MAM) constitute hot weather period which is also called as pre-monsoon. In general, this period is known for severe convective activity

such as thunderstorms, hailstorms etc, over land areas. Over Indian region thunderstorms are typically observed during pre-monsoon season (March-May) (Tyagi et al., 2013). In order to study these events in detail first synoptic conditions have to be verified and therefore the same over Pune and Mahabaleshwar are explained in the following.

Pune (Case: 24 April 2011)

During this period in 2011, a maximum temperature of $\sim 38^{\circ}\text{C}$ was reported over Maharashtra as per India Meteorological Department (IMD) Daily Weather Report (IDWR). On 23rd April 2011, the IDWR showed the trough/wind discontinuity at 0.9 km AMSL from east Rajasthan to Lakshadweep area which persisted across west Madhya Pradesh, Marathwada, south Madhya Maharashtra, north interior Karnataka and coastal Karnataka with an embedded cyclonic circulation over east Rajasthan and neighborhood. Further on 24th the trough/wind discontinuity at 0.9 km AMSL were running from east Rajasthan to Kerala, Madhya Maharashtra and other places with the embedded cyclonic circulation over east Rajasthan and neighborhood. On 25th it is observed that the trough/wind discontinuity at 0.9 km AMSL runs from east Rajasthan to south Tamil Nadu across Madhya Maharashtra with an embedded cyclonic circulation over east Rajasthan and neighborhood. During these days, Pune's weather remained dry (very hot) with a temperature of 38°C . According to IDWR report Pune experienced a squall at 1610 IST on 24th April from northwest to southeast direction with a wind speed of 68 Kmph, fall in temperature by 14°C and rise in pressure by 2hPa. It was also reported that, at 0830 hrs IST on 25th April 2011 the Rain gauge in Automatic Weather Station had recorded 25.6mm of rainfall over Pune for the preceding 24hrs.

Mahabaleshwar (Case: 25 April 2013)

On 24th April 2013 the IDWR showed the cyclonic circulation persisted over north Rajasthan and neighbourhood and it was extending upto 1.5km a.s.l. The trough/wind discontinuity in the low levels from the above cyclonic circulation was running over south Tamil Nadu across west Madhya Pradesh, Vidarbha, Marathwada and interior Karnataka. On 25th the cyclonic circulation had moved spreading over east Rajasthan and adjoining northwest Madhya Pradesh and it was extending upto 2.1 kms AMSL. The trough/ wind discontinuity in the low levels spreading from the above cyclonic circulation to south Tamil Nadu across same above mentioned regions except west Madhya Pradesh. Further on 26th the cyclonic circulation persisted in the same region as that of 25th and it was extending upto 1.5 kms AMSL. The trough/wind discontinuity in the lower levels then extended from

the above cyclonic circulation to coastal Karnataka across interior Maharashtra and north interior Karnataka. A cyclonic circulation extending up to 0.9 km AMSL was lying over south Tamil Nadu and adjoining Comorin area. During these days, temperature of 32°C was noted over Mahabaleshwar. According to IDWR report, observation at 0830 hrs IST on 24th April 2013 had shown a probability (between 51-75%) of rain or thundershower over Pune and neighborhood areas for next 24hrs. Further observation at 0830 hrs IST on 26th April 2013 had shown that Rain gauge in Automatic Weather Station recorded 19.4mm of rainfall over Mahabaleshwar for the preceding 24hrs with a remark that it was a rainy day.

Hence the present study considered the thunderstorm occurred on 24th April 2011 over Pune and the one on 25th April 2013 over Mahabaleshwar to address the present objective initially.

DATA USED

Ground based Microwave Radiometric Profiler used in the present study is MP-3000A (manufactured by Radiometrics Corporation, USA), which is a 35 channel Temperature, Water vapor and liquid water profiler. The MP-3000A incorporates mainly two radio frequency (RF) subsystems in the same cabinet sharing a single antenna and antenna pointing system. Temperature profiles can be obtained by measuring the radiation intensity, or brightness temperature, at points along the side of the oxygen absorption band at 60 GHz, whereas water vapor profiles can be obtained by observing the intensity and shape of emission from pressure broadened water vapor lines. The line near 22 GHz is suitable for ground based profiling in relatively moist areas. Radiometer retrieves temperature and relative humidity profiles with a temporal resolution of 2 minutes and its spatial resolution varies with altitude as follows: up to 500m with 50m, 500m to 2km with 100m and 2 to 10km with 250m. Apart from obtaining the vertical profiles, radiometer also provides surface parameters i.e. temperature and relative humidity, integrated products like vapor and liquid and also cloud base height.

RESULTS AND DISCUSSIONS

As a first step we have analyzed thermodynamic state of atmosphere based on single events from each station i.e. a thunderstorm occurred on 25 April 2013 over Mahabaleshwar and 24 April 2011 over Pune. (Synoptic conditions of these events are discussed in Section 3 above). Later composite analysis of all the events occurred over both stations has been attempted as a part of comparative study. It is to be noted that in the Variation in surface parameters to Variation in stability indices the results are

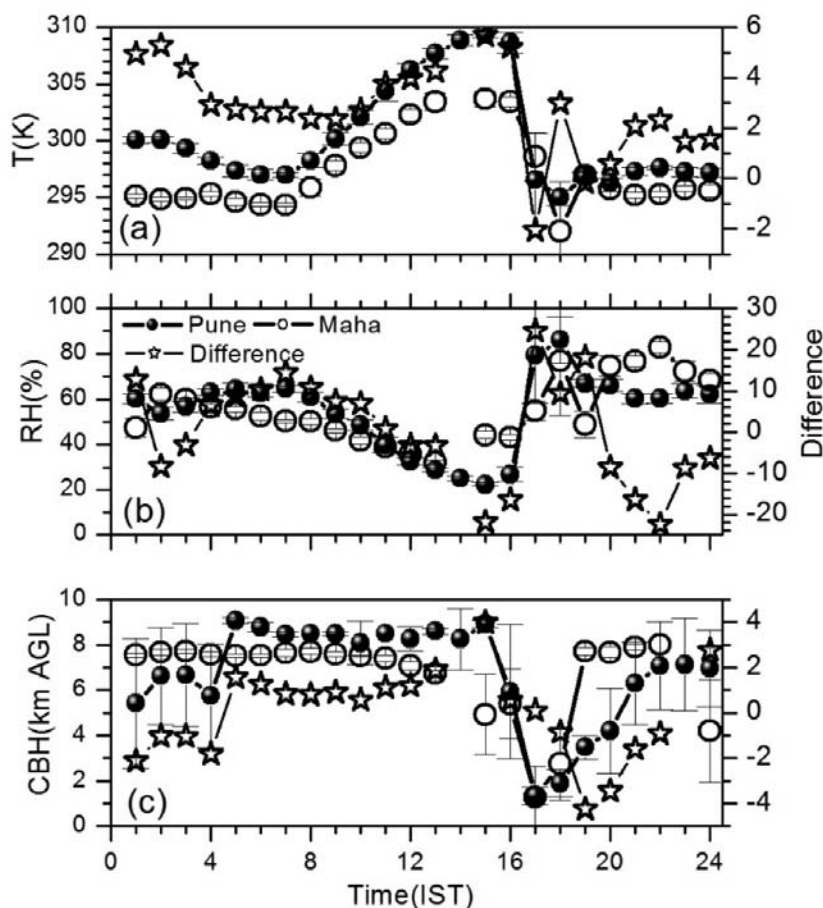


Figure 2. Diurnal variation of atmospheric parameters (temperature, RH and CBH) observed over Mahabaleshwar and Pune along with corresponding differences.

discussed based on individual events and the difference has been calculated as Pune minus Mahabaleshwar.

Variation in surface parameters

It is well known that severe convective activity such as thunderstorms occurring in pre-monsoon is very much dependent on three basic components i.e. moisture, instability and lifting mechanism. As air near the surface is lifted higher in the atmosphere and supersaturated, available water vapor condenses into small water droplets which form clouds. Therefore, studying the variation of background atmospheric field is very important. The variations in surface temperature, RH and cloud base height (CBH) over Mahabaleshwar and Pune are shown in Figure 2. There is a significant variation in all these parameters before, during and after the development of the storm. Our analysis has also brought out the obvious fact of drop in temperature and 100% increase in surface RH during the event. During day time maximum temperature observed was 305 K over Mahabaleshwar but it was ~ 310 K over Pune. During the event the temperature dropped to

297K over Mahabaleshwar and it was ~295K over Pune. The difference in temperature observed between Pune and Mahabaleshwar was about 6° K before the thunderstorm, less during the thunderstorm (~-2 °K) and negligible after the storm i.e. ~1-2 °K (see Figure 2). It is seen that before the storm, the RH was between 40-60 % and after the storm it was in the range 60-80% over both the stations. Differences in RH noticed during the storm are ~30 % higher over Pune compared to Mahabaleshwar. After the storm it decreased to 10-20% over Pune compared to Mahabaleshwar. Interestingly it is seen that moisture content in morning hours over Pune was 10% higher than that at Mahabaleshwar. This shows that the surface moisture availability was higher over Pune compared to Mahabaleshwar. In the pre environment ~2 hour before the storm the CBH (above ground level) at Mahabaleshwar was low which indicates abundant low-level moisture. But in morning hours it showed presence of ice clouds with CBH as high as 8km. The variation of CBH over Pune was similar to that of Mahabaleshwar showing high CBH in morning hours. CBH difference (~1-1.5 Km) was found to be negligible before and very less during the thunderstorm.

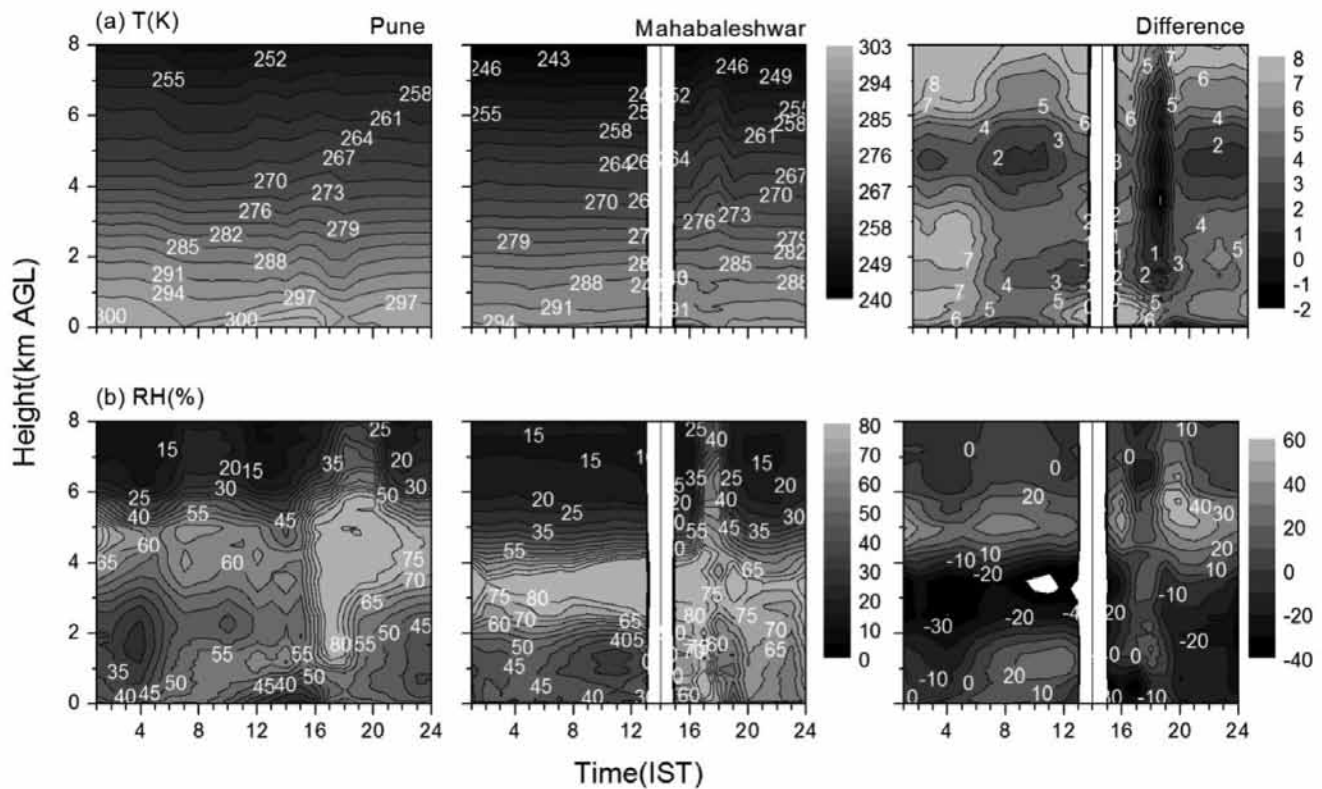


Figure 3. Time-height cross-section of (a) temperature and (b) RH observed over Mahabaleshwar and Pune along with corresponding difference.

Time-height variability of temperature and moisture

A vertical profile (Figure 3) of temperature and RH shows significant diurnal variation over Mahabaleshwar. It is observed that there was not much of variation in temperature before and after the event whereas it was varying significantly during the event over Mahabaleshwar. Over this region, there exists not only a temporal variation but also a vertical variation; i.e. below 2km the temperature variation is similar to surface variability and above that the condition reverses. In case of Pune, the diurnal variation is similar to that of surface temperature but in vertical direction there is a significant variation below 2km altitude. During the storm below 2km and above 6km the temperature over Pune was higher ($\sim 8^{\circ}\text{K}$) whereas in the mid layer the condition reverses where the difference was negative ($\sim 3^{\circ}\text{K}$).

From the variation of RH, over both the regions there is a significant variation in ϕ moisture content. Over Mahabaleshwar, RH variability clearly showed moistening of middle layer throughout the day. During the event the RH had increased to 100% maximum up to 8km altitude. Over Pune, RH variability clearly shows moistening of middle layer throughout the day but the moisture content before the development of storm was less compared to

Mahabaleshwar. The vertical extent of moisture over Pune was less compared to Mahabaleshwar. Interestingly over Pune, increase of moisture content below 1km altitude started increasing in early morning hours itself where it was almost 40% higher than Mahabaleshwar (Figure 3 third row). This is even seen between 4-6 km altitudes but from 2-4km the condition reverses.

The moisture availability over these locations can be clearly seen from vapor as well as equivalent potential temperature (EPT). During the thunderstorm the vapor showed maximum of 16g m^{-3} over both the regions extending up to ~ 8 (4) km altitude at Mahabaleshwar (Pune). Interestingly it was observed over Pune that, below 1km altitude the vapor content had started increasing prior to the event and also there existed vapor in lower altitude after the event too. In general, it suggests abundance of low level moisture over Pune as compared to Mahabaleshwar. From the difference (Figure 4) it may be observed that before, during and after the storm lower troposphere records higher availability of vapor at Pune ($\sim 8\text{-}10\text{ g m}^{-3}$) when compared to Mahabaleshwar. In general, during stable conditions EPT increases with altitude where as if EPT decreases with height, convection can occur. The equivalent potential temperature of air parcel at different altitudes provides a measure of instability of the air column. Over Pune it is clearly seen that in morning hours, the

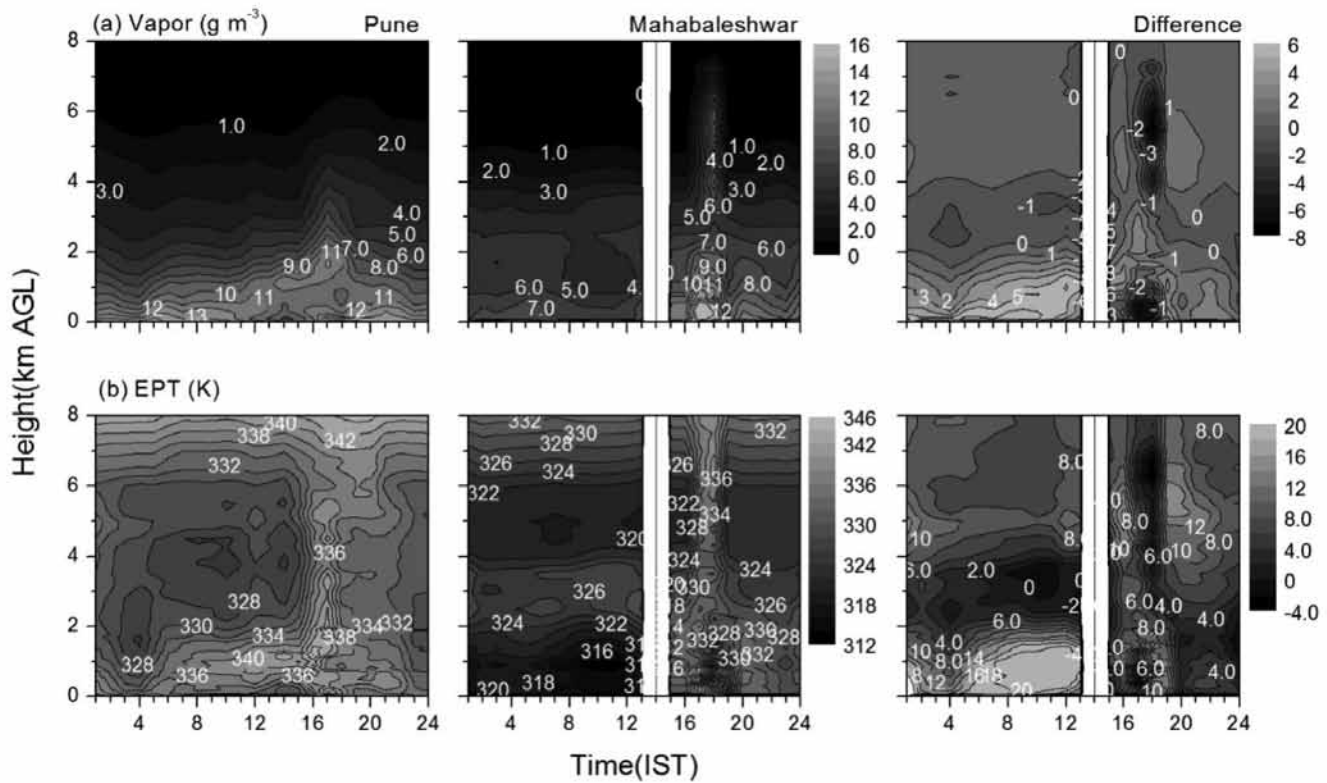


Figure 4. Time-height cross-section of (a) vapor and (b) EPT observed over Mahabaleshwar and Pune along with corresponding difference.

atmosphere was stable and few hours before the storm the instability started developing. The growth of instability is seen building up over Pune from quite early hours unlike that at Mahabaleshwar. Interestingly, the temperature difference between the surface and mid-troposphere was found to be negative ($\sim -4\text{K}$), which clearly indicates that the atmosphere was more unstable over low altitude station during thunderstorm compared to high altitude station. This suggests that the abundant moisture content in the mid troposphere over low altitude station helps in formation of deep convective clouds over Pune.

Variation in stability indices

The significant variation in atmospheric parameters before $\sim 2-4$ hours of the storm noticed in the earlier section is to be seen as associated with thermodynamic/stability indices. To understand the thermodynamic evolution of the boundary layer convective instability, variation of thermodynamic indices has to be examined (Feltz et al., 2003) which can also help in explaining the prerequisites necessary for genesis of the thunderstorm activity (Madhulatha et al., 2013). In Figure 5 are presented the variation of stability indices during these two days along with difference between these two stations. A short description of the indices used in the present study is furnished in Table 1.

Initially the variation of dew point temperature at 850hPa, which is an alternative parameter providing information on moisture variability, may be considered. The diurnal variation of T_{d850} and their corresponding difference has shown that, it was almost same before the event over the two stations with negligible difference. During and after the event the difference showed negative (~ -10 to -2°K) suggesting that T_d at that particular level is higher at Mahabaleshwar compared to Pune indirectly showing moisture content at that level was higher at Mahabaleshwar.

Now taking up the variability in the other seven thermodynamic indices: Lifted Index (LI) is calculated assuming the parcel of air near the surface as lifted to 500 hPa. Expected temperature parcel at 500 hPa is then subtracted from the actual (environmental) 500 hPa temperature. This difference in LI can be positive, negative or zero and would indicate the different types of stability of the parcel of air. A positive value of LI means stable atmosphere, negative means possibility of convection and zero means neutral atmosphere. From the variation of LI it is seen that it varied between -2 to $+2$ during the morning time over Mahabaleshwar but it was negative over Pune. Few hours before the event, LI was more negative $\sim -10^\circ\text{C}$ over Mahabaleshwar just before the storm and after the storm; LI showed positive values which suggested the atmosphere as stable. Variation over Pune was not as clear

Characteristics of pre-monsoon convective activity over two contrasting environments from microwave radiometer data – A case study

Table 1. List of different thermodynamic indices studied.

S. No	Thermodynamic Indices
1	Lifted Index (LI) Mainly considers temperature difference between an air parcel lifted adiabatically T_p and the temperature of the environment at a given pressure in the troposphere, usually at 500hPa, and is given by $T_{p500} - T_{500}$
2	Humidity Index (HI) , given by $(T - T_d)_{850} + (T - T_d)_{700} + (T - T_d)_{500}$
3	Total Total Index (TTI) , given by $T_{850} + T_{d850} - 2T_{500}$
4	K-Index (KI) , given by $(T_{850} - T_{500}) + T_{d850} + (T_{700} - T_{d700})$
5	Showalter Index (SI) This index mainly considers the difference between the observed temperature at 500 hPa (T_{500}) and the temperature of an air parcel after it has been lifted pseudo- adiabatically to 500 hPa from 850 hPa.
6	Convective temperature (Conv Temp) Mainly explains the surface heating results in rising of parcel without any mechanical lift.
7	Convective Available Potential Energy [$J kg^{-1}$] CAPE is a measure of amount of energy that is available during convection (VenkatRatnam et al., 2013) and it is a potential indicator of the convective activity in the atmosphere.

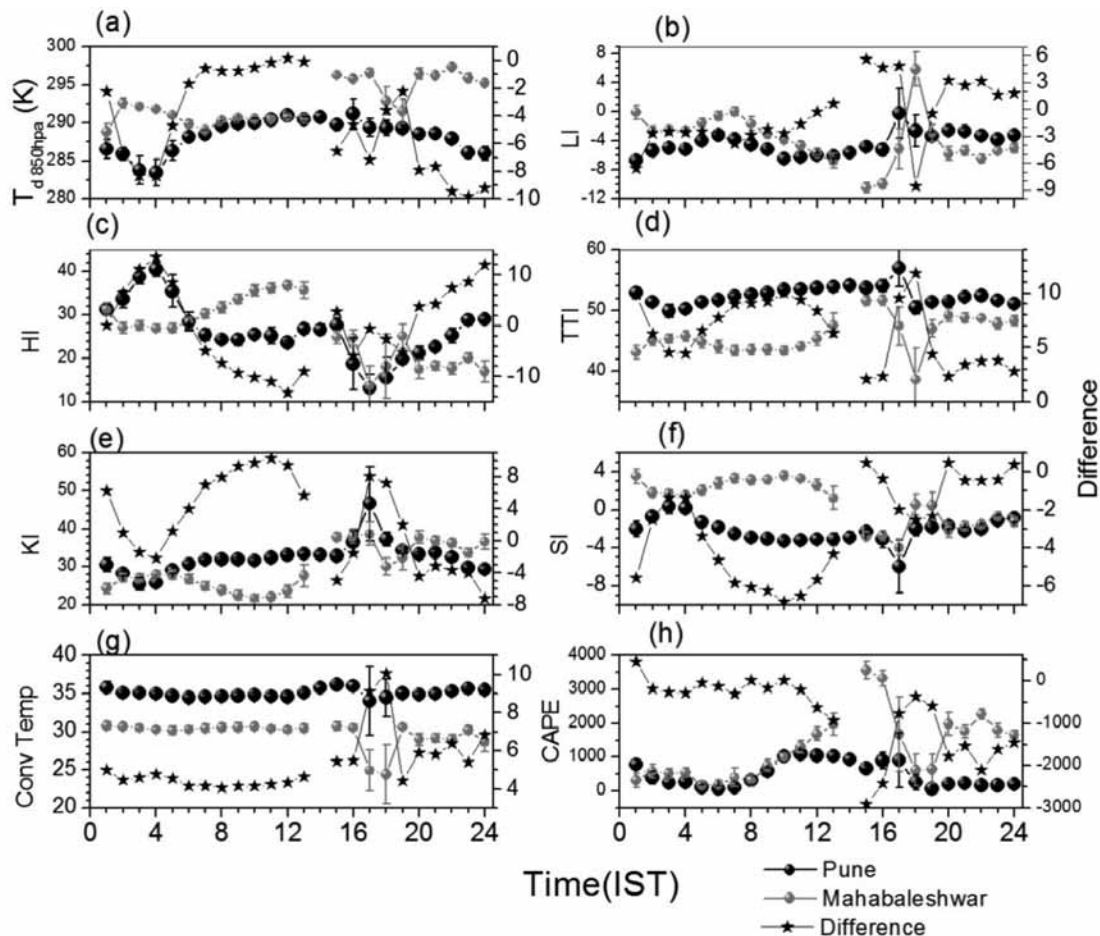


Figure 5. Diurnal variation of eight different thermodynamic indices observed over Mahabaleshwar and Pune along with corresponding differences.

as at Mahabaleshwar but LI showed that the atmosphere was unstable in morning hours itself and later it became stable. These features are even clear from the associated differences.

Stability of atmosphere as well as moisture variability for different pressure levels can be explained using HI, TTI and KI. HI variation shows significant temporal as well as regional difference. Interestingly over both the stations it was low during the event with negligible differences. Variation of HI had suggested that moisture variability at various pressure levels (or altitudes) play a significant role during these convective events. The difference was negative (~ -10 °C) suggesting the moisture variability over Pune was higher compared to Mahabaleshwar. The TTI and KI showed different variations over these two regions with very high values over Pune. It is well known that the values >44 in TTI indicate the possibility of thunderstorm occurrence. It is interesting to note from Figure 5, that TTI was found to be higher (>50) at Pune as compared to Mahabaleshwar (40-50), which suggest that the thunderstorm potential is higher at Pune. This was even clear from the temporal variation of the difference which was positive throughout varying from 0 to 10 °C

Also KI values >40 indicate convective potential. The temporal variation of KI has shown that, over Pune it varied from 30-45 whereas over Mahabaleshwar it was from 20-35 °C. During the event it was much higher at Pune and even the temporal variation of the regional difference was almost positive. Thus the higher positive KI values at Pune indicate higher thunderstorm potentials as compared to Mahabaleshwar.

Showalter Index (SI) in the present study, was used to assess 850hPa parcel stability/instability. Negative SI indicates that the upper planetary boundary layer (PBL) is unstable with respect to the middle troposphere. The more negative the SI the more unstable the troposphere and the more buoyant the acceleration will be for rising parcels of air from the upper PBL. The values of SI from -4 to -7 indicate the large instability. Negative values (up to ~ -4) before the storm and higher value of SI (~ -8) during the thunderstorm at Pune indicate the higher to extreme atmospheric instability over the station. On the other hand, Mahabaleshwar station showed positive values before the storm and less negative (~ -3) during the storm which was less compared to Pune. This indicates higher atmospheric instability over Pune before and during the thunderstorm as compared to Mahabaleshwar. This is even clear from the difference, especially before the storm where it showed a negative difference.

Convective temperature mainly, explains the surface heating effect resulting from the rising of an air parcel with no mechanical lifting. Convective temperature at Pune was observed to be $\sim 37^\circ\text{K}$ before, $\sim 33^\circ\text{K}$ during and $\sim 34-35^\circ\text{K}$ after the thunderstorm while it was ~ 30 , ~ 22 and $27-30$

$^\circ\text{K}$ before, during and after the thunderstorm respectively at Mahabaleshwar. The difference showed positive throughout suggesting the convective temperature over Pune was higher than that at Mahabaleshwar thus confirming the potential of thunderstorm occurrence as higher over Pune compared to Mahabaleshwar. But in the case of CAPE, it showed very high (4000 J kg^{-1}) over Mahabaleshwar prior to the event ($\sim 3-4$ hours before) whereas over Pune it was comparatively less ($\sim 1500 \text{ J kg}^{-1}$). In general, both regions showed the atmosphere was unstable before the event. The difference between Pune and Mahabaleshwar was negative suggesting CAPE was comparatively higher at Mahabaleshwar than at Pune.

Composite analysis of stability indices: a comparison

The discussion thus far presented reveals a significant variation in atmospheric parameters/thermodynamic indices before $\sim 2-6$ hours of the storm over both the regions. Now the variations in these eight indices within ± 04 hours of the occurrence of storm (Figure 6 and 7) may be examined first by verifying individual cases, then mean of all the cases for each region and later difference of the mean (i.e. Pune minus Maha) for the two thunderstorms occurred over Pune (24th April and 26th May 2011) and the three over Mahabaleshwar (16th March, 25th April and 01st May 2013). In general, all the indices showed significant temporal as well as regional difference. Also while considering individual cases (Figure 6), most of the variables/indices did not show significant regional difference. Hence for a quantitative analysis mean of all the cases for that particular region along with the corresponding difference (Figure 7) were considered.

It is observed from the mean variation that T_d at 850 hPa was less at Pune compared to Mahabaleshwar. This is even clear from the difference of the mean that it was negative before, during and after the event suggesting that over all amount of moisture at that level was higher at Mahabaleshwar. Among the other represented thermodynamic indices, LI, HI, SI showed a negative difference whereas TTI, KI and Conv Temp showed positive difference. Positive difference in TTI and KI suggested higher low level moisture availability at Pune compared to Mahabaleshwar. Also it is well known that lower (higher) values in LI, HI, SI (TTI, KI and convective temperature) suggest higher instability and therefore higher probability of occurrence of thunderstorm. The difference associated with these variables (graythick line on Figure 7) suggests that the strength of instability is more over Pune compared to Mahabaleshwar. In case of CAPE, it showed negative before the storm suggesting instability is higher over Mahabaleshwar but the condition reverses during and after the storm.

Characteristics of pre-monsoon convective activity over two contrasting environments from microwave radiometer data – A case study

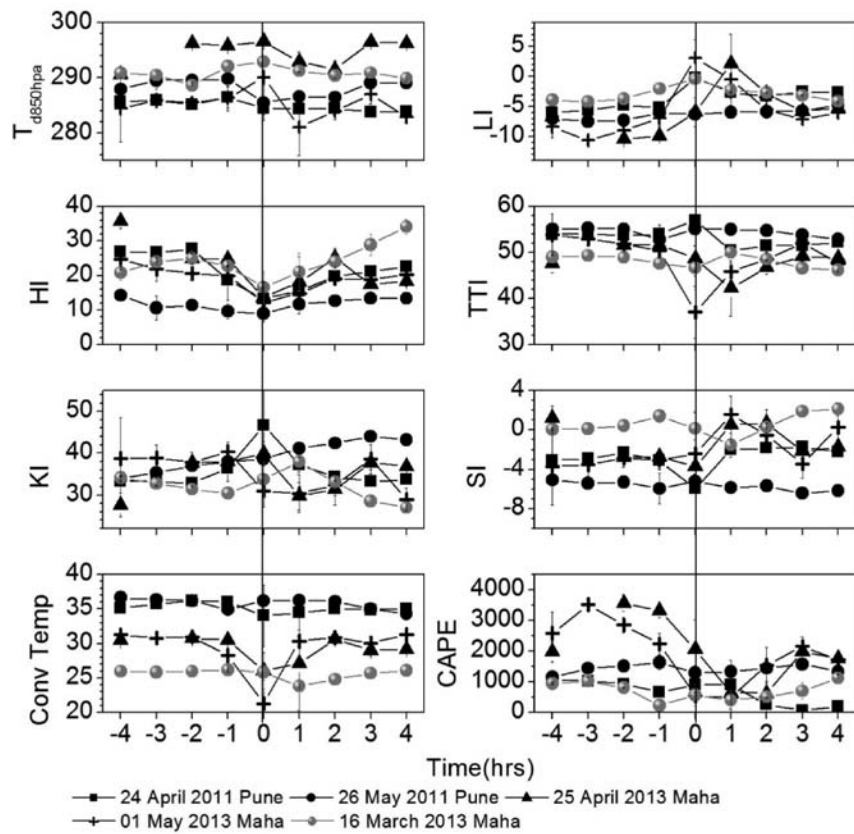


Figure 6. Variation of eight different thermodynamic indices for all individual cases, mean of all cases over Pune and Mahabaleshwar along with difference of the mean within ± 04 hours of the occurrence of storm.

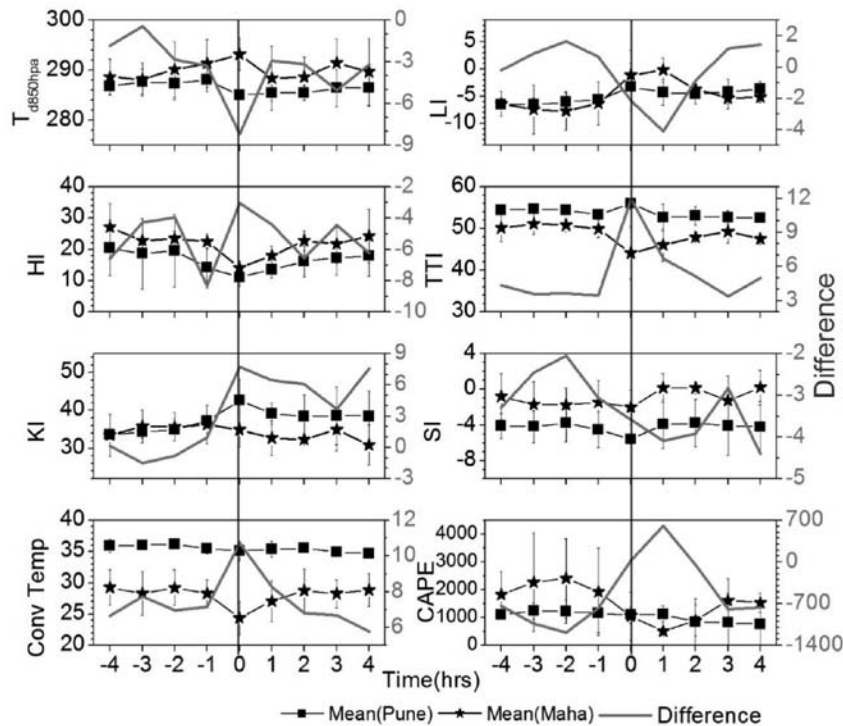


Figure 7. Same as Figure 6 but for mean of all cases over Pune and Mahabaleshwar along with difference of the mean within ± 04 hours of the occurrence of storm.

Entire analysis (single case and difference of the mean) shows appreciable regional difference in all the atmospheric parameters and thermodynamic indices before, during and after the storm occurrence. This variation may be possibly due to the fact that Pune is a plane surface compared to Mahabaleshwar. There is a possibility of warm air advection to be stronger in lower troposphere creating a potential instability with accumulation of low level moisture and strong radiative heating of the earth's surface leading to the initiation of deep convection. In case of Mahabaleshwar, though there is a warm air advection which is lifted by orography too there lies a possibility of cold air gets advected over that. It is documented in literature that, cold air blowing up to the height of mountain is blocked by mountains but above that height (of mountain) cold air flows above the warm air (Van Delden 2001). These processes over the two regions create a difference in the formation of cloud and precipitation i.e. over Pune there is a chance of formation of rain bearing clouds which precipitates heavily and in other place, convective clouds appear in the lower mountain ranges. Also the cold air flow over warm air in the mountain region may limit the clouds from growing deeper over observational site, Mahabaleshwar. All these factors can possibly cause a regional difference.

SUMMARY

The main objectives of the present work are to understand the thermodynamic state of the atmosphere before, during and after the thunderstorm events at two different geographical locations using well established microwave radiometric observations. Initially, we have demonstrated the variability in surface field and vertical profiles of atmospheric parameters over these two regions and later the variations associated with thermodynamic indices using single case. Most of the atmospheric parameters showed significant variations with positive differences between Pune and Mahabaleshwar in surface fields like temperature before thunderstorm, while surface relative humidity (RH) recorded negative differences. Interestingly the thermodynamic indices associated with the storms over both the regions showed significant variation. These differences (single case and difference of the mean) in various indices are significant and suggest a high thunderstorm potential at Pune compared to Mahabaleshwar. The present analysis suggests that there is a regional difference in thermodynamic features during the evolution of thunderstorm and shows the robustness of ground based microwave radiometry for the study of convective events. Further study with more number of cases can help establish the presently obtained results and inferences.

ACKNOWLEDGMENTS

Authors are thankful to Director, IITM for encouragement. IITM is fully funded by Ministry of Earth Sciences, Govt of India. Thanks are due to Dr. C.K. Unnikrishnan and Dr. S.G. Narkhedkar for constructive suggestions and objective reviewing. Authors are also thankful to Prof.B.V.S.Murthy and Chief Editor for carrying out editing.

Compliance with Ethical Standards

The authors declare that they have no conflict of interest and adhere to copyright norms.

REFERENCES

- Browning, K. A., 1980. Review Lecture : Local weather forecasting, In proceedings of Roy. Soc. London A., v.371, pp: 179–211.
- Chan, P. W., 2009. Performance and application of a multi-wavelength ground based microwave radiometer in intense convective weather, *Meteorol. Zeit.*, v.18, no.3, pp: 253–265.
- Chan, P. W., and Hon, K. K., 2011. Application of ground-based, multichannel microwave radiometer in the nowcasting of intense convective weather through instability indices of the atmosphere, *Meteorol. Zeit.*, v.20, no.4, pp: 431–440.
- Farr, Tom. G., Paul, A. Rosen., Edward Caro., Robert Crippen., Riley Duren., Scott Hensley., Michael Kobrick., Mimi Paller, Ernesto Rodriguez., Ladislav Roth., David Seal., Scott Shaffer., Joanne Shimada., Jeffrey Umland., Marian Werner., Michael Oskin., Douglas Burbank and Douglas Alsdorf., 2007. The shuttle radar topography mission, *Rev. Geophys*, RG2004, doi:10.1029/2005RG000183, v.45.
- Feltz, W. F., Smith, W. L., Howell, H. B., Knuteson, R. O., Woolf, H., and Revercomb, H., 2003. Near-continuous profiling of temperature, moisture, and atmospheric stability using the Atmospheric Emitted Radiance Interferometer (AERI), *J. Appl. Meteorol.*, v.42, pp: 584–597.
- Lambert, W. C., Wheeler, M., and Roeder, W., 2005. Objective lightning forecasting at Kennedy Space Center and Cape Canaveral Air Force Station using cloud-to-ground lightning surveillance system data, Paper presented at Conference on Meteorological Applications of Lightning Data, Amer. Meteor. Soc. San Diego, Calif.
- Madhulatha, A., Rajeevan, M., VenkatRatnam, M., JyotiBhate and Naidu, C. V., 2013. Nowcasting severe convective activity over southeast India using groundbased microwave radiometer observations, *J. Geophys.Res.*, v.118, pp: 1–13.
- Rajeevan, M., Kesarkar, A., Thampi, S. B., Rao, T. N., Radhakrishna, B., and Rajasekhar, M., 2010. Sensitivity of WRF cloud microphysics to simulations of a severe thunderstorm event over southeast India, *AnnalesGeophysicae.*, v.28, pp: 603–619.
- Rajeevan, M., Madhulatha, A., Rajasekhar, M., Bhate, J., Kesarkar, A., and Apparao, B. V., 2012. Development of a perfect

Characteristics of pre-monsoon convective activity over two contrasting environments from microwave radiometer data – A case study

- prognosis probabilistic model for prediction of lightning over south-east India, *J. Earth. Syst. Sci.*, v.121, pp: 355–371.
- Reap, R. M., 1994. 4-h NGM based probability and categorical forecasts of thunderstorms and severe local storms for the contiguous U.S, *NWS Tech. Proc. Bull.*, National Weather Service. Silver Spring. Md., v.419, pp: 14.
- Tyagi, B., Satyanarayana, A. N. V., and NareshKrishna,V, 2013 Thermo dynamical structure of atmosphere during pre-monsoon thunderstorm season over Kharagpur as revealed by STORM data. *Pure Appl. Geophys.*, doi:10.1007/s00024-012-0566-5.,v.170, pp: 675–687.
- Van Delden Aarnout., 2001. The synoptic setting of thunderstorms in Western Europe, *Atmos Res.*, v.56, pp: 89-110.
- VenkatRatnam, M., DurgaSanthi, Y., Rajeevan, M., and Vijaya Bhaskara Rao, S., 2013. Diurnal variability of stability indices observed using radiosonde observations over a tropical station: Comparison with microwave radiometer measurements, *Atmos. Res.*, v.124, pp: 21–33.
- Ware, R., Carpenter, R., Guldner, J., Liljegren, J., Nehr Korn, T., Solheim, F., and Vandenberghe, F., 2003. A multichannel radiometric profiler of temperature, humidity, and cloud liquid, *Radio Sci.*, doi:10.1029/2002RS002856.,v.44, no.3, pp: 8079.
- Ware, R., Anthes, R., Blanchette, L., Eilts, M., Gultepe, I., Heckman, S., Jackson, M., MacDonald, A., Marshall, R., Murakami, M., Nelson, M., Markin, V., Rajeevan, M., Serafin, R., and Xie, Y., 2014. Thermodynamic Profiling and Humidity Mapping for Local High-Impact Weather Prediction, *Proceeding. WMO Technical Conference on Meteorological and Hydrological Services*
- Wilson, J. W., and Mueller, C. K., 1993. Nowcasts of thunderstorm initialization and evolution, *Weather Forecasting.*, v.8, pp: 113–131.

Long range forecast of rainfall during southwest monsoon in the states of Maharashtra and Goa

Onkari Prasad^{*1}, O.P. Singh² and K. Prasad³

¹43, Ritu Apartments, A-4 Paschim Vihar, New Delhi-110063

²B44, First Floor, Parshvnaath Paradise, Mohan Nagar, Distt: Ghaziabad-201007 (U.P.)

³D-104, Seema Apartments, Sector 11, Dwarka, New Delhi-110085

*Corresponding Author: prasadonkari123@yahoo.in

ABSTRACT

The close relationship known between the activity of South Indian Ocean Convergence Zone and southwest monsoon rainfall for India as a whole also exists for all the four meteorological subdivisions of the states of Maharashtra and Goa (viz., Konkan & Goa, Madhya Maharashtra, Marathwada and Vidarbha). The present study has shown that long range forecast of rainfall for southwest monsoon season as a whole (June-September), bi-monthly periods of August+ September and for the month of September could be prepared for all the four subdivisions. Forecast for seasonal rainfall, at the district level, could be prepared for all districts of the region except the 4 districts of Madhya Maharashtra, namely, Nasik, Pune, Satara and Sangli. For the months of July and September forecast could be prepared for the majority of the districts. For August rainfall forecasting could be possible for the districts of the subdivision of Marathwada only. Forecast for rainfall in the month of June could not be prepared for any of the subdivisions/districts.

Key Words: Long Range Forecast, South Indian Ocean convergence zone, Southwest monsoon and Maharashtra and Goa.

INTRODUCTION

Maharashtra and Goa are two contiguous western states of India with 36 and 2 districts respectively (Figure 1 and 2). Based on rainfall characteristics, the districts of Maharashtra and Goa have been clubbed together to form four meteorological subdivisions, namely, Konkan & Goa, Madhya Maharashtra, Marathwada and Vidarbha (Figure 1 & Table 1). All the four subdivisions receive rainfall during Southwest Monsoon (SWM) (June-September) and also during Northeast Monsoon (NEM) (October-December). The contribution of SWM (NEM) rainfall to the annual total is 94% (5%) in Konkan and Goa, 83% (12%) in Madhya Maharashtra, 84% (11%) in Marathwada and 88% (7%) in Vidarbha. Goa's annual rainfall is 3040.5 mm. Most of the annual rainfall (91%) is received during southwest monsoon season alone. As these two states receive rainfall mainly during southwest monsoon, a reliable advance information on it is a necessity for sustenance and development of the two states. It is in this context that the possibility of issuing long range forecast of southwest monsoon rainfall, in the states at district level, has been attempted by the authors and the results are discussed in the following.

Data Used and Method of Analysis

Subdivision and district level rainfall during Southwest monsoon and South Indian Ocean Convergence Zone

(SIOCZ) Activity Index (SAI) values for a period of 43 years (1972-2015, except for 1978 when cloud data were not available) have been used in the study. Rainfall data were not available for the recently created district of Palghar. Also the data for the district of Mumbai Suburban were available for a limited period (1972-1989) only. Regression equations have been developed between SAI and rainfall using the data for a period of 32 years (1972-2004 except 1978) and data for the remaining 11 years (2005-2015) have been used for forecast verification.

RAINFALL

Long Period Average (LPA) of monthly, seasonal and annual rainfall for the subdivisions and their districts are given in Table 1. The Coefficient of Variation (C.V.) is highest in Marathwada for monthly as well as for the seasonal rainfall. The frequency of occurrence of deficient rainfall is lowest in the subdivision of Konkan & Goa. The rainfall of the subdivision was deficient in 7 years only during the period of 66 years (1950-2015). The number of deficient rainfall years during the said period in the subdivisions of Madhya Maharashtra, Marathwada and Vidarbha are 17, 21 and 13 respectively. Long range forecast of rainfall for the subdivision of Marathwada and its districts assumes a special significance because of high variability in monthly and seasonal rainfall and high frequency of occurrence of deficient rainfall.



Figure 1. Districts of Maharashtra.

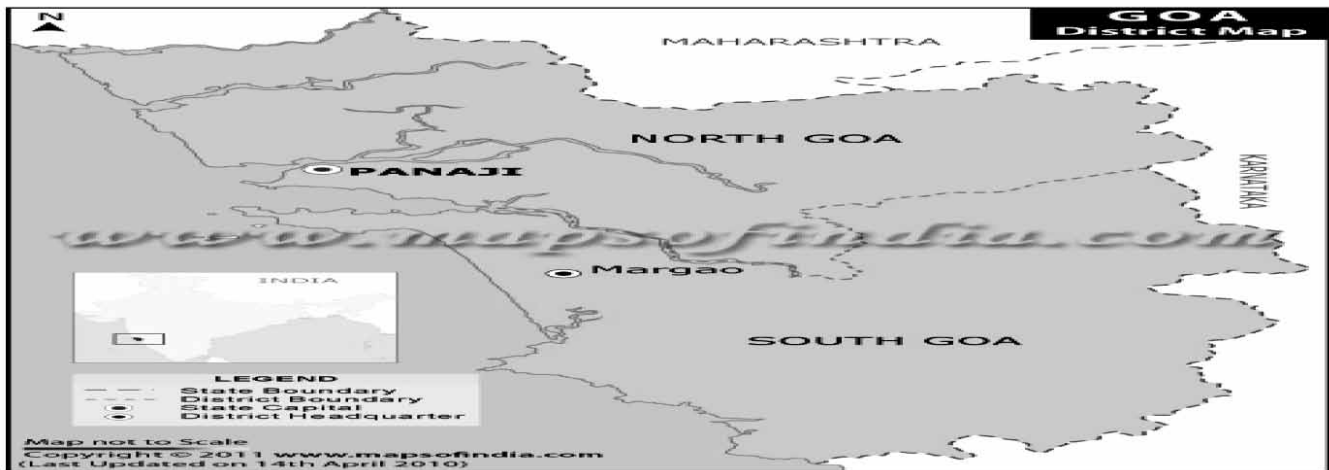


Figure 2. Districts of Goa.

South Indian Ocean Convergence Zone (SIOCZ) Activity Index (SAI)

The first set of 16 values of SAI, pertaining to the years 1972-1989, except 1978 and 1981 based on the features developing in the activity of SIOCZ during April-May, were assigned while proposing SIOCZ model (Gupta and Prasad, 1992). Beginning from the year 1990, SAI values are assigned on the real time basis and used for preparing forecasts (Prasad et al., 2010 a,b; Prasad and Singh, 2012; Prasad et al., 2014, 2016b,c). The values of SAI for the period 1972-2015 are reproduced here in Table 2.

Correlation between SAI and Rainfall

The Correlation Coefficients (CCs) between SAI and rainfall are given in Table 3. The value of CCs significant

at 95% and 99% level, are 0.34 and 0.44 respectively. The CCs are small and not significant in the month of June in any of the subdivisions/districts of both the states. The CCs are significant in July for the subdivisions and 24 districts of the states. There is considerable reduction in CCs values during August. However, the CCs are significant for Marathwada subdivision and its 7 districts. The CCs are significant for all the four subdivisions and 32 districts of the states during September. The number of districts where CCs are significant increases from bimonthly period of Jun+ Jul to Aug+ Sep. For the seasonal rainfall, the CCs are significant in all the subdivisions and their districts, except in 4 districts of Madhya Maharashtra, namely, Nasik, Pune, Satara and Sangli. The regression coefficients in the subdivisions and districts where CCs are significant are included in Table 4.

Table 1. Long period average rainfall (mm) during southwest monsoon season in meteorological subdivisions and districts of the states of Maharashtra & Goa. [Period: 1901-2000, Source: India Meteorological Department]

Subdivision/ District	Jun	Jul	Aug	Sep	Jun-Sep	Annual	Jun-Sep rainfall as % of Annual
Konkan & Goa	678.5	1079.5	676.2	341.4	2775.6	2959.1	94
Thane	434.5	924.1	575.2	319.6	2253.4	2368.1	95
Mumbai City	496.2	695.1	421.1	297.9	1914.7	2024.8	95
Mumbai suburban	540.1	803.5	514.9	316.0	2152.5	2239.9	96
Raigarh	619.3	1200.4	805.3	400.6	3025.5	3183.6	95
Ratnagiri	821.8	1237.3	782.8	374.6	3216.5	3433.6	94
Sindhudurga	854.3	1014.8	593.2	290.7	2753.0	2984.6	92
North Goa	873.0	1050.9	610.3	290.9	2825.1	3099.8	91
South Goa	870.4	997.2	572.4	279.1	2726.6	3006.3	91
Madhya Maha.	144.2	249.9	178.3	154.8	727.3	874.3	83
Nandurbar	131.7	282.6	203.4	145.9	763.5	830.0	92
Dhule	116.2	165.4	116.0	113.2	510.9	592.1	86
Jalgaon	131.1	201.4	172.6	136.7	641.7	734.3	87
Nasik	149.7	309.0	227.6	174.0	860.4	979.4	88
Ahmednagar	108.1	100.6	80.3	149.2	438.2	571.8	77
Pune	165.8	333.2	224.5	166.6	890.1	1042.5	85
Satara	199.5	427.6	279.1	173.3	1079.5	1282.5	84
Sholapur	100.7	92.1	92.9	169.7	455.4	618.8	74
Sangli	102.1	143.8	97.8	124.2	467.9	680.1	69
Kolhapur	281.2	602.1	367.9	158.6	1409.8	1658.3	85
Marathwada	140.5	181.6	164.6	182.0	668.7	800.6	83
Aurangabad	131.6	167.1	138.9	161.7	597.6	719.8	83
Jalna	139.2	169.4	157.8	139.8	606.2	722.8	84
Beed	121.5	130.6	123.7	189.4	565.2	692.7	82
Parbhani	154.2	211.7	194.9	194.7	755.4	895.4	84
Hingoli	174.4	230.6	217.9	151.9	774.8	904.3	86
Osmanabad	139.0	158.5	146.1	198.5	638.8	778.4	82
Latur	142.7	195.1	196.5	173.5	707.9	855.4	83
Nanded	154.3	239.3	219.0	191.1	803.4	936.9	86
Vidarbha	172.2	332.2	284.8	176.7	968.5	1101.7	88
Buldhana	146.2	205.6	171.6	138.3	661.7	776.1	85
Akola	139.0	228.5	178.5	137.5	683.7	793.9	86
Wasim	159.8	246.1	209.1	161.2	776.5	893.2	87
Amraoti	148.1	272.3	232.1	159.0	811.5	933.2	87
Yeotmal	170.9	285.7	233.5	165.8	855.8	990.9	86
Wardha	173.5	307.1	247.7	175.0	903.2	1047.6	86
Nagpur	176.5	338.2	283.8	183.2	981.8	1132.8	87
Bhandara	186.9	425.7	395.8	203.5	1211.9	1361.8	89
Gondia	189.3	440.1	419.3	204.1	1253.9	1397.1	90
Chandrapur	189.9	403.6	355.4	201.5	1150.4	1299.2	89
Gadchiroli	200.3	466.0	402.2	208.7	1277.3	1427.1	89

Long range forecast of rainfall during southwest monsoon in the states of Maharashtra and Goa

Table 2. South Indian Ocean Convergence Zone Activity Index (SAI). [Period: 1972-2015] *Cloud data were not available in 1978 after 16 March.

Year	1972	1973	1974	1975	1976	1977	1978	1979	1980	1981	1982
SAI	20	6	15	4	10	9	*	16	7	7	14
Year	1983	1984	1985	1986	1987	1988	1989	1990	1991	1992	1993
SAI	3	13	14	16	17	1	8	7	14	16	9
Year	1994	1995	1996	1997	1998	1999	2000	2001	2002	2003	2004
SAI	8	10	9	9	7	5	14	6	16	6	16
Year	2005	2006	2007	2008	2009	2010	2011	2012	2013	2014	2015
SAI	16	7	6	7	15	8	9	18	7	14	15

Table 3. Correlation coefficients between SAI and rainfall (mm) in the subdivisions and districts of Maharashtra and Goa. The CCs significant at 95% level or more are shown in bold italics. [Period: 32 years (1972-2004 except 1978)]

Subdivision/District	Jun	Jul	Aug	Sep	Jun+ Jul	Jul+ Aug	Aug+ Sep	Jun-Sep
Konkan & Goa	-0.06	<i>-.40</i>	-.10	<i>-.67</i>	<i>-.43</i>	<i>-.41</i>	<i>-.43</i>	<i>-.63</i>
Thane	-0.06	<i>-.41</i>	.12	<i>-.63</i>	<i>-.42</i>	-.25	-.31	<i>-.51</i>
Mumbai City	.07	-.11	-.08	<i>-.63</i>	-.04	-.15	<i>-.48</i>	<i>-.42</i>
Raigadh	-.20	<i>-.38</i>	-.07	<i>-.61</i>	-.41	<i>-.36</i>	<i>-.35</i>	<i>-.56</i>
Ratnagiri	.07	-.27	-.16	<i>-.64</i>	-.20	-.32	<i>-.44</i>	<i>-.46</i>
Sindhudurga	-.02	<i>-.38</i>	-.26	<i>-.54</i>	-.30	<i>-.43</i>	<i>-.46</i>	<i>-.50</i>
North Goa	.00	<i>-.43</i>	-.17	<i>-.51</i>	-.33	<i>-.42</i>	<i>-.38</i>	<i>-.45</i>
South Goa	-.08	-.22	-.24	<i>-.58</i>	-.22	-.31	<i>-.46</i>	<i>-.45</i>
Madhya Maha.	-.07	<i>-.52</i>	-.01	<i>-.49</i>	<i>-.40</i>	<i>-.39</i>	<i>-.35</i>	<i>-.55</i>
Nandurbar	-.18	<i>-.53</i>	-.03	<i>-.42</i>	<i>-.48</i>	<i>-.34</i>	-.29	<i>-.45</i>
Dhule	-.17	-.30	-.01	<i>-.52</i>	<i>-.35</i>	-.22	<i>-.37</i>	<i>-.48</i>
Jalgaon	.04	<i>-.34</i>	-.16	<i>-.57</i>	-.23	<i>-.36</i>	<i>-.45</i>	<i>-.49</i>
Nasik	-.03	<i>-.41</i>	.27	<i>-.58</i>	-.27	-.07	-.15	-.29
Ahmednagar	.10	<i>-.45</i>	-.24	<i>-.40</i>	-.20	<i>-.46</i>	<i>-.49</i>	<i>-.50</i>
Pune	-.05	-.28	.04	<i>-.40</i>	-.23	-.15	-.16	-.25
Satara	-.04	<i>-.41</i>	.09	-.31	-.28	-.23	-.09	-.29
Sholapur	.00	-.31	<i>-.35</i>	-.33	-.26	-.45	<i>-.44</i>	<i>-.46</i>
Sangli	-.02	<i>-.39</i>	-.16	-.06	-.23	<i>-.38</i>	-.11	-.26
Kolhapur	-.24	-.31	.06	-.30	<i>-.42</i>	-.25	-.08	<i>-.37</i>
Marathwada	.08	<i>-.49</i>	<i>-.55</i>	<i>-.53</i>	<i>-.34</i>	<i>-.68</i>	<i>-.69</i>	<i>-.67</i>
Aurangabad	.15	<i>-.37</i>	-.32	<i>-.48</i>	-.10	<i>-.50</i>	<i>-.55</i>	<i>-.52</i>
Jalna	.04	-.28	<i>-.34</i>	<i>-.47</i>	-.23	<i>-.45</i>	<i>-.56</i>	<i>-.54</i>
Beed	.09	<i>-.38</i>	<i>-.56</i>	<i>-.46</i>	-.26	<i>-.62</i>	<i>-.66</i>	<i>-.58</i>
Parbhani	.05	<i>-.45</i>	<i>-.51</i>	<i>-.57</i>	-.31	<i>-.62</i>	<i>-.73</i>	<i>-.69</i>
Hingoli	.30	<i>-.47</i>	<i>-.34</i>	<i>-.58</i>	-.16	<i>-.58</i>	<i>-.55</i>	<i>-.59</i>
Osmanabad	-.08	-.28	<i>-.43</i>	<i>-.42</i>	-.29	<i>-.47</i>	<i>-.57</i>	<i>-.56</i>
Latur	.07	<i>-.38</i>	<i>-.58</i>	<i>-.52</i>	-.29	<i>-.63</i>	<i>-.59</i>	<i>-.63</i>
Nanded	-.02	<i>-.56</i>	<i>-.59</i>	<i>-.54</i>	<i>-.48</i>	<i>-.72</i>	<i>-.71</i>	<i>-.73</i>
Vidarbha	-.15	<i>-.44</i>	-.10	<i>-.68</i>	<i>-.46</i>	<i>-.40</i>	<i>-.54</i>	<i>-.61</i>
Buldhana	.03	<i>-.44</i>	-.18	<i>-.50</i>	-.32	<i>-.52</i>	<i>-.40</i>	<i>-.50</i>
Akola	-.03	<i>-.45</i>	-.05	<i>-.55</i>	<i>-.38</i>	<i>-.36</i>	<i>-.38</i>	<i>-.48</i>
Wasim	.14	<i>-.39</i>	-.22	<i>-.46</i>	-.19	<i>-.45</i>	<i>-.45</i>	<i>-.46</i>
Amraoti	-.22	<i>-.38</i>	.11	<i>-.63</i>	<i>-.53</i>	-.15	-.30	<i>-.51</i>
Yeotmal	-.03	<i>-.52</i>	<i>-.35</i>	<i>-.62</i>	<i>-.50</i>	<i>-.61</i>	<i>-.63</i>	<i>-.72</i>
Wardha	.03	<i>-.41</i>	.11	<i>-.52</i>	-.33	-.18	-.26	<i>-.34</i>
Nagpur	-.20	-.21	-.16	<i>-.69</i>	-.27	-.27	<i>-.60</i>	<i>-.54</i>
Bhandara	-.18	-.30	-.02	<i>-.70</i>	<i>-.35</i>	-.27	<i>-.45</i>	<i>-.49</i>
Gondia	-.20	<i>-.39</i>	.08	<i>-.65</i>	<i>-.43</i>	-.23	-.29	<i>-.46</i>
Chandrapur	-.17	<i>-.44</i>	-.07	<i>-.63</i>	<i>-.41</i>	-.31	<i>-.41</i>	<i>-.48</i>
Gadchiroli	-.21	-.31	-.06	<i>-.60</i>	<i>-.37</i>	-.25	<i>-.37</i>	<i>-.43</i>
No. of districts where CC is significant at 95% level or more ($\geq .34$)	Nil	24	10	32	15	23	30	32

Table 4. Regression coefficients between SAI and rainfall for the subdivisions and their districts where CC is significant at 95% level or more. The CC is not significant in any subdivision/district during the month of June.

Subdivision/ District	Jul		Aug		Sep		Jun+ Jul		Jul+ Aug		Aug+ Sep		Jun-Sep	
	a	b	a	b	a	b	a	b	a	b	a	b	a	b
Konkan Goa	-19.8	1219.1			-22.9	556.1	-11.0	964.0	-12.1	998.9	-13.7	667.4	-49.3	3262.7
Thane	-21.1	1061.5			-24.7	553.8	-11.8	755.9			-9.5	560.4	-42.9	2636.6
Mumbai City					-27.8	604.5					-15.9	578.8	-34.8	2402.0
Raigadh	-22.6	1375.4			-23.4	626.6	-15.8	1050.0	-13.3	1129.2	-13.8	754.8	-59.1	3609.6
Ratnagiri					-24.5	602.3					-16.7	760.5	-45.3	3593.6
Sindhudurga	-20.5	1206.3			-19.0	466.9			-16.1	1003.3	-15.3	633.6	-52.1	3352.3
North Goa	-25.4	1300.8			-16.5	417.5			-16.8	1043.0	-12.4	601.4	-50.1	3445.5
South Goa					-21.2	474.5					-17.0	642.0	-52.4	3356.4
MadhyaMaha.	-6.3	298.2			-7.2	224.9	-3.6	237.7	-3.3	249.4	-3.7	212.7	-14.6	900.8
Nandurbar	-12.1	400.9			-9.0	221.7	-8.1	306.2	-6.4	328.5			-25.5	1081.1
Dhule					-7.8	184.0	-3.2	181.3			-3.9	161.0	-14.3	684.6
Jalgaon	-4.5	232.4			-9.1	211.3			-3.6	230.1	-5.9	219.5	-15.6	799.1
Nasik	-7.6	359.2			-9.7	262.4								
Ahmednagar	-4.2	135.4			-7.6	220.9			-3.4	127.1	-5.1	169.9	-13.3	580.7
Pune					-22.9	556.1								
Satara	-9.2	480.0												
Sholapur			-4.8	151.0					-4.0	135.7	-6.9	201.1	-15.7	627.6
Sangli	-4.0	154.3							-2.6	129.8				
Kolhapur	-12.1	746.7					-9.5	595.5					-21.4	1841.5
Marathwada	-7.2	242.6	-10.0	286.1	-10.9	268.9	-3.1	180.7	-8.6	264.3	-10.4	277.5	-27.2	929.6
Aurangabad	-4.2	184.5			-9.2	239.2			-4.3	190.3	-6.8	217.7	-15.5	721.7
Jalna			-5.9	223.2	-9.1	231.8			-5.0	209.7	-7.5	227.5	-19.7	796.1
Beed	-6.0	186.4	-9.9	241.4	-10.5	276.1			-7.9	213.9	-10.2	258.8	-25.6	833.6
Parbhani	-9.1	287.9	-13.6	364.9	-12.8	287.4			-11.3	326.4	-13.2	326.1	-34.6	1094.0
Hingoli	-10.0	318.2	-9.9	328.3	-11.6	265.8			-10.0	323.2	-10.7	297.0	-28.7	1071.4
Osmanabad			-7.3	216.4	-9.0	266.5			-5.3	187.8	-12.6	305.6	-20.4	771.1
Latur	-6.3	233.1	-13.0	319.5	-12.2	291.8			-9.7	276.3	-8.1	241.4	-30.9	967.6
Nanded	-13.7	82.8	-15.8	419.0	-13.5	294.2	-7.0	271.1	-14.7	400.9	-14.6	356.6	-43.3	1255.6
Vidarbha	-8.7	388.1			-11.4	259.7	-5.4	294.4	-5.2	356.3	-6.6	292.1	-24.1	1173.1
Buldhana	-5.7	244.5			-7.9	195.0			-4.3	238.1	-5.4	213.3	-16.2	814.7
Akola	-8.2	291.6			-9.0	205.6	-4.4	225.1	-4.6	259.9	-5.0	216.9	-18.9	884.3
Wasim	-7.0	303.4			-10.2	255.5			-5.9	291.7	-7.5	267.8	-19.2	981.2
Amraoti	-7.3	317.7			-11.1	243.8	-5.1	249.0			-4.1	244.7	-18.4	987.9
Yeotmal	-10.6	364.3	-7.6	342.8	-12.4	256.9	-5.5	271.7	-9.1	353.6	-10.0	299.8	-31.2	1143.1
Wardha	-9.3	354.0			-10.6	247.8					-3.9	242.6	-16.5	1003.9
Nagpur					-13.9	295.0					-8.3	307.2	-25.6	1195.4
Bhandara					-13.3	302.1	-6.5	337.4			-6.8	341.4	-26.6	1357.5
Gondia	-11.9	519.5			-13.1	308.3	-8.6	387.0			-5.4	347.7	-28.0	1469.5
Chandrapur	-10.8	456.1			-11.6	270.9	-7.2	341.7			-6.7	325.0	-27.8	1333.3
Gadchiroli	-10.8	541.3			-11.0	281.2	-7.7	409.5			-6.4	364.8	-28.7	1550.6

Table 5a. Summary of verification of forecasts of monthly rainfall. The CCs is not significant in any of the subdivisions/districts in the month of June.

Subdivision & No. of Districts in it	Subdivision & No. of districts where CCs is significant	% of 'Useful' forecast in the subdivision & mean % of 'Useful' forecast in the districts		Subdivision & No. of districts where CCs was significant	% of 'Useful' forecast in the subdivision & mean % of 'Useful' forecast in the districts		Subdivision & No. of districts where CCs was significant	% of 'Useful' forecasts in the subdivision & mean % of 'Useful' forecasts in the districts	
		July			August			September	
		1972-2004	2005-2015		1972-2004	2005-2015		1972-2004	2005-2015
Konkan & Goa 7	Yes 4	87	73	No Nil	-	-	Yes 7	84	73
		80	80		-	-		78	71
Madhya Maha. 10	Yes 7	94	91	No 1	-	-	Yes 6	66	82
		76	68		78	82		71	65
Marathwada 8	Yes 6	72	55	Yes 7	81	100	Yes 8	62	64
		75	61		80	86		65	69
Vidarbha 11	Yes 11	78	73	No 1	-	-	Yes 11	78	55
		81	65		84	82		78	55

Forecast Verification

For the purpose of verification of forecasts at subdivision as well as district level, only two broad categories of rainfall, namely, 'Excess/Normal' and 'Deficient/Scanty' are used. A forecast has been termed 'Useful' if the realized as well as the forecast rainfall are in the same broad category or they become so if Model Error (M.E.) denoted in mm is taken into account. The forecasts in a year are considered reasonably good, if they are in 'Useful' category in 60% of the districts of a subdivision. As the satellite observed cloud/OLR data required for assigning SAI are available for a limited period of time, the desired accuracy of ± 1 in assigning the value of SAI could not be achieved. Hence it is presumed that there could be an error of ± 2 in the assigned value of SAI in a year (Table 2). Accordingly the M.E. in forecast rainfall becomes twice the value of the coefficient 'a' of the regression equations. In order to compare forecast rainfall with the realized rainfall, which is available in %, the M.E. was converted into % of Long Period Average (LPA) rainfall. For describing rainfall we have used the categorization of rainfall based on % departure from normal as used in IMD: 'Excess' (E), R/F >20%, 'Normal' (N) 19% to -19%, 'Deficient' (D) -20% to -59%, 'Scanty' (S) -60% to -99% and 'No Rain' (NR) -100%. The results of verification for a period of 11 years (2005-2015) have been included in Tables 5 & 6.

Forecast of monthly rainfall

The CCs are not significant in any of the subdivisions/districts during June. The M.E. in the subdivisions and

their districts, in the order they appear in Tables 4, and where the CCs are significant are: Jul (**4**,5,4,4,5; **5**,9,4,5,8,4,6,4; **8**,5,9,9,9,6,11; **5**,6,7,6,5,7,6,5,5,5), Aug (Sholapur-10;**12**,8,16,14,9,10,13,14; Yeotmal-7); Sep (**10**,10,13,8,11,12,10,14; **8**,11,10, 12,9,10,7; **11**,11,12,10,11,14,9,13,12; **9**,10,11,10,9,12,9,10,9,8,9,7). The bold figure refers to the value of M.E. for the subdivision. Summary of verification is given in Table 5a. For the month of July, the % of 'Useful' forecast, during the period of development of the model equations, is 94% in Madhya Maharashtra and the least (72%) in Marathwada. With slightly reduced percentages, this trend is present during the forecast verification period also. The % of 'Useful' forecast has varied from 81% in Vidarbha to 75% in Marathwada. During the month of August, the CCs are significant in one district each in Madhya Maharashtra and Vidarbha, i.e., Sholapur and Yeotmal respectively. The % of 'Useful' forecasts in these 2 districts during the period of development of the model equations (forecast verification period) are 78% (82%) and 84% (82%) respectively. August rainfall in the districts of Marathwada is well correlated with SAI. With the exception of Aurangabad, the CCs are significant in all the remaining 7 districts of the subdivision. The % of 'Useful' forecast for the subdivision and the mean % of 'Useful' forecasts in the districts during the period of development of the model equations are 81% and 80% respectively. The respective figures for the period of verification are 100% and 86%. The situation improves remarkably during September, when the CCs become significant in the districts of the subdivisions of Konkan & Goa, Marathwada and Vidarbha. The % of 'Useful' forecast during the period of development of the

Table 5b. Summary of verification of forecasts of bi-monthly rainfall.

Subdivision & No. of Districts in it	Subdivision & No. of districts where CCs is significant	% of 'Useful' forecast in the subdivision & mean % of 'Useful' forecast in the districts		Subdivision & No. of districts where CCs is significant	% of 'Useful' forecast in the subdivision & mean % of 'Useful' forecast in the districts		Subdivision & No. of districts where CCs is significant	% of 'Useful' forecast in the subdivision & mean % of 'Useful' forecast in the districts	
		Jun+ Jul 1972-2004	2005-2015		Jul+ Aug 1972-2004	2005-2015		Aug+ Sep 1972-2004	2005-2015
Konkan & Goa 7	Yes 2	87 81	100 91	Yes 3	87 86	100 88	Yes 7	84 84	91 91
Madhya Maha. 10	Yes 3	87 89	64 83	Yes 4	84 79	100 84	Yes 5	81 87	100 98
Marathwada 8	Yes 1	81 84	64 64	Yes 8	91 83	82 80	Yes 8	84 80	91 85
Vidarbha 11	Yes 6	84 84	82 79	Yes 4	91 84	82 79	Yes 11	87 81	100 87

model equations for the subdivisions' rainfall has varied from 84% for Konkan & Goa to 62% for Marathwada. The corresponding figures for the forecast in the districts have varied from 78% in Konkan & Goa and Vidarbha to 65% in Marathwada. The figures for the subdivisions for the period of verifications have varied from 82% in Konkan & Goa to 55% in Vidarbha. The corresponding figures for the forecasts in the district are 71% in Konkan & Goa to 55% in Vidarbha. There is some reduction in the % of 'Useful' forecast for the subdivision of Vidarbha for the month of September during the period of verification.

A comparison of % of 'Useful' forecasts in the districts of Maharashtra and Goa with those in the districts of A.P. and Telangana has shown that (i) during July, the forecasts % in Konkan & Goa is comparable to those in the districts of A.P. and higher than that in the districts of Telangana. The % of 'Useful' forecast is lower in the districts of other subdivisions as compared to A.P. and comparable to those in the districts of Telangana, (ii) during August, forecasts are not available for the districts of Konkan & Goa. The forecast % is higher than that in the districts of A.P. and comparable to that in the districts of Telangana, (iii) in September, the % of 'Useful' forecast in the districts of Vidarbha are lower than that in the districts of A. P. and Telangana. The forecast % in the remaining subdivisions is comparable to those in A.P. and Telangana.

Forecast of bi-monthly rainfall

The M.E. in the subdivisions and their districts, in the order as they have appeared in Tables 4, and where the CCs is significant are: Jun+ Jul (2,3,3; 4,8,8; 4,7; 4,5,5,5,4,5,5,5), Jul+Aug (3,3,4,4; 3,5,4,8,9,4; 10,6,6,12,11,9,7,10,13; 3,5,5,5,7), Aug+Sep (5,4,9,5,6,7,5,8; 4,7,8,7,10; 2,9,10,13,14,12,9,14,14; 6,7,6,8,4,10,4,7,5,3,5,5,4). The

summary of verification of forecasts in respect of bi-monthly rainfall are given in Table 5b. It may be noted that the number of districts where CCs are significant for the bi-monthly period of Jun+ Jul has reduced to 12 as compared to 24 for the month of July (Table 5a). This is due to the effect of rainfall in the month of June. In the subdivision of Vidarbha, where CCs are significant in the majority of the districts, the % of 'Useful' forecast has varied from 84% during the period of development of the equations to 82% during the period of verification. The corresponding figures for mean % of 'Useful' forecasts in the districts are 84% and 79%. Rainfall of Jul+ Aug is well correlated with SAI in all the districts of Marathwada. Also the mean % of 'Useful' forecasts in the districts, both during the period of model development and verification, are high: 91% and 82% respectively. There is a jump in the number of districts where CCs are significant for the rainfall during the bi-monthly period of Aug+ Sep and it is now in 31 districts (out of 36). The exceptions are: 5 districts of Madhya Maharashtra. The improvement is seen in the % of 'Useful' forecasts also. It is now between 81% to 87% for the subdivisions during the development of model equations and 91% to 100% during the period of verification. The corresponding figures for the mean % of 'Useful' forecasts in the districts are 80% to 87% and 85% to 98% respectively. In conclusion, there is a distinct possibility of issuing forecasts of rainfall for the bi-monthly period of Aug+ Sep. Forecast for the bi-monthly period of Jul+ Aug could also be issued for the districts of Marathwada. Similarly, Forecast for the bi-monthly period of Jun+ Jul could also be issued for the majority of the districts of Vidarbha.

A comparison of 'Useful' forecasts during the bi-monthly periods in the districts of Maharashtra & Goa with those in A.P. and Telangana has shown that (i) during

Long range forecast of rainfall during southwest monsoon in the states of Maharashtra and Goa

Table 5c. Summary of verification of forecasts of seasonal rainfall.

Subdivision & No. of districts in it	Subdivision & No. of districts where CCs is significant	% of 'Useful' forecast in the subdivision & mean % of 'Useful' forecasts in the districts	
		1972-2004	2005-2015
Konkan & Goa 7	Yes 7	94 88	100 90
Madhya Maha. 10	Yes 6	97 84	73 92
Marathwada 8	Yes 8	91 85	100 93
Vidarbha 11	Yes 11	84 87	100 91

Table 6. Subdivision-wise details of forecasts where it was in 'Useful' category in less than 60% of the districts where CCs was significant.

Month/ Period	Subdivision (No. of districts), No. of districts (figures in Italics) where CCs is significant and years with % of districts (in bracket) where forecast was in 'Useful' category . The figure, given at the bottom in the right hand corner of each block, refers to the % of forecasts which were not in 'Useful' category out of the number of total forecasts issued during the period (2005-2015).			
	Konkan & Goa (7)	Madhya Maha. (10)	Marathwada (8)	Vidarbha (11)
Jun	<i>Nil</i> -	<i>Nil</i> -	<i>Nil</i> -	<i>Nil</i> -
Jul	4 2006(50) 2007(25) 2008(25) 7%	7 2005(14) 2008(29) 2009(43) 4%	6 2005(0) 2006(0) 2007(50) 2008(0) 2012(23) 8%	8 2005(0) 2008(12) 2011(50) 2012(12) 5%
Aug	<i>Nil</i> -	1 <i>Nil</i>	7 2008(57) 2013(28) 3%	1 <i>Nil</i>
Sep	7 2005(0) 2009(14) 2014(0) 4%	6 2005(0) 2011(33) 2012(50) 2014(33) 2015(16) 8%	8 2005(0) 2009(50) 2011(12) 3%	11 2005(0) 2008(54) 2012(0) 2013(45) 2014(36) 2015(27) 5%
Jun+ Jul	2 <i>Nil</i>	3 2008(33) 8%	1 2006(0) 2007(0) 2008(0) 2011(0) 36%	6 2008(43) 2011(57) 2012(28) 5%
Jul+ Aug	3 2015(33) 3%	4 2005(50) 2008(50) 2015(50) 7%	8 2007(50) 2008(25) 2%	4 2008(25) 2%
Aug+ Sep	7 2015(57%) 1%	5 <i>Nil</i>	8 2005(37) 1%	11 2012(45) <1%
Jun-Sep	7 2015(43%) 1%	6 <i>Nil</i>	8 <i>Nil</i>	11 2008(55) <1%

the period of Jun+ Jul, the % of 'Useful' forecasts was lower in Marathwada but nearly the same in the districts of other subdivisions as compared to the districts in A.P. The % of 'Useful' forecasts in the districts of Marathwada was comparable and it was higher in the districts of other subdivisions of Maharashtra and Goa as compared to the districts of Telangana, (ii) during Jul+ Aug, the % of 'Useful' forecasts was higher in the districts of Konkan

& Goa as compared to those in the districts of A.P. and Telangana. In other subdivisions it was comparable to those in the districts of A.P. and Telangana, (iii) during Aug+ Sep, the % of 'Useful' forecasts in the districts of Madhya Maharashtra is higher than that in the districts of A.P. and Telangana. In the remaining subdivisions, it is either higher or comparable to that in the districts of A.P. and higher than that in the districts of Telangana.

Forecast of seasonal rainfall

Except for 4 districts of the subdivision of Madhya Maharashtra, namely, Nasik, Pune, Satara and Sangli, the CCs are significant in all other districts (Table 3). The M.E. in the subdivisions and their districts are: 4,4,4,4,4,3,4,4,4; 4,7,6,5,6,7; 8,5,6,9,9,7,6,9,11; 5,5,6,5,5,7,4,5,4,4,5,4. The summary of verification of seasonal forecasts is given in Table 5c. The % of 'Useful' forecasts is high: 84% -100%, except for the subdivision of Madhya Maharashtra, where it is 73%. The mean % of 'Useful' forecasts in the districts has varied from 84% in Madhya Maharashtra to 88% in Konkan & Goa during the period of development of model equations. The figure for the period of verification is more than 90%. These results point towards the possibility of issuing operational long range forecasts of seasonal rainfall in the districts of Maharashtra and Goa. The % of 'Useful' forecasts in the districts of Maharashtra & Goa is comparable to that in the districts of A.P. and it is higher than that in the districts of Telangana.

Reduction in Number of Districts in 'USEFUL' Category of Forecast in Some Years

The % of forecasts which are not in 'Useful' category during the period of verification (2005-2015) for each month, bi-monthly periods and the whole SWM season have been worked out. For example, the number of districts where CCs are significant in the Konkan & Goa subdivision during the month of July are 4. During 11 year verification period, a total of 44 forecasts had been issued. 3 out of those, i.e., 7% forecasts were not in 'Useful' category. The details in respect of % of such not in 'Useful' forecasts category have been included in Table 6. It follows from Table 6 that, during the bi-monthly period of Jun+ Jul except for rainfall in just a lone district in Marathwada, i.e., Nanded, the % of forecasts which were not in 'Useful' category is <10%. This is an encouraging result. The corresponding figures for Aug+ Sep and seasonal rainfall, which are 1% or less, are still more encouraging. Intra-seasonal changes in the activity of SIOCZ are responsible for reduction in number of districts in 'Useful' category of forecasts, as it had been discussed in district level forecasts for the states of Andhra Pradesh (Prasad, et al., 2016b) and Telangana (Prasad, et al., 2016c). Due to lack of space, it could not be possible to include OLR/weekly mean cloudiness maps and discussions on intra-seasonal changes and their impact on forecasts in the districts of Maharashtra and Goa.

CONCLUSIONS

1. The close relationship between the activity of South Indian Ocean Convergence Zone and Indian Summer

Monsoon Rainfall, also holds good for southwest monsoon rainfall in the states of Maharashtra and Goa.

2. Long range forecast of southwest monsoon seasonal rainfall could be issued for all the districts of the states of Maharashtra and Goa except for 4 districts of Madhya Maharashtra, namely, Nasik, Pune, Satara and Sangli. Forecasts could also be issued for a number of districts in July, August and September and bi-monthly periods of Jul+ August and August+ September.

3. Long range forecast of rainfall in the districts of Marathwada, the subdivision which is prone to occurrence of deficit rainfall, could be issued for the season as a whole, bi-monthly periods and also for monthly rainfall, except for the month of June.

4. The % of 'Useful' forecast varies from month to month and also from one subdivision to another. For the month of July, the best forecasts are available for the subdivision of Madhya Maharashtra, followed by Konkan & Goa, Vidarbha and Marathwada. In August the best forecasts are available for Marathwada. However, the forecasts are not available for this month in the remaining subdivisions. In September, the best forecast are available for Madhya Maharashtra followed by Konkan & Goa, Marathwada and Vidarbha.

5. A comparison of the % of 'Useful' forecasts in Maharashtra & Goa with those in the state of Telangana has shown that July forecast for the former zone is slightly better than that in Telangana. August forecast is comparable to that in Telangana. September forecast % is lower in Vidarbha and in other subdivisions it is comparable to that in Telangana. During the bi-monthly period of Jun+ Jul, the % of 'Useful' forecast is lower in Marathwada and in the remaining subdivisions it is comparable to that in Telangana. During Jul+ Aug, the % of 'Useful' forecast is higher in Konkan & Goa. In the remaining subdivisions it is either comparable to or slightly higher than that in Telangana. During Aug+ Sep, the % of 'Useful' forecast is higher in Madhya Maharashtra. In other subdivisions it is either higher or comparable to those in Telangana. For the season as a whole, the % of 'Useful' forecasts in the districts of Maharashtra & Goa is better than that in Telangana.

6. The forecasts for the month of June are not available for any of the subdivisions/districts. In the remaining months, the forecast is not available for all the districts of the subdivisions. Similarly, seasonal forecast is not available for four districts of Madhya Maharashtra. SAI values used here for preparing forecast in Maharashtra and Goa, had been calibrated with Indian Summer Monsoon Rainfall (ISMR) data which represents June-September total rainfall for India as a whole. These SAI values are unable to take care of the characteristics of rainfall distribution in subdivisions and their districts. For improvement in results, a new set of SAI values calibrated with subdivision/district level rainfall data has to be worked out.

ACKNOWLEDGMENTS

Rainfall data had been supplied by Additional Director General of Meteorology (Research), India Meteorological Department, Pune. The map showing the districts of Maharashtra and Goa have been downloaded from the site 'www.mapsofindia.com'. OLR data have been downloaded from NOAA/Climate Prediction Centre's web site. Figures showing OLR anomaly /Zonal weekly mean cloudiness fields have been drawn using GrADS software developed by COLA/IGES. Authors thank Dr. U.S. De for constructive suggestions and evaluation of the manuscript. They also thank Prof. B.V.S. Murty and Chief Editor for apt editing and useful suggestions to enhance quality of the manuscript.

Compliance with Ethical Standards

The authors declare that they have no conflict of interest and adhere to copyright norms.

REFERENCES

- Gupta, G. R., and Onkari Prasad, 1992. Role of Southern Hemispheric Equatorial Trough in long range forecasting, *Jalvigyan Saameeksha*, - A publication of Indian national Committee on Hydrology, v.7, pp: 83-97.
- Onkari Prasad, Singh, O. P., and Subramanian, S.K., 2010a. Seasonal forecast of southwest monsoon rainfall-District level, *J. Ind. Geophys. Union*, v.14, no.2, pp: 93-113.
- Onkari Prasad, Singh, O. P., and S. Prasad, 2010b. South Indian Convergence Zone model: A new approach to long range forecasting of summer monsoon rainfall in India, Part-I: Role of south Indian convergence zone in the development of Indian summer monsoon, *J. Ind. Geophys. Union*, v.14, no.4, pp: 233-248.
- Onkari Prasad, Singh, O. P., and K. Prasad, 2014. South Indian Convergence Zone model: A new approach to long range forecasting of summer monsoon rainfall in India, Part-VI: Merits of the model and limitations in seasonal forecasting of rainfall in India, *Indian summer monsoon*, *J. Ind. Geophys. Union*, v.18, no.3, pp: 363-386.
- Onkari Prasad, Singh, O. P., and K. Prasad, 2016b. District level long range forecast of rainfall during southwest monsoon in Andhra Pradesh, *J. Ind. Geophys. Union*, v.20, no.2, pp: 254-264.
- Onkari Prasad, Singh, O. P., and K. Prasad, 2016c. District level long range forecast of rainfall during southwest monsoon in Telangana, *J. Ind. Geophys. Union*, v.20, no.4, pp: 434-441.

Cloud Aerosol Interactions and its influence on Cloud Microphysical parameters during Dry and Wet spells of Indian Summer Monsoon using CAIPEEX data

G.R. Chinthalu*, T. Dharmaraj, M.N. Patil, A.R. Dhakate and Devendraa Siingh

Indian Institute of Tropical Meteorology, Pune 411008 India

*Corresponding author: chintalu@tropmet.res.in

ABSTRACT

The variations of cloud condensation nuclei (CCN), aerosol and cloud particle concentration (PCASP), cloud droplet effective radius (CDPR_e), and Liquid water content (LWC) have been measured using instrumented aircraft over Hyderabad, Bengaluru and Bareilly in India during Cloud Aerosol Interactions and Precipitation Enhancement Experiment (CAIPEEX-2009). Three intensive observation periods (IOPs) i.e. 17-22 June and 13 July representing the dry spells, and the IOP during 16-25 August, representing wet spells of Indian summer monsoon were analyzed. Cloud droplet size is highly sensitive to liquid water content and temperature in the cloud environment. The CDPR_e and LWC show strong linear correlation during both dry spells and wet spells of ISMR. The mid level clouds C_M ~ 2000 meters are more favorable for coalescence of cloud droplets leading to growth of CDPR_e > 14 μm required for warm rain formation.

Key words : Cloud condensation nuclei (CCN), Aerosol and cloud particle concentration (PCASP), Cloud droplet effective radius (CDPR_e), Liquid water content (LWC) and Indian Summer Monsoon.

INTRODUCTION

The Indian Summer Monsoon Rainfall (ISMR) during a four-month period (June-September) shows large variations in the interannual and intraseasonal time scale due to embedded dry and wet spells. Droughts over India impact the economy of the country leading to major loss of agricultural productivity and livelihood of a large population (Swaminathan, 1987). Following Deka et al., (2010) the definition of spell is based on the duration of consecutive wet and dry days. A wet spell is a sequence of wet days and it begins and ends the day after and the day before a dry day. In this study a wet day (W) is considered as one where the precipitation is ≥1 mm and above. Obviously, dry day (D) is the one where there is no precipitation or is < 1 mm. The important aspect of dry spells of the Indian summer monsoon have been reported by Krishnamurti et al., (2010) regarding the formation of a blocking high around Arabian Peninsula located at 3-9 km above sea level. Studies on the aerosol-cloud interaction over Indian summer monsoon zone and associated dry and wet spells have not received adequate attention due to lack of extensive in-situ field observations. It is in this context CAIPEEX-2009 (Cloud Aerosol Interaction and Precipitation Enhancement Experiment -2009) was taken up with the main objectives as: (i) to simultaneously measure microphysics of aerosols, CCN, cloud parameters (number concentration, liquid water content, particle size, etc.) and large-scale meteorological conditions to document and (ii) to analyse the data towards understanding the pathways through which aerosols interact with clouds

and influence precipitation over the continental Indian monsoon region.

Aerosols cloud interactions and warm rain formation

Aerosols modulate the weather and climate by perturbing the radiative budget through direct absorption and scattering of solar radiation (the direct effect) and altering the cloud microphysical properties by acting as cloud condensation nuclei (the indirect effect) (Jayaraman, 2001; Kaufman and Koren, 2006; Devara et al., 2009; Manoj et al., 2012). Sarkar and Kumar (2007) reported rain-bearing cloud height along the east and west coasts and peninsular India to be 3-6 km. Leiming et al., (2006) reported that usually marine and continental clouds show different precipitation efficiencies. The different cloud condensation nuclei (CCN) size distributions and composition play a major role in precipitation development particularly in warm clouds. Warner and Twomey (1967) concluded that droplet concentration in clouds forming in air contaminated by smoke from cane fires is greatly increased leading to much retarded coalescence process causing less rain. Enhanced aerosol concentrations also suppress warm rain processes by producing a narrow droplet spectrum which inhibits collision and coalescence processes (Squires and Twomey, 1960, Warner, 1968, Rosenfeld, 1999). Elevated concentrations of CCN contains higher concentrations of smaller cloud droplets, which slows their coalescence into raindrops (Squires, 1958). This can lead to suppression of precipitation in shallow and short-lived clouds (Warner,

1968). The CCN fraction at a given super saturation (CCNS) is the subset of the overall aerosol population, which can be activated to cloud droplets at a higher super saturation. The CCN and condensation nuclei (CN) indicate strong dependence of (CCN/CN) on particle size. For this reason, they play a significant role in the CCN budget and in the cloud-mediated effects of aerosols on climate (Adams and Seinfeld, 2003; Pierce et al., 2007).

METHODOLOGY

Description of CAIPEEX aircraft and its instrumentation

The PA-31T instrumented aircraft was used during the CAIPEEX programme. The instruments include (i) Passive Cavity Aerosol Spectro Photometer (PCASP: DMT -100X) for aerosol particle measurements inside the clouds in the range of 0.1-3.0 μm (ii) An aerosol counter (DMT-100) to measure cloud condensation nuclei (CCN) which form at different super-saturations in the range of 0.1 - 1.2 %. (iii) The cloud droplet probe (CDP), which measures the concentration and size distribution of cloud droplets in the size range from 2-50 μm . [The effective radius (R_{eff}) is measured using the CDP probe which is referred as (CDPre) the cloud droplet size distribution in the range 3-50 μm .] (iv) DMT LWC-100 to measure liquid water content (LWC) in the range of 0-3 gm^{-3} . Details of the cloud-aerosol instrumentation and CAIPEEX experiment are described by Kulkarni et al., (2012).

Data and synoptic weather conditions

Data used are daily aircraft observations viz., (a) CCN (b) aerosol concentrations (c) CDPre (d) LWC (e) Flight track data (f) radiosonde data (g) Composite daily wind field at 700 hPa from NCEP/NCAR- Reanalysis and (h) Meteosat-7 visible satellite imagery.

Intensive observation periods

During June 8-20, 2009 there was a prolonged hiatus in the further advance of the monsoon. A Depression was formed over the Arabian Sea during June 23-24, 2009 and the monsoon revived and further advanced as reported by IMD (2009). Thus 17-22 June and 13 July, 2009 were identified as dry and 16-25 August as wet spells of monsoon. Daily flight routes were accordingly planned based on the prevailing weather conditions. The aircraft base stations in India are shown in Figure 1 and the flight tracks for dry and wet spells are illustrated in Figure 2a-b. The aircraft data measured over Hyderabad, Bengaluru and Bareilly are utilized in this study.

The daily flight routes

During the experiment, aircraft measurements were conducted near Hyderabad (17.38°N, 78.48°E) during the dry spell. While in the wet spell, the aircraft observations were continued near Bengaluru (12.97 °N, 77.59°E) and Bareilly (28.35°N, 79.41°E). Figure 2a shows the aircraft route map for 17 June, 2009 over Hyderabad. The aircraft flight track extending up to about 7 km with low cloud depth reveals a weak convective activity and the same is evident from the satellite imagery for this day. Figure 2b shows aircraft flight tracks on July 13, 2009. On this day the well developed clouds attained high vertical depths, height extending above 7 km, which caused intense convective activity. Figure 2c shows the 17 June, 2009 Meteosat-7 0600 UTC visible satellite imagery representing the Indian sub-continent and adjoining ocean areas such as Indian Ocean, Arabian Sea and Bay of Bengal. Satellite imagery clearly depicts few isolated shallow clouds over Hyderabad, which indicates subdued convective activity and dry weather. Similarly Figure 2d depicts the 13 July, 2009 Meteosat-7 0600 UTC visible satellite imagery showing the prevalence of dense thick convective rain bearing clouds over Bengaluru and major parts of Indian land mass representing wet monsoon conditions.

Daily mean values of air-borne measurements were calculated from instantaneous values for respective dates of observations over the study region and discussed. Warm clouds form when a large number of water droplets having a wide range of radius, collide with each other and interact with suspended aerosol particles present in atmosphere which act as a seed for the development of cloud. When the effective radius (R_{eff}) of the droplet, under conditions, is < 14 μm the rain rate is limited by the rate of coalescence of cloud drops (Rosenfeld et al., 2012).

RESULTS AND DISCUSSIONS

Cloud base characteristics during dry and wet spells

The cloud base heights, referred as lifting condensational level (LCL) for air parcel and air temperature during dry spell derived from radiosonde data, are shown in table-1. The cloud base temperature during the dry spell varies between 11.5 to 16.5 °C, with a mean of 13.8 °C. Cloud base height varies between 2060 and 3044 meters and the mean height is ~ 2742 meters. The cloud temperature is one of the responsible parameters which might enhance or suppress the growth of CDPre. Cloud base height and temperature during wet spell are shown in table-2. While the cloud base temperature during the wet spell varies between 16.0 to 23.7°C with a mean of 20.8 °C, the cloud base height varies between 1299 and 1828 meters and the

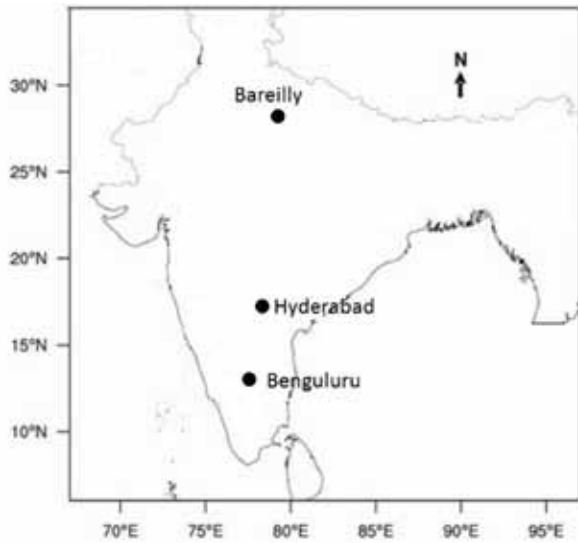


Figure 1. Map showing IOP base stations of Hyderabad, Bengaluru and Bareilly.

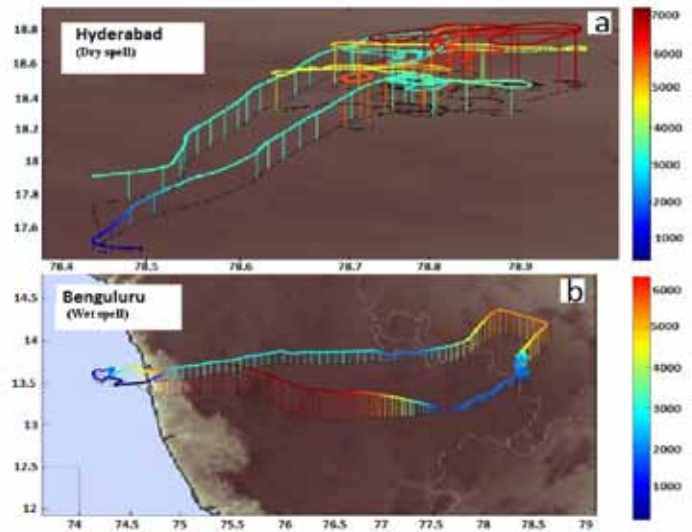


Figure 2a. Flight tracks over Hyderabad during dry phase on 17 June, 2009.

Figure 2b. Flight tracks over Bengaluru during wet phase on 13 July, 2009.



Meteosat 17 June 2009, 0600 UTC Visible

Figure 2c. The Meteosat-7 visible imagery for 17 June 0600 UTC, 2009 in dry phase.

mean height is ~ 1556 meters. It may be observed that the cloud base height is comparatively lower during the wet spell than in dry spell.

Most cloud drops in convective clouds nucleate at the cloud base and grow with height since more vapour condenses on the nucleated drops as the rising air cools. The modal size and width of the cloud drop increases with the vertical distance above cloud base (D) (Rogers and Yau,



Meteosat 13 July 2009, 0600 UTC Visible

Figure 2d. The Meteosat-7 visible imagery for 13 July 0600 UTC, 2009 in wet phase.

1989; Rosenfeld and Givati, 2006; Freud and Rosenfeld, 2012). The cloud drop coalescence becomes more efficient with increasing D . The raindrops in convective clouds cannot form by diffusional growth alone; also efficient drop coalescence is required for warm rain to form. Mixing of the cloud with ambient dry air evaporates some of the cloud drops and dilutes the rest of them; this would decrease the ability of the cloud to form warm rain.

Cloud Aerosol Interactions and its influence on Cloud Microphysical parameters during
Dry and Wet spells of Indian Summer Monsoon using CAIPEEX data

Table 1. Cloud base height estimated by LCL height and temperature during dry spell, 17-22 June, 2009.

Date	Temperature (°C)	LCL (m)
17/6/2009	13.5	3203
18/6/2009	11.5	3024
19/6/2009	12.2	3044
20/6/2009	13.9	2730
21/6/2009	16.5	2060
22/6/2009	15.3	2395

Table 2. Cloud base height estimated by LCL height and temperature during wet spell, 13 July 16-25 August, 2009.

Date	Temperature (°C)	LCL (m)
13/7/2009	16.0	1828
16/8/2009	23.0	1524
23/8/2009	21.8	1456
24/8/2009	23.7	1299
25/8/2009	19.9	1677

Table 3. Cloud microphysics data during dry spell monsoon period 2009.

Dates	Cloud level	CCN (cm ⁻³)	CDPre (μm)	PCASP(cm ⁻³)	LWC(g/m ³)
17/6/2009	C _L	10x10 ³	4.5	5 x10 ³	0.57
	C _M	30 x10 ³	11	20 x10 ³	2.5
18/6/2009	C _L	2 x10 ³	4.25	5 x10 ³	1.0
	C _M	8 x10 ³	12	20 x10 ³	2.9
19/6/2009	C _L	5.5 x10 ³	4.2	13 x10 ³	0.16
	C _M	9 x10 ³	6.4	20 x10 ³	0.28
20/6/2009	C _L	5 x10 ³	5.4	2.25 x10 ³	1.2
	C _M	15 x10 ³	12	8 x10 ³	2.5
21/6/2009	C _L	20 x10 ³	4.9	4 x10 ³	1.0
	C _M	79 x10 ³	12	11.5 x10 ³	3
22/6/2009	C _L	1 x10 ³	5.2	4 x10 ³	0.9
	C _M	3.5 x10 ³	15.2	15 x10 ³	3.1

* Column PCASP refers to aerosol number concentration (cm⁻³)

Cloud aerosol interactions during dry spell

The cloud microphysical characteristics during the dry spell are shown in table-3. The daily mean values of aerosol number concentration (cm⁻³) and cloud droplets sizes (CDPre) at two cloud levels are designated as C_L - cloud at low level (surface to 2000 meters), and C_M -cloud at medium level (2000 to 8000 meters). These two levels, in fact correspond to a single cloud.

Cloud aerosol interactions during dry spell are presently discussed with respect to cloud microphysics data (Table 3). The aerosol number concentration (cm⁻³) is observed to vary in the range from 2.25 x 10³ to 13.0 x 10³ cm⁻³ for low level clouds, C_L with the mean value of aerosol as 15.75 x 10³ cm⁻³. Similarly Table 3 also shows

the variability of CCNs from C_L to C_M level, with the minimum and maximum as 8.0 x10³ and 20.0 x 10³ cm⁻³ respectively and mean value prevailing at C_M as 24.083 x 10³ cm⁻³. From Table 3 the mean value of LWC at C_L is of the order of 0.80 gm⁻³ and the corresponding mean of LWC at C_M is 2.38 gm⁻³. It indicates that the low LWC at C_L does not favor faster conversion to a larger drop size due to availability of less water. In comparison, the mean LWC at C_M is higher than at C_L, which indicates that as LWC increases the CDPre size also increases. The CDPre shows variations between 4.2-12 μm except for the case of 22 June when the CDPre exceeded the threshold and on other days it was lower. The CCN was observed to increase up to 79 x 10³ cm⁻³ in dry spell. The high concentration of CCN leads to suppression of coalescence. Also if the

Table 4. Cloud microphysics data during wet spell monsoon period, 2009.

Dates	Cloud Level	CCN (cm ⁻³)	CDPRE(μm)	PCASP(cm ⁻³)	LWC(g/m ³)
13/7/2009	C _L	5x10 ³	5.2	4.5 x10 ³	0.5
	C _M	12 x10 ³	19	12 x10 ³	1.8
16/8/2009	C _L	14 x10 ³	2.8	0.4 x10 ³	0.6
	C _M	52 x10 ³	15.4	4.5 x10 ³	6.5
23/8/2009	C _L	20 x10 ³	4.2	1.725 x10 ³	1.2
	C _M	58 x10 ³	14.5	6.5 x10 ³	3.9
24/8/2009	C _L	1 x10 ³	1.8	9 x10 ³	1.0
	C _M	10 x10 ³	15.2	35.8 x10 ³	4.4
25/8/2009	C _L	4 x10 ³	2	2 x10 ³	0.9
	C _M	25 x10 ³	19	18 x10 ³	5.4

* Column PCASP refers to aerosol number concentration (cm⁻³)

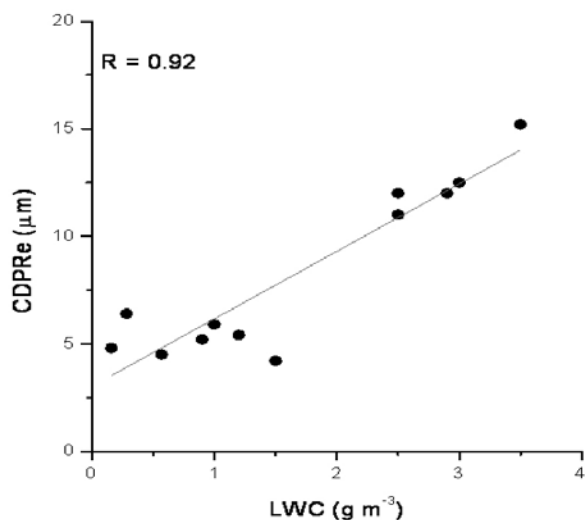


Figure 3. Relationship between CDPRe and LWC for dry monsoon days, 17-22 June, 2009.

clouds evaporate before acquiring a sufficient depth for considerable droplet growth by coalescence they may not precipitate and may lead to reduced rainfall activity causing dry monsoon conditions.

Cloud aerosol interactions during wet spells

The cloud aerosol interactions in the cloud environment during wet spells are discussed with reference to Table-4. The mean aerosol number concentration is $3.525 \times 10^3 \text{ cm}^{-3}$. The aerosol number concentration at C_L varies in the range of 0.4×10^3 to $9.0 \times 10^3 \text{ cm}^{-3}$. Aerosol (CCN) at cloud level C_M varies in the range of 10.0×10^3 to $58.0 \times 10^3 \text{ cm}^{-3}$. The LWC is significantly low at C_L, and increases sharply at C_M. LWC plays a significant role in faster conversion to a larger droplet. On all days of study period during wet spells the CDPRe had crossed the threshold limit of warm rain formation. CDPRe was a maximum of 19 μm

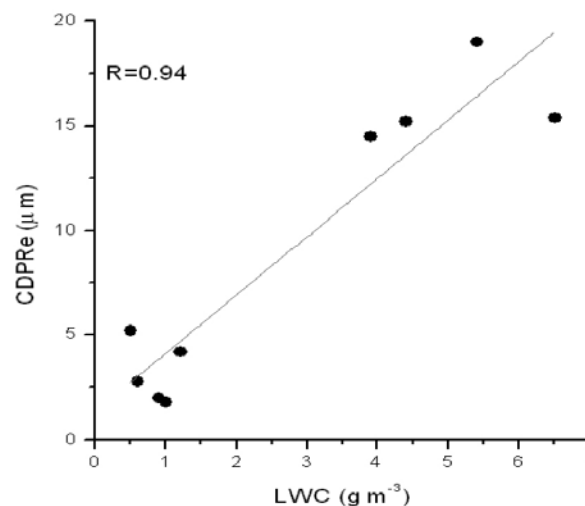


Figure 4. Relationship between CDPRe and LWC for wet monsoon days, 13 July and 16-25 August, 2009.

on 13 July and 25 August, 2009. Aerosol at C_L are less in number as compared to C_M which indicates that sufficient number of hygroscopic aerosols was available at C_M. This is also supported by the increase in LWC at C_M levels. The condensation and coalescence process depends on the cloud environment temperature during the formation and growth of clouds which is discussed in the later part of the paper. The ratio of increase in (CDPRE) size at C_L to C_M is nearly 1:3 indicating the growth of cloud droplets as more effective at C_M level during both the phases. CCN was observed to attain a value of $58 \times 10^3 \text{ cm}^{-3}$ during wet spell. The lower number of CCN is favorable for efficient coalescence processes which shows the significance of cloud condensation nuclei during wet monsoon spells.

The threshold values for onset of rain were also observed in deeper convective clouds. Rosenfeld and Gutman (1994) showed a threshold of 12-14 μm when comparing Reff with ground based radars.

Cloud Aerosol Interactions and its influence on Cloud Microphysical parameters during Dry and Wet spells of Indian Summer Monsoon using CAIPEEX data

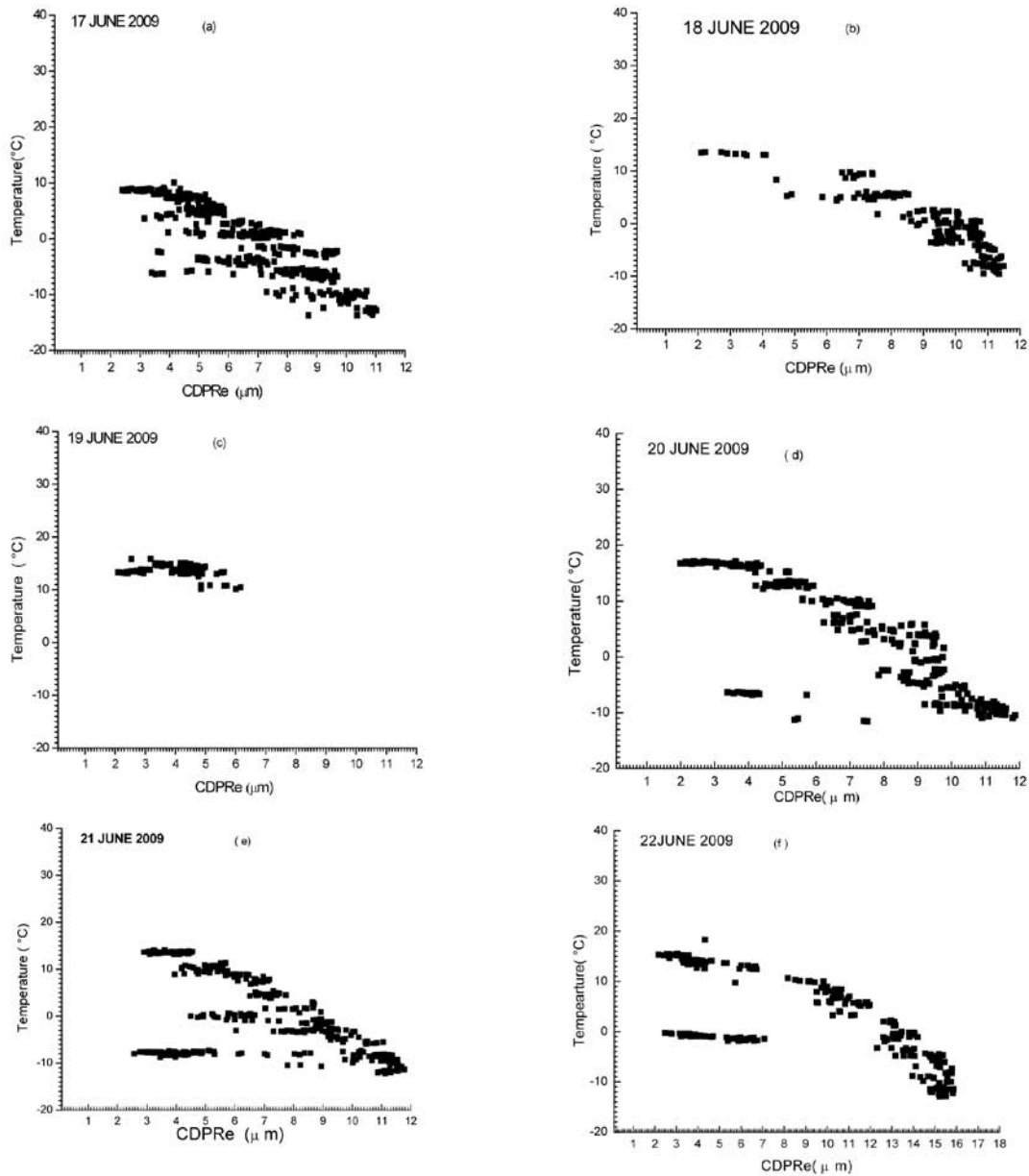


Figure 5. (a-f) Scatter plot of Temperature and CDPRe during 17-22 June, 2009.

According to Gerber (1996) significant coalescence starts when the main body of the cloud drop size distribution exceeds $(Reff_c)$ effective radius for efficient coalescence, which is $15 \mu\text{m}$, as opposed to the situation in which the largest drops from the tail of the distribution grow to isolated drizzle. It must be emphasized that most cloud drops in convective clouds nucleate at the cloud base and grow with height as more vapor condenses on the nucleated drops as the rising air cools. This trend was also observed during almost all days of dry and wet spells.

Figure 3 shows a positive linear correlation coefficient of 0.92 between CDPRe and LWC during dry phase of monsoon for the period 17-22 June, 2009. CDPRe increase

with rise in LWC suggests that both the parameters are highly sensitive and play a significant role in cloud formation and precipitation. It can be seen that the cloud formation is initiated within the C_L level and growth of cloud is enhanced at the C_M level; at both these levels the CDPRe and LWC increase linearly. The threshold value of $14 \mu\text{m}$ for CDPRe required for warm rain initiation during the dry spells was limited due to low values of LWC. Also, in case of non precipitating clouds, high concentration of CCN may cause the cloud to lose condensed water due to increased evaporation of smaller droplets that increases mixing of the cloud with ambient air (Wang et al., 2003; Xue et al., 2008).

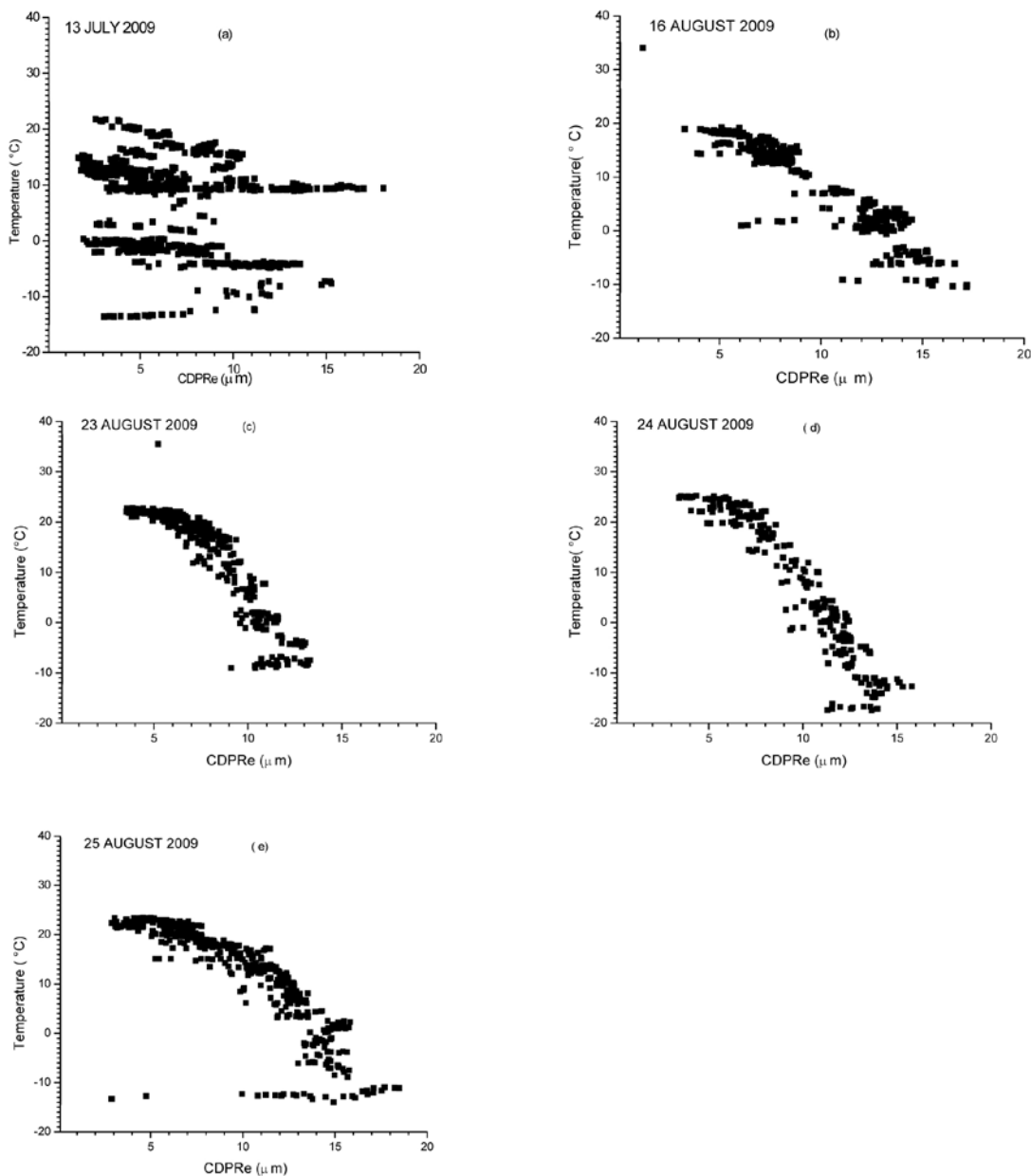


Figure 6. (a-e) Scatter plot of Temperature and CDPRe during 13 July and 16-25 August, 2009.

Figure 4 show strong positive linear correlation (coefficient 0.94) between CDPRe and LWC during the wet spells. The CDPRe tends to rise sharply with rise in LWC. It can be seen that during the wet spells, the CDPRe had crossed the threshold limit of 14 μm on almost all days. The reason for the significant growth in the size of CDPRe during wet spell may be increase in the availability of highly hygroscopic sea salt aerosol. From correlation analysis of CDPRe and LWC during dry and wet spells it is observed that these parameters show similar trend. However during the wet spells, the convective activity increases due to hygroscopic aerosol and incursion of significant moisture from marine environment. The fundamental causes for

the existence of this threshold are provided in Freud and Rosenfeld (2012).

Temperature and CDPRe variations during dry spells

Figure 5a-f shows scatter plots of cloud temperature (varying in the ranges of -15 to 10°C and -15 to 20°C) and CDPRe during the dry spells. Variations in CDPRe and temperature indicate the nature of coalescence occurring in the cloud environment. At higher temperature the CDPRe grows slowly. As the cloud temperature falls with increase in cloud altitude, CDPRe increase in size at various

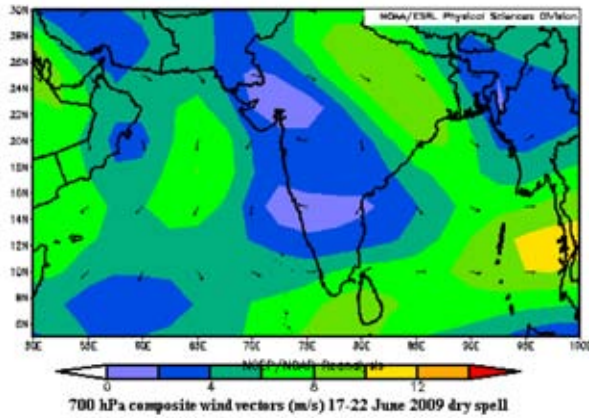


Figure 7a. Composite wind vectors (m s^{-1}) at 700 hPa level during 17-22 June, 2009 for dry period.

temperature intervals. At higher temperature the cloud droplets undergo slow coalescence. As temperature falls with altitude, the process of coalescence becomes faster and the resultant droplet grows larger to a maximum size of $11 \mu\text{m}$ at altitude C_M and a minimum of $4.2 \mu\text{m}$ at C_L . This trend was noticed on all days of the observation during the dry spells. Figure 5c shows certain deviations with respect to other days of the observation. It can be clearly seen that the temperature varies in the range of $10\text{-}16^\circ\text{C}$, which implies the cloud had dissipated partially due to rainfall or evaporation at the C_L level. The CDPRe shows $4.2 \mu\text{m}$ at C_L while it is $6.4 \mu\text{m}$ at C_M . This marginal rise in CDPRe indicates the prevalence of very low cloud depth and hence the coalescence process is rather inefficient in such environment.

Figure 6a-e depicts scatter plots of cloud temperature and CDPRe during the wet spells. Cloud temperature varies between -15 to 25°C . The temperature and CDPRe variation shows similar trend as observed during the dry spell. As temperature falls at higher altitude, growth of CDPRe increases to a maximum of $19 \mu\text{m}$ at C_M and a minimum of $5 \mu\text{m}$ at C_L . Fluctuation in CDPRe shows cloud droplets attaining maximum size at lower temperature and minimum at higher temperature. These fluctuations can be attributed to the dissipation of cloud due to rainfall or evaporation in the cloud environment or phase transformation from water to ice and vice-versa.

Variations of wind field during dry and wet spells

The wind data used in our analysis are obtained from the NCEP/NCAR Reanalysis data sets for the period from 1948 to present. These data are made available for purpose of research using state-of-the-art analysis/forecast system. A large subset of this data is available from PSD in its original 4 times daily format and as daily averages. The 4x daily data is considered for local ingestion process such

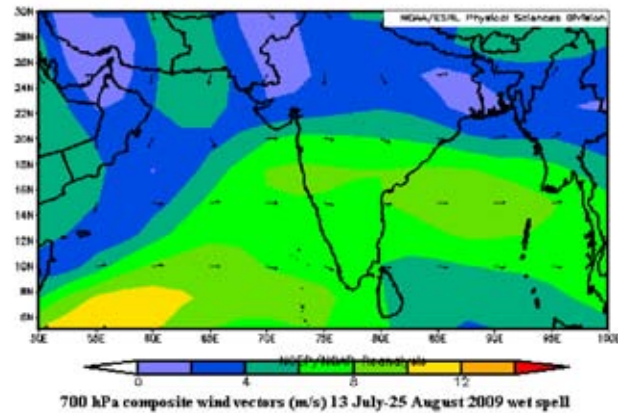


Figure 7b. Composite wind vectors (m s^{-1}) at 700 hPa level during July 13- 25 August, 2009 for wet period.

as 0Z, 6Z, 12Z, and 18Z forecasted values, and only those were used to make the daily time series data sets. The daily NCEP/NCAR 700 hPa wind field (ms^{-1}) during dry and wet spells was analyzed to supplement the inferences drawn from air-borne measurements.

Figure 7a shows the composite analysis of 700 hPa wind field during dry spell, indicating the winds as blowing from northwesterly direction from the adjoining desert region. The transport of non hygroscopic aerosols from the desert regions of Saudi Arabia and Thar desert of Rajasthan might lead to the inhibition of CDPRe during the dry spell. The predominant northwesterly flow devoid of moisture and loaded with mineral dust from the adjoining desert region of Saudi Arabia during the dry spell corroborates the findings of Krishnamurti et al., (2010). In the drought (normal) year, during the pre-monsoon (March-May) season the higher aerosol loading and higher optical depth were associated with weak (strong) winds over India (Bhawar and Devara, 2010).

During dry spells, although the winds from Arabian Sea are southwesterly, they are not strong and confine to the ocean areas. They do not reach the west coast of India resulting in suppressed rainfall activity. During the wet spells (Figure 7b) the wind speeds gained significant momentum and increased drastically to $10\text{-}12 \text{ms}^{-1}$ blowing in the southwesterly direction, from Arabian Sea reaching up to central India. Strong south westerlies carrying abundant moisture loaded with highly hygroscopic sea salt aerosols favor strong convective activity, and thus helped in the revival of monsoon. Sateesh (2012) reported that when there was very strong wind ($> 10 \text{ms}^{-1}$) direct sea-spray production takes place by breaking of wave crests. Also Feingold et al., (1999) reported that sea salt particles are very efficient CCN due to its hygroscopic property. This suggests that the large scale wind forcing across the sea has a considerable influence on regional weather over interior Indian land mass and associated cloud microphysical parameters.

CONCLUSIONS

Analysis of aircraft measured data during CAIPEEX-2009 reveals the following significant characteristics of aerosol cloud interactions and cloud microphysical parameters.

i) There is a linear relationship between cloud droplet effective radius and liquid water content.

ii) During dry spell CDPRe was $< 14 \mu\text{m}$ on all the days of aircraft observation at C_L and CDPRe in the medium cloud level C_M , exceeds the threshold value of $> 14 \mu\text{m}$ required for warm rain initiation during wet spells which implies that the collision and coalescence process is more efficient at cloud levels above 2000 meters during the wet spells.

(iii) The LWC and CDPRe are highly sensitive to cloud environmental temperature due to processes such as cloud water evaporation and phase transformation from ice to water.

(iv) During dry spells the flow of North westerly winds, which carry mineral dust aerosols from adjoining desert regions of Saudi Arabia and Thar desert of Rajasthan, appears to be one of the reasons for the low amount of LWC in cloud environment thus acting as limiting factor for the enhancement of CDPRe.

(v) The winds during wet spells at 700 hPa were significantly stronger and predominantly southwesterly with $\sim 10\text{-}12 \text{ ms}^{-1}$ velocity. They carry highly hygroscopic sea salt aerosols from the Arabian sea. Hence wind force plays major role during wet spells of Indian summer monsoon influencing the cloud microphysics.

(vi) The cloud seeding operations for rainfall enhancement is more likely to be successful during the prevalence of strong southwesterly wind flow from Arabian sea (velocity $> 10\text{-}12 \text{ m/s}$.)

(vii) For better understanding of cloud microphysics this study recommends more aircraft observations over rain shadow regions of India during monsoon for generating longer multiyear data sets.

ACKNOWLEDGEMENTS

The authors thank, Director, IITM, Pune for encouragement. CAIPEEX Program was funded by Ministry of Earth Sciences (MoES), Govt. of India. Satellite Imagery data provided by Meteosat-7 Dundee station. NCEP/NCAR Reanalysis derived data provided by the NOAA/OAR/ESRL PSD, Boulder, Colorado, USA, from their Web site at <http://www.esrl.noaa.gov/psd>, are acknowledged. Authors are thankful to Dr. S.C. Bhan and Prof. B.V.S. Murthy for critical evaluation of the manuscript. They also thank Prof. B.V.S. Murthy and Chief Editor for apt editing.

Compliance with Ethical Standards

The authors declare that they have no conflict of interest and adhere to copyright norms.

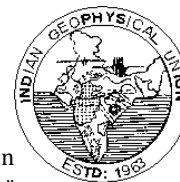
REFERENCES

- Adams, P. J., and Seinfeld, J. H., 2003. Disproportionate impact of particulate emissions on global cloud condensation nuclei concentrations. *Geophys. Res. Lett.*, doi: 10.1029/2002GL016303., v.30, pp: 1239.
- Bhawar, R.L., and Devara, P.C.S., 2010. Study of successive contrasting monsoons (2001-2002) in terms of aerosols variability over a tropical station Pune, India. *Atmos. Chem. Phys.*, v.10, pp: 29-37.
- Deka, S., Borah M., and Kakaty S.C., 2010. Statistical modeling of wet and dry spell frequencies over North-East India. *J Appl and Natural Sci.*, v.2, no.1, pp: 42-47.
- Devara, P.C.S., Manoj, M.G., and Jaya Rao, Y., 2009. Role of aerosols in monsoon clouds and precipitation: an observational perspective. *Mausam. Diamond Jubilee Volume*, pp: 155-162.
- Feingold, G., William, R., Cotton, Sonia, M., Kreidenweis, Janel, and Davis, T., 1999. Impact of giant cloud condensation nuclei on drizzle formation in marine stratocumulus: Implications for cloud radiative properties. *J. Atmos. Sci.*, v.56, pp: 4100-4117.
- Freud, E.D., and Rosenfeld., 2012. Linear relation between convective cloud drop number concentration and depth for rain initiation. *J. Geophys. Res.*, D02207, doi: 10.1029/2011JD016457., pp: 117.
- Gerber, H., 1996. Microphysics of marine stratocumulus clouds with two drizzle modes. *J. Atmos. Sci.*, v.53, pp: 1649-1662.
- India Meteorological Department, Govt. of India 2009. South-West Monsoon: End of Season Report, pp: 1-12.
- Jayaraman, A., 2001. Aerosol radiation cloud interaction over the tropical Indian Ocean prior to the onset of the summer monsoon. *Curr. Sci.*, v.81, no.11, pp: 1437-1445.
- Kaufman, Y. J., and Koren, I., 2006. Smoke and pollution aerosol effect on cloud cover. *Sci.*, v.313, pp: 655-658.
- Krishnamurti, T.N., Thomas, A., Simon, A., and Vinay Kumar, 2010. Desert Air Incursions an Overlooked Aspect, for the Dry Spells of the Indian summer Monsoon. *J. Atmos. Sci.*, v.67, pp: 3423-3441.
- Kulkarni J.R., Maheshkumar R.S., Morwal S.B., Padma kumari B., Konwar M., Deshpande C.G., Joshi R.R., Bhalwankar R.V., Pandithurai G., Safai P.D., Narkhedkar S.G., Dani K.K., Nath A., Nair Sathy, Sapre V.V., Puranik P.V., Kandalgaonkar S.S., Mujumdar V.R.,
- Leiming Z., Michelangeli D., Peter, V., and Taylor, A., 2006. Influence of aerosol concentration on precipitation formation in low-level warm stratiform clouds. *J. Aero. Sci.*, v.37, pp: 203-217.

Cloud Aerosol Interactions and its influence on Cloud Microphysical parameters during
Dry and Wet spells of Indian Summer Monsoon using CAIPEEX data

- Manoj, M.G., Devara, P.C.S., Susmitha Joseph., and Sahai, A.K., 2012. Aerosol indirect effect during the aberrant Indian Summer Monsoon breaks of 2009, *Atmos. Environ.*, v.45, pp: 665-672.
- Pierce, J. R., and Adams, P. J., 2007. Efficiency of cloud condensation nuclei formation from ultrafine particles. *Atmos. Chem. Phys.*, v.7, pp: 1367-1379.
- Rogers, R. R., and Yau, M.K., 1989. A short course in cloud physics, 3 ed., Pergamon Press.
- Rosenfeld, D., 1999. TRMM observed first direct evidence of smoke from forest fires inhibiting rainfall. *Geophys. Res. Lett.*, v.26, pp: 3105-3108.
- Rosenfeld, D., Wang, H., and Rasch, P. J., 2012. Role of cloud drop effective radius and LWP in determining rain properties in marine stratocumulus. *Geophys. Res. Lett.* DOI: 10.1029/2012GL052028., v.39.
- Rosenfeld, D., and Givati, A., 2006. Evidence of orographic precipitation suppression by air pollution induced aerosols in the western U.S. *J. Appl. Meteor. and Clim.*, v.45, pp: 893-911.
- Rosenfeld, D., and Gutman, G., 1994. Retrieving microphysical properties of cloud tops by multispectral analysis of AVHRR data. I. *Atmos. Res.*, v.34, pp: 259-283.
- Sarkar, S.K., and Kumar, A., 2007. Recent studies on clouds and precipitation phenomena for propagation characteristics over India. *Ind. J. Radio and Space Phys.*, v.36, pp: 502-513.
- Sateesh, S.K., 2012. Atmospheric chemistry and climate. *Curr. Sci.*, v.102, no.3, pp: 426-439.
- Squires, P., and Twomey, T., 1960. The relation between cloud drop number and the spectrum of cloud nuclei in Physics of Precipitation. *Geophys. Monogr.Ser.*, edited by H.Weickmann, AGU, Washington D.C, v.5 ,pp: 211-219.
- Squires, P., 1958. The microstructure and colloidal stability of warm clouds. Part I—The relation between structure and stability. *Tellus.*, v.10, pp: 256-261.
- Swaminathan, M. S., 1987. Abnormal monsoons and economic consequences: the Indian experience. In *Monsoons* (eds., Fein, J.S and Stephens, P.L) John Wiley, Washington, DC, pp: 121-133.
- Wang, S., Wang, Q., and Feingold, G., 2003. Turbulence, condensation, and liquid water transport in numerically simulated nonprecipitating stratocumulus clouds. *J. Atmos. Sci.*, v.60, pp: 262-278.
- Warner, J., 1968. A reduction in rainfall associated with smoke from sugar cane fires: and inadvertent weather modification?. *J. Appl. Meteorol.*, v.7, pp: 247-251.
- Warner, J., and Twomey, S., 1967. The production of cloud nuclei by cane fire and the effects on cloud droplet concentration. *J. Atmos. Sci.*, v.24, pp: 704-706.
- Xue, H., Feingold, G., and Stevens, B., 2008. Aerosols effects on clouds, precipitation and the organization of shallow cumulus convection. *J. Atmos. Sci.*, v.65, pp: 392-406.

NEWS AT A GLANCE



FORTH COMING EVENTS:

- * 1st Triennial Congress of Federation of Indian Geosciences Association (FIGA), 53rd Annual Convention of Indian Geophysical Union (IGU) & 34th Annual convention for Association of Hydrologists of India (AHI) on “Geosciences for Sustainability” will be held at Indian School of Mines, Dhanbad during November 8-10, 2016.
- * 2nd International Conference on Green Energy & Expo will be held during November 28-30, 2016 at Atlanta, USA.
- * A seminar on HS_DT — Hydrodynamic Stability and Dynamo Theory, ID 833012 will be held during 09 Dec 2016 - 20 Dec 2016 at Warangal, Telangana State, India. For details visit

Event website: http://nitw.ac.in/media/uploads/HS_DT_Brochure_2.pdf

Awards and Recognition

Ministry of Earth Sciences presented the following awards to Earth system scientists of India during its annual convention. Awards were presented by Hon. Minister of Govt of India Shri Dr. Harsh Vardhan on July 27, 2016, during the Celebration of 10 Years of Ministry of Earth Sciences (2006-2016) & Foundation Day Function held at Vigyan Bhawan, New Delhi.

- * **Life Time Achievement Award 2016**
In recognition of her outstanding contribution to Earth System Science Prof. Sulochana Gadgil was honoured with “Life Time Excellence Award in Earth System Science” for the year 2016.
- * **National Award in Ocean Science & Technology for the year 2016**
Dr. M. Dileep Kumar was awarded, in recognition of his outstanding contribution to Ocean Science & Technology with “National Award in Ocean Science & Technology” for the year 2016.
- * **National Award in Atmospheric Science & Technology for the year 2016**
Prof. P.V. Joseph was awarded, in recognition of his outstanding contribution to Atmospheric Science &

Technology with “National Award in Atmospheric Science & Technology” for the year 2016.

- * **National Award in Geoscience & Technology for the year 2016.**

Prof. Shyam Sundar Rai was awarded, in recognition of his outstanding contribution to Geoscience & Technology with “National Award in Geoscience & Technology” for the year 2016.

- * **National Award in Polar Science & Cryosphere for the year 2016.**

Dr. S. Shivaji was awarded, in recognition of his outstanding contribution to Polar Science & Cryosphere with “National Award in Polar Science & Cryosphere” for the year 2016.

- * **Young Researcher Award in the field of Earth System Science for the year 2016.**

Dr. Anoop Kumar Mishra was awarded, in recognition of his outstanding research contributions in the field of Earth System Science with “Young Researcher Award in the field of Earth System Science” for the year 2016

- * **Young Researcher Award 2016**

Dr. Kunal Chakraborty, was awarded Young Researcher Award-2016 for his outstanding scientific contributions in the field of Bio-Physical Coupling Process in Indian Ocean.

- * **Certificate of Merit for 2016**

Shri. N. Kiran Kumar, Scientist & In-charge Web Based Services was awarded Certificate of Merit-2016 for his outstanding scientific contributions in the field of Ocean Sciences.

- * **Certificate of Best Employee for 2016**

Shri. Dasari Prasad, Asst. Manager, INCOIS was awarded Best Group-B Employee Award-2016.

- * Dr. P.M. Kessarkar, Scientist of National Institute of Oceanography, Goa has been awarded Raman Research Fellowship -2016.

News Item: Prof. Boyd's 90th Birthday Celebrations



I am happy to publish this important news item. Dr. D. Atchuta Rao, former Honorary Secretary of IGU (1983-1993), communicated this information for my use. I have taken the liberties to publish this mainly to motivate the students and young researchers seeing the details.....P.R. Reddy

"During 25th Geophysical Conference of ASEG-PESA-AIG 2016 held at Adelaide from 21st to 24th August, my revered Guru, Prof. David Boyd's 90th birth day was celebrated by his students and admirers and he was also honored by the ASEG (Australian Society of Exploration Geophysicists).

I was in Adelaide (South Australia) during 1974-76 as a post doctoral fellow at the University of Adelaide and worked with Prof. David Boyd, a very respected and eminent Geophysicist, and again visited in 1990 & 1995 attending conferences.

On the invitation of my friends and a number of Prof. Boyd's students, who have now attained high stature in the Geophysical profession in Australia, my wife and I went to Adelaide and attended the conference and was present at this momentous occasion of the 90th birth day celebrations and paid my respects to my teacher, who enriched my life in many ways. It was really an exciting experience to be with him and other friends after a gap of 20 years".....D. Atchuta Rao

Outstanding Contribution to Indian Space Programme



Dr. Krishnaswamy Kasturirangan was born on 20 October, 1940, in Ernakulam, Kerala, India. He graduated in Science with Honours, and obtained his Master of Science degree in Physics, from Bombay University. He received his Doctorate Degree in Experimental High Energy Astronomy in 1971, working at the Physical Research Laboratory, Ahmedabad.

Dr. Kasturirangan was responsible for directing the Indian Space programme for over 9 years, as Chairman of ISRO and the Space Commission and as Secretary to the Government of India in the Department of Space, before laying down office on 27 August 2003. He was subsequently nominated as a member of Rajya Sabha, the Upper House of Indian Parliament from 2003 to 2009. During this period, he also served as Director of National Institute of Advanced Studies, Bangalore. Between June 2009 and May 2014, he was a member of the Planning Commission of Government of India.

Dr. Kasturirangan is presently the Chancellor of Jawaharlal Nehru University, Satish Dhawan Chair of Engineering Eminence of Indian National Academy of Engineering, Professor Emeritus at NIAS and Member, Atomic Energy Commission.

He was earlier the Director of ISRO Satellite Centre, overseeing the development of new generation spacecraft, the Indian National Satellite (INSAT-2) and the Indian Remote Sensing Satellites (IRS-1A and 1B) as well as scientific satellites. He was also the Project Director for India's first two experimental earth observation satellites, Bhaskara-I and II.

Under his leadership, the programme witnessed several major milestones including the successful launching and operationalisation of the India's prestigious launch vehicles, the Polar Satellite Launch Vehicle and the Geosynchronous Satellite Launch Vehicle. Studies on the advanced version of the GSLV, GSLVMk-III, were also completed including defining their full configuration. Further, he also oversaw the development and launching of some of the world's best civilian remote sensing satellites, IRS-1C and 1D, realization of new generation INSAT communication satellites, besides ocean observation satellites IRS-P3/P4. He also led the initiative for India to enter the planetary exploration era by an extensive studies leading to the definition of Chandrayaan-I. These efforts have put India as a pre-eminent space-faring nation among the handful of six countries that have major space programmes. As an Astrophysicist, Dr. Kasturirangan's interests include research in high energy X-ray and gamma ray astronomy as well as optical astronomy. Defining India's most ambitious space based High Energy Astronomy observatory and initiating a related activities was also an important milestone under his leadership. He has made extensive and significant contributions to studies of Cosmic x-ray and gamma ray sources and effect of cosmic x-rays in the lower atmosphere.

He has published more than 250 papers, in international and national journals, in the areas of astronomy, space science and space applications. He is a Fellow of the Indian Academy of Sciences, Indian National Science Academy, National Academy of Sciences of India, Indian National Academy of Engineering,

Astronautical Society of India, National Telematics Forum, The Indian Meteorological Society and The Third World Academy of Sciences.

Dr. Kasturirangan is a member of several important scientific academies and educational institutions, both within India and abroad. He is a recipient of the three civilian awards from the Government of India, the Padma Shri (1982), Padma Bhushan (1992) and Padma Vibhushan (2000).

Dr. Kasturirangan is the recipient of Honorary Doctorate from 16 universities;

Banaras Hindu University (1994), Andhra University (1995), S. V. University, Tirupati (1996), Sri Krishna Devaraya University, Ananthpur (1998), Anna University, Chennai (1998), Roorkee University, Roorkee (1999), IIT, Bombay (2000), ChatrapatiShahujiMaharaj University, Kanpur (2000), GurunanakDev University, Amritsar (2001), University of Calcutta, Calcutta (2002), Indira Gandhi National Open University (IGNOU), New Delhi (2003), Punjab University, Chandigarh (2003), Visvesvaraya Technological University, Belgaum (2004), Alagappa University, Karaikudi (2006), Mysore University, Mysore (2007); SRM University, Chennai (2008).

He is an Academician of the Pontifical Academy of Sciences, Vatican, a Honorary Fellow of Cardiff University, a Member of the International Astronomical Union and the International Academy of Astronautics. He has chaired some of the prestigious international committees, such as, the International Committee on Earth Observation Satellites (CEOS), Panel for Space Research in Developing countries of COSPAR/ICSU and the committee meeting at senior

official level of UN-ESCAP, that led to the adoption of the "Delhi Declaration" by the Ministers of the region (1999-2000). He has won several awards including Shanti Swarup Bhatnagar Award in Engineering, Shri Hari Om Ashram Dr. Vikram Sarabhai Prerit Award in Aerospace, M.P. Birla Memorial Award in Astronomy, Shri M.M.Chugani Memorial Award in Applied Science, H.K.Firodia Award in Science Technology, Rathindra Puraskar and Desikothama from Visvabharati, Shantiniketan, Dr.M.N.Saha Birth Centenary Medal for outstanding contributions in the field of Space, Aryabhata Award of ASI, Aryabhata Medal of INSA, ISRO Lifetime Achievement Award, GM Modi Award by GM Modi Science Foundation, Asutosh Mookerjee Memorial Award by the Indian Science Congress, Award of Jewel of Ruia, Ruia College Alumni Association, Maharana Udai Singh Award by Maharana of Mewar Charitable Foundation, Rajayogindra Award, Maharaja of Mysore, Vikram Sarabhai Memorial Gold Medal, Indian Science Congress, Dharma Vira Memorial Citation & Gold Medal and JK Lakshmipat University Laureate Award.

International recognitions include 'Brock Medal' of International Society of Photogrammetry and Remote Sensing, Allan D Emil Memorial Award of the International Astronautical Federation, Lifetime Achievement Award of Asia-Pacific Satellite Communications Council, Singapore and Theodore Von Karman Award by International Academy of Astronautics. He has been conferred the Award of "Officer of the Legion d'honneur" by the President of the French Republic.

Dr. Kasturirangan was felicitated by Indian Geophysical Union (IGU) with "Millennium Award" in December, 1999, for his outstanding contribution to Indian Space science.

P.R.Reddy

In the absence of a robust controlling mechanism Sand mining will be more disastrous compared to Global warming

P.R.Reddy

Director Grade Scientist (Retd), CSIR-NGRI, Hyderabad-500 007

E-mail: parvatarreddy@gmail.com

ABSTRACT

In almost all the international conferences associated with Pollution, monsoon aberrations, environmental issues scientists invariably present their studies covering "Global warming and Climate change". We hardly come across an international conference that covers studies on sand mining. While fully agreeing that global warming and climate change impacts the land and ocean ecosystem and resultant ill effects on life it is presented in this small write up the necessity to give due importance to steps that would curb illegal sand mining. If we continue to ignore introduction of robust controlling mechanism we will irrevocably suffer due to sand mining resultant permanent negative impact on our environment.

Key words: Sand mining, Global warming, Instream mining, Channel Morphology, National Building Codes

PREAMBLE:

All of us at one time or the other might have come across a situation where in choosing between one set back over the other has become a necessity. Many of us, who have limited capability to wriggle out of the crisis, might have weighed options and chosen one or the other believing the Almighty would save us.

Presently majority of those who are exposed to the existing camouflaged reality (influenced by never ending media hype and business options` based global politics), finding difficult to weigh the options, are coming to the conclusion that global warming is more disastrous. However, in reality sand mining is as disastrous if not more due to various reasons. If global warming is a devil sand mining is the deep blue. Devil can change its decisions depending on its moods and preferences and can leave one by just making him sweat. In case of the deep blue neither we know its depth nor can change its set behaviour. And as such when someone falls in the deep blue sea, irrespective of his swimming expertise, he will not be sure where he would move and when he would be saved. While global warming scenario is expected to be reversed, during mini ice age expected to surface during 2030-2040 period (at least for a limited period) due to the Sunspot minimum impact, sand mining resultant setbacks can never be reversed as sand accumulated over thousands if not millions of years cannot be replenished through any means. Even though these options have some setbacks experiments to lessen global warming through hard and soft Climate engineering exercises have shown some good results in arresting the coastal belt erosion due to global warming resultant rising of sea levels. Also in the recent past carbon dioxide

removal (CDR) method or a solar radiation management (SRM) method have yielded some useful results. CDR methods address the warming effects of greenhouse gases by removing carbon dioxide (CO₂) from the atmosphere. CDR methods include ocean fertilization, and carbon capture and sequestration. SRM methods address the climate change by increasing the reflectivity of the Earth's atmosphere or surface. Aerosol injection and space-based reflectors are examples of SRM methods. SRM methods do not remove greenhouse gases from the atmosphere, but can be deployed faster with relatively immediate global cooling results compared to CDR methods. We do know that these geo-engineering interventions need to be introduced in a controlled way to minimise environmental instability. In addition, as Rida Bilgram of Sustainability forum has pointed out "...The 21st of March 2016 marked 100 days since the historic climate agreement was struck in Paris between 195 countries, setting the first long-term goal for carbon emissions reduction. It was bolstered, too, by the World Economic Forum, whose work demonstrates that global leaders for the first time perceive the failure to mitigate and adapt to climate change as the top risk in terms of greatest potential impact. While the Paris agreement is officially due to enter into force in 2020, it is already shaping public policy and corporate action. Pre- and post-Paris, governments have not been the only actors motivated to commit and act. Business was a key voice leading up to COP21, and the role of business is even more crucial as we shift from the negotiation table to the massive systemic change that is required to keep global warming to 1.5°-2° Celsius. We expect to see more ambition and action from business in a post-Paris world through exploring low carbon business models, setting science-

based targets and being more active on internal carbon pricing, as well as the shadow pricing of other resources such as water. More than 400 companies already use or are considering an internal carbon price to future-proof their business, as CDP reports.”

I only detail these initiatives to impress upon the readers that there is a percentage of hope for bringing out a positive change in case of global warming. Nothing of that sort of hopeful solutions can be invented in replenishing removed volume of sand from river channels. We need actions that can at least arrest the degradation by properly propagating the problem.

IMPACTS OF SAND MINING:

For thousands of years, sand and gravel have been used in the construction of roads and buildings. Today, demand for sand and gravel continues to increase. Mining operators, in conjunction with cognizant resource agencies, must work to ensure that sand mining is conducted in a responsible manner. Unfortunately, this is not in practice.

Excessive in-stream sand-and-gravel mining causes the degradation of rivers. In-stream mining lowers the stream bottom, which may lead to bank erosion. Depletion of sand in the streambed and along coastal areas causes the deepening of rivers and estuaries, and the enlargement of river mouths and coastal inlets. It may also lead to saline-water intrusion from the nearby sea. The effect of mining is compounded by the effect of sea level rise. Any volume of sand exported from streambeds and coastal areas is a loss to the system. Excessive in-stream sand mining is a threat to bridges, river banks and nearby structures. Sand mining also affects the adjoining groundwater system and the uses that local people make of the river.

In-stream sand mining results in the destruction of aquatic and riparian habitat through large changes in the channel morphology. Impacts include bed degradation, bed coarsening, lowered water tables near the streambed, and channel instability. These physical impacts cause degradation of riparian and aquatic biota and may lead to the undermining of bridges and other structures. Continued extraction may also cause the entire streambed to degrade to the depth of excavation. Sand mining generates extra vehicle traffic, which negatively impairs the environment. Where access roads cross riparian areas, the local environment may be impacted.

Removing sediment from the active channel bed in river sand mining interrupts the continuity of sediment transport through the river system, disrupting the sediment mass balance in the river downstream and induces channel adjustments (usually incision) extending considerable distances (commonly one km or more) beyond the extraction site. The magnitude of the impact basically depends on the magnitudes of the extraction relative to

bed load sediment supply and transport through the reach. Government of India guide lines point out that mining within or near riverbed has a direct impact on the stream's physical characteristics, such as channel geometry, bed elevation, substratum composition and stability, in-stream roughness of the bed, flow velocity, discharge capacity, sediment transport capacity, turbidity, temperature etc. Alteration or modification of the above attributes may cause hazardous impact on ecological equilibrium of riverine regime. This may also cause adverse impact on in-stream biota and riparian habitats. This disturbance may also cause changes in channel configuration and flow-paths. Furthermore, the process of in-stream mining and gravel washing produces fine sediments under all flow conditions, resulting in a deposition of fine sediment in riffles as well as other habitats at low discharge. Excess sediment is considered the greatest pollutant in waters and constitutes one of the major environmental factors in the degradation of stream fisheries. However, in-stream mining may contribute additional sediment to downstream reaches due to the disruption of substrate stability. Once sediment enters the stream, it is best to let natural geomorphological and hydrological processes reach a dynamic equilibrium, rather than further exacerbating the situation by additional disturbance.

Several studies, including those in USA, have documented the bed degradation caused by the two general forms of in-stream mining: (1) pit excavation and (2) bar skimming. Bed degradation, also known as channel incision, occurs through an important primary process: head-cutting. In head-cutting, excavation of a mining pit in the active channel lowers the stream bed, creating a nick point that locally steepens channel slope and increases flow energy. During high flows, a nick point becomes a location of bed erosion that gradually moves upstream. Head-cutting mobilizes substantial quantities of streambed sediments, which are then transported downstream to deposit in the excavated area and locations further downstream. In gravel-rich streams, effects downstream of mining sites may be short-lived when mining ends, because the balance between sediment input and transport at a site can re-establish itself relatively quickly. Effects in gravel-poor streams may develop rapidly and persist for many years after mining has finished. Regardless of downstream effects, head-cutting in both gravel-rich and gravel-poor streams remains a major concern. Head cuts often move long distances upstream and into tributaries, in some watersheds moving as far as the headwaters or until halted by geologic controls or man-made structures.

Impacts of sand mining can be broadly classified into three categories:

- **Physical**
The large-scale extraction of streambed materials, mining and dredging below the existing streambed,

In the absence of a robust controlling mechanism Sand mining will be more disastrous compared to Global warming



Figure 1. (a,b,c): Sand mining to a depth of 30 feet in Uttara pinakini river stream in Kalludi in Gauribidanur Taluk, Karnataka. (Source:<https://www.researchgate.net/figure/267856891-fig-1-Fig-1-sand-mining-to-a-depth-of-30-feet-in-uttara-pinakani-river-stream-in-kalludi-in>)

and the alteration of channel-bed form and shape leads to several impacts such as erosion of channel bed and banks, increase in channel slope, and change in channel morphology. These impacts may cause: (1) the undercutting and collapse of river banks, (2) the loss of adjacent land and/or structures, (3) upstream erosion as a result of an increase in channel slope and changes in flow velocity, and (4) downstream erosion due to increased carrying capacity of the stream, downstream changes in patterns of deposition, and changes in channel bed and habitat type.

- **Water Quality**
Mining and dredging activities, poorly planned stockpiling and uncontrolled dumping of overburden, and chemical/fuel spills will cause reduced water quality for downstream users, increased cost for downstream water treatment plants and poisoning of aquatic life.
- **Ecological**
Mining which leads to the removal of channel substrate, re-suspension of streambed sediment, clearance of vegetation, and stockpiling on the

streambed, will have ecological impacts. These impacts may have an effect on the direct loss of stream reserve habitat, disturbances of species attached to streambed deposits, reduced light penetration, reduced primary production, and reduced feeding opportunities.

(Source: http://ponce.sdsu.edu/three_issues_sandminingfacts01.html)

EXISTING SCENARIO:

In spite of number of government guidelines, Supreme Court and several High Court orders the serene and peaceful environment associated with many rivers has been completely destroyed beyond recognition by illegal sand mining. The serene environment used to be associated with slow but steady river flows of clear waters has been replaced by angry and muddy gushing waters that run through deep gorges created by absence of sandy column, ignoring wails of number of bore wells and tube wells (its children present along and near its banks), which basically thrive on river flows (mother`s milk).The plight

of infiltration galleries and infiltration wells is much worse. They erected in thick saturated sand zones (in drought hit Rayalaseema on Bahuda and Cheyyair river beds) that used to quench thirst of thousands of nearby villagers completely lost their bearings with exposed foundations and disjointed frames. Many of the bridges, minor dams too are going to become victims of sand mining due to sand mining extending to depths of 30 to 40 feet in place of permitted depth of mining, which is restricted to 3m / water level, whichever is less. Due to unregulated sand-mining, the bed of Pinakini River in the vicinity of the Gauribidanur town, Kolar District, Karnataka, India has been denuded of all sand. Despite protests from local environmental groups and citizens — because of collaboration between politicians, the local police, and some village groups — the mining has led to extensive and irreversible environmental damage. (Source: <https://en.wikipedia.org/wiki/Gauribidanur#Geography>)

The existing scenario needs to be changed, at least partly to save one and all. Can we not impress upon those who matter that disaster is lurking to strike a big blow in different parts of our country where conjunctive use of surface and ground waters alone can sustain agriculture and quench the thirst of millions? Is it not time for all those who are knowledgeable and wise throw away the blinkers and protest the savage actions of sand mafia instead of getting enamoured by international scientific deliberations on global warming and climate change that can never come to a definite conclusion regarding the impact of Man and Nature? Global warming and climate change do affect us but the impact can be lessened to a reasonable extent due to concerted efforts by many governments. If the presently fixed targets are met the negative impact could be reduced considerably in the next 3 to 4 decades. In addition many scientists counter the very negative impact theory attributed, through wealth of data bringing an amount of optimism. But sand mining if continued to thrive we will see millions struggling for want of a pot of water in less than a decade. It is true that the ongoing monsoon vagaries are due to significant changes in sea surface temperature, deep sea turbulences, polar ice melting resultant sea water rise, variations in velocity and direction of winds blowing from oceans towards landmasses and vice versa, impact of aerosols travelling from deserts towards plains and mountains, greenhouse gases emission. Significant efforts are being made locally, regionally and globally to lessen the impact. In case of sand mining some insignificant restrictions are made at local level, which are regularly flouted by powerful sand mafia, in collusion with influential politicians and real estate magnets. The initiative to arrest this catastrophe will not be opposed by the common man, if he is exposed to the reality.

NEED FOR IMPLEMENTATION OF STANDARD BUILDING CODES:

The quality control authorities have pointed out that builders prefer river sand as it is cheaper and binds well in preparing concrete compared to marine and desert sands. The important standard setting bodies in India are taking steps to promote the usage of alternatives to sand and gravel. Bureau of Indian Standards, the National Standards Body of the country, considering the scarcity of sand and coarse aggregates from natural sources, has evolved number of alternatives, which are ultimately aimed at conservation of natural resources apart from promoting use of various waste materials without compromising in quality. These measures include permitting in the Concrete Code (IS 456) as also in the National Building Code of India, the use of slag - a waste from steel industry, fly ash - a waste from thermal power plants, crushed over-burnt bricks and tiles - waste from clay brick and tile industry, in plain cement concrete as an alternative to sand/natural aggregate, subject to fulfilling the requirements of the Code. This Code, further, encourages use of fly ash and ground granulated blast furnace slag as part replacement of ordinary Portland cement in plain as well as reinforced cement concrete. The Indian Standard on concrete mix design (IS 10262) has been upgraded to include guidance and examples of designing concrete mixes using fly ash and slag. Provisions for compliance for requisite quality of concrete made using fly ash and slag have been duly covered for the manufacturers of ready-mixed concrete in the Indian Standard Code of practice for RMC (IS 4926). BIS has also formulated an Indian Standard Specification for artificial lightweight aggregates covering manufactured aggregates, such as foamed blast furnace slag, bloated clay aggregate, sintered fly ash aggregate and cinder aggregate (IS 9142). A series of Indian Standards has also been formulated on various precast concrete products such as solid and hollow concrete blocks, light weight concrete blocks, autoclaved aerated concrete blocks, preformed foam concrete blocks, partial prefabricated concrete flooring and roofing units, concrete pipes, etc, all permitting use of fly ash and slag.

Ministry of Environment and Forests (MOEF), through concerted efforts identified various bottlenecks in implementing well thought out norms. The system of preparing an Environment Management Plan (EMP) report for clearance from the Government of India prior to implementation of mining project has been a positive step of minimizing the negative impacts. However, irrespective of the quality of the prepared plan document Government should ensure periodical on spot monitoring mechanism to ensure proper execution of the project. SUSTAINABLE SAND MINING MANAGEMENT GUIDELINE, released

In the absence of a robust controlling mechanism Sand mining will be more disastrous compared to Global warming

by MOEF in September, 2015 is an excellent document. In this manual of 54 pages, it is clearly pointed out that "The implementation of these Guidelines on Sustainable Sand Mining is not possible till States create a robust mechanism to monitor the mining operation and measure the mined out mineral. The entire exercise of Environment Impact Assessment and Environment Management Plan aims towards making the mining process environmentally sustainable. The Environment Clearance letter indicates the EC capacity that is the quantity of material which can be mined in a year. If this quantity is not measured, and much more mineral than envisaged in the EC is mined out then the entire process of EC is rendered futile. Keeping above objective in mind it is required of the State / State Agencies to create and establish a robust system to monitor and measure the mined out mineral at each lease location and its transportation in State."

The details given above expose us to the reality; we know the problem and we have some solutions but we do not have needed will power and organised execution

machinery to impose the standards, as we do not want to come in the way of Sand mafia, which is backed by powerful lobbies. Unless this mindset is changed and every individual connected with usage of sand be exposed to the gravity of the situation we cannot stop the impending catastrophe. This is the bitter truth. I urge the earth scientists, who have needed capabilities, to spare couple of hours of their invaluable time and put in a concerted effort to address this problem instead of brushing aside the problem as "non scientific".

ACKNOWLEDGEMENTS

I support all the initiatives taken up by the scientific, technical, non technical, administrative, governmental and non- governmental channels to contain this dreadful manmade disaster. I am benefitted by number of technical and popular articles by experts in structuring this research note. One can treat this research note as an "Appeal" made to safe guard the interests of the present and the future generations.

ANNOUNCEMENT

20th Convention of the Indian Geological Congress (IGC) will be organised under the auspices of MECL and GSI at Chitnavis Centre/BSNL Auditorium, Nagpur, from October 3 to 5, 2017. The Convention will deliberate especially on the theme “Make in India: Challenges and Opportunities for Domestic Iron and Steel Industry and Its Innate Mineral-raw Materials”, which has been split into the following sub-themes:

- Make in India: The domestic Iron and Steel Industry (ISI): current production and trade avenues, development and diversification in perspective – an overview.
- Long-term planning, hurdles & challenges before the iron & steel industry for expansion and foreign trade besides meeting the domestic demands.
- Reviews on mineral raw-materials – metallic and non-metallic Present & future demands and supplies, imports & exports.
- Recent developments in exploration, new techniques and targets – exploratory drilling tools, geophysical surveys, logging techniques and advancements in investigation technologies of iron-ores.
- Broad aspects of occurrences and origin of iron-ore deposits.
- Up-to-date review on resources, reserves and inventories on iron ores of India – Are we making use of our potentials optimally?
- Deposits of alloying metals to steel manufacture – sufficiency and non-sufficiency. Their application in grade development and quality improvement of steel.
- Geological data on classical iron-ore deposits.
- Mining methods and environmental issues of open-cast iron-ore mining.
- Development of new beneficiation techniques of low-grade iron-ores – latest practices in major steel-producing countries.
- Govt. initiatives and motivation to scale up exploration and production of iron-ores and Ferro-alloy minerals.
- Sustainability of Indian metallurgical coal in perspective and status of other energy sources to meet demands of the steel industry.
- Emerging safety and health issues related to steel industry.
- Miscellany: Research, education, training, exploration of sea-bed deposits and planetary bodies for supply of minerals at exhaustion limits.

Contributions both for oral and poster presentations are solicited by 31st December, 2016.

They need to be transmitted by e-mail either to the Editor, IGC, Roorkee,
on “igcroorkee@gmail.com” or “igcroorkee@ymail.com”.

The contributions can also be sent to Shri S.N. Rao, Organizing Secretary, IGC, 20th Convention & GM (Geology), CMPDIL, Nagpur. E-mail: raosnrao@gmail.com, Cell: 09437287197 or Shri Vijay V. Mugal, Convention Convenor and Director, GSI, Central Region, Nagpur.

Full details on the Convention can be known by visiting IGC website “www.igcroorkee.net,” or through enquiry, addressed to Prof. V.K.S. Dave, Secretary, IGC, 35-A, Civil Lines, Roorkee - 247667 (Uttarakhand).

E-mails: igcroorkee@gmail.com, igcroorkee@ymail.com,
Tel. 01332-277827, Cell: 09219414329.

GUIDELINES TO AUTHORS

The Journal of Indian Geophysical Union (J-IGU), published bimonthly by the Indian Geophysical Union (IGU), is an interdisciplinary journal from India that publishes high-quality research in earth sciences with special emphasis on the topics pertaining to the Indian subcontinent and the surrounding Indian Ocean region. The journal covers several disciplines of earth sciences such as the Geosphere, its watery and gaseous envelopes (the Hydrosphere, the Cryosphere and the Atmosphere), and life (the Biosphere). It also publishes articles on Space and Planetary sciences. J-IGU welcomes contributions under the following categories:

- Research papers reporting development of new theoretical methods, new techniques of data processing, development of area specific models, new experimental findings and results.
- Review articles providing comprehensive overview of a significant research field related to earth system sciences

In addition, J-IGU also welcomes short communications on opinion and report on scientific activity, personal information, book reviews and news and views.

The manuscript should be submitted electronically as a single pdf file including the main text, figures, tables, and any other supplementary information along with the signed "Declaration Letter". The manuscript should be submitted by email (jigu1963@gmail.com) to the Chief Editor.

After acceptance of the manuscript the corresponding author would be required to submit all source files (text and Tables in word format) and figures in high resolution standard (*.jpg, *.tiff, *.bmp) format. These files may be submitted to the Editor as a single *.zip file along with the "Copyright Transfer Statement".

IMPORTANT INFORMATION

Ethics in publishing

J-IGU is committed to ensuring ethics in publication and takes a serious view of plagiarism including self-plagiarism in manuscripts submitted to the journal. Authors are advised to ensure ethical values by submitting only their original work and due acknowledgement to the work of others in case used in the manuscript. Authors must also refrain from submitting the same manuscript to more than one journal concurrently or publish the same piece of research work in more than one journal, which is unethical and unacceptable. Chief Editor of J-IGU is committed to make every reasonable effort to investigate any allegations of plagiarism brought to his attention, as well as instances that came up during the peer review process and has full authority to retract any plagiarized publication from the journal and take appropriate action against such authors if it is proven that such a misconduct was intentional.

Similarly, Chief Editor, Associate Editors, Editorial board members and Reviewers are also expected to follow ethical norms of publishing by ensuring that they don't use any unpublished information, communicated to them for editorial or review purpose, in their own research without the explicit written consent of the author. They are also expected to keep manuscript/ data/ observations/ any other information related to the peer review confidential to protect the interest of the authors. Reviewers should refrain from reviewing the manuscripts in which they have conflicts of interest resulting from competitive, collaborative, or other relationships or connections with any of the authors, companies, or institutions connected to the manuscript.

Conflict of interest

All authors are requested to disclose any actual or potential conflict of interest including any financial, personal or other relationships with other people or organizations within three years of beginning the submitted work that could inappropriately influence, or be perceived to influence, their work.

Submission declaration

Submission of a manuscript implies that the work has not been published previously and it is not under consideration for publication elsewhere, and that if accepted it will not be published elsewhere in the same or any other form, in English or in any other language, without the written consent of the publisher. It also implies that the authors have taken necessary approval from the competent authority of the institute/organization where the work was carried out.

Copyright

After acceptance of the manuscript the corresponding author would be required to sign and submit the "Copyright Transfer Statement".

MANUSCRIPT PREPARATION

The corresponding author should be identified (include E-mail address, Phone/Mobile number). Full affiliation and postal address must be given for all co-authors.

Abstract:

An abstract of not more than 300 words must be included.

Text:

The manuscript should be structured to include a front page containing the title, Author(s) name, affiliation and address of the institute where the work was carried out, a short title, and 5-to-6 index terms/Key words. Author(s) present address, if different from the above mentioned address,

may be given in the footnote. The corresponding author should be identified with an asterisk and his/her email ID should be provided. This page should be followed by the main text consisting of Abstract, Introduction, Methods/ Techniques/ Area description, Results, Discussion, Conclusions, Acknowledgements, and References. Tables and Figures with captions should be inserted in the main text of the manuscript at appropriate places. Text should be 1.5 spacing with 12 pt font; lines should be numbered.

Figures/ Illustrations:

All figures should be provided in camera-ready form, suitable for reproduction (which may include reduction) without retouching. Figures in high-resolution (at least 300 dpi) standard formats (*.jpg, *.tiff, *.bmp) are acceptable. Figures should be numbered according to their sequence in the text. References should be made in the text to each figure. Each figure should have a suitable caption.

Tables:

Authors should take note of the limitations set by the size and layout of the journal. Table should not exceed the printed area of the page. They should be typed on separate sheets and details about the tables should be given in the text. Heading should be brief. Large tables should be avoided and may be provided as supplementary information, if required.

Equations:

Equations should be numbered sequentially with Arabic numerals and cited in the text. Subscripts and Superscripts should be set off clearly. Equation writing software that presents each equation as an object in MS Word will be accepted. Style and convention adopted for the equations should be uniform throughout the paper.

References:

All references to publications cited in the main text should be presented as a list of references following the text and all references in the list must be cited in the text. References should be arranged chronologically, in the text. The list of references should be arranged alphabetically at the end of the paper.

References should be given in the following form:

Kaila, K.L., Reddy, P.R., Mall, D.M., Venkateswarlu, N., Krishna, V.G., and Prasad, A.S.S.R.S., 1992. Crustal structure of the west Bengal Basin from deep seismic sounding investigations, *Geophys. J. Int.*, v.111, no., pp: 45-66.

REVIEW PROCESS:

All manuscripts submitted to the journal are peer-reviewed. It is advisable to send the contact details of **4 potential reviewers** along with the manuscript to expedite the review process. Chief Editor has the option to select reviewers from the list or choose different reviewers. The review process usually takes about 3 months. All enquiries regarding the manuscript may be addressed to the Chief Editor. It is helpful to have the list of several potential reviewers covering various research topics/themes/ sub themes, to avoid delay in choosing the right persons. Authors and learned experts may help in developing a reference manual, which could be updated from time to time.

GALLEY PROOF:

Technical editing of manuscripts is performed by the editorial board. The author is asked to check the galley proof for typographical errors and to answer queries from the Chief Editor. Authors are requested to return the corrected proof **within two days** of its receipt to ensure uninterrupted processing. The Chief Editor will not accept new material in proof unless permission from the editorial board has been obtained for the addition of a "note added in proof". Authors are liable for the cost of excessive alterations to galley proof.

PUBLICATION CHARGES:

There are no page charges for publication and printing charges for b/w figures, provided length of **printed manuscript is not more than 10 pages. For every additional page Rs.3000/ is charged**, basically to meet publication costs. Also, in view of substantial cost involved in printing of color figures, author will be charged for printing of pages containing color figures @ Rs.2,500/- per page. The charges may be revised at any time based on cost of printing and production. Author will receive an estimate/ invoice of the additional page charges, color figures reproduction cost along with the galley proof. It is the responsibility of the author to remit the additional page charges and/ or color figures reproduction cost **within one month** of the receipt of the estimate/invoice.

The corresponding author will receive a soft copy (pdf format) of his/her published article. Should the author desire to purchase reprints of his/her publication, he/she must send the duly signed Reprint Order Form (accompanies the galley proof and contains price details) along with the corrected galley proof to the Chief Editor. The reprint charges must be paid **within one month** of sending the Reprint Order Form.

Any payment related to additional page charges, printing of color figures and/ or purchase of reprints should be made in the form of a Demand Draft in the name of **Treasurer, Indian Geophysical Union**, payable at **Hyderabad**.

You may download the pdf file from: <http://www.j-igu.in/IGU-Guide-forAuthors.pdf>